Università di Genova

Dottorato di Ricerca in Ingegneria dei Modelli delle Macchine e dei Sistemi per l'Energia, l'Ambiente e i Trasporti Curriculum Ingegneria delle Macchine e dei Sistemi per l'Energia, l'Ambiente e la Propulsione

XXXVI Ciclo

Numerical and experimental study of the flow in side-channel blowers

Shahabeddin Zarei

Supervisors: Prof. Edward Canepa, Prof. Andrea Cattanei

A thesis submitted to the University of Genoa for the degree of Doctor of Philosophy

January 2024

I am filled with overwhelming emotions, reflecting on the incredible journey that has led me to this point – the completion of my PhD thesis.

First and foremost, I want to express my deepest appreciation to both of you. Your unwavering support, love, and encouragement throughout my life have been the bedrock upon which I have built my achievements. Your sacrifices, guidance, and belief in my abilities have been my greatest motivators. This journey would not have been possible without your constant presence and the values you instilled in me.

I would also like to extend my heartfelt gratitude to Professor Edward Canepa and Professor Andrea Cattanei. Your guidance and mentorship have been instrumental in shaping not only my academic journey but also my personal and professional growth. Your commitment to excellence, patience, and encouragement during the challenging moments of my PhD journey have been invaluable. Your expertise, insights, and dedication have significantly contributed to the successful completion of my thesis.

Professor Cattanei, your ability to elucidate complex concepts and provide insightful feedback has been enlightening. Your encouragement to explore innovative ideas and pursue excellence has been a driving force behind my academic endeavors.

Professor Canepa, your support and guidance in navigating the intricacies of research methodology and data analysis have been instrumental. Your commitment to fostering a collaborative and intellectually stimulating environment has truly enriched my academic experience.

Together, your collective mentorship has shaped my research, refined my analytical skills, and broadened my perspective. Your belief in my potential has been a source of inspiration, and I am profoundly grateful for the impact you've had on my academic journey.

In essence, without your guidance, Mom and Dad's unwavering support, and the mentorship of Professors Canepa and Cattanei, the completion of my thesis would not have been possible. Your contributions have left an indelible mark on my academic and personal development.

As I embark on the next chapter of my journey, I carry with me the lessons, knowledge, and values you have imparted. I am truly blessed to have had such wonderful parents and mentors, and for that, I am eternally thankful.

With deepest gratitude and love,

January 2024

Contents

Figures

Tables

Nomenclature

a_c	Shear area of casing
a_i	Shear area of impeller
A_b	Area of blade
A_r	Chanel area
A_R	Area at any radial location
BF	Blade blockage factor
c_a	Axial clearance
c_r	Radial clearance
C_c	Shear stress coefficient of casing
C_D	Orifice discharge coefficient
C_i	Shear stress coefficient of impeller
C_P	Specific heat at constant pressure
d_A, d_B	Channel depth at station A and B
dX_G	Peripheral distance
D_h	Hydraulic diameter
f_r, f_c	Rotor and Casing friction factor
F_s	Fraction of periphery occupied by impeller seal
g	Acceleration due to gravity
H	Head
H_b	Airfoil blade height
H_1, H_2	Total enthalpy of fluid at inlet and exit of impeller blade
k_b	Blade turning loss coefficient
k_{in}, k_{out}	Inlet and outlet port loss coefficient
$k_,$	Blade mixing loss
k_{se}	Sudden expansion loss
k_t	Channel turning loss coefficient
K_t	Head loss coefficient
l	Airfoil blade chord length or flow path length
L_1, L_2	Length of blading at inlet and outlet edges
$\dot{m}$	Mass flow rate

M_{OT}	Impeller tip Mach number
$\dot{M}_A$	Mass flow rate through annular channel
$\dot{M}_B$	Mass flow rate through blading
N_B	Number of blades
N_s	Specific speed
P	Pressure
W_S	Casing depth
W_R	Rotor depth
h	Rotor height
r_{in}	Rotor inner radius
r_{out}	Rotor outer radius
D_{out}	Casing outer radius
ω	Rotational speed
η	Efficiency
T_{out}	Temperature of outlet
V_θ	Tangential velocity
V_c	Circulatory velocity
Φ	Non-dimentionalized flow rate
ψ	Non-dimentionalized pressure rise

Abstract

Regenerative machines are known for their ability to achieve high heads at low flow rates while exhibiting stable performance curves. Despite being the subject of scientific inquiry since the 1940s, the precise mechanism responsible for generating high pressure in regenerative flow compressors remains incompletely understood. In this study, we conducted experimental and numerical analyses on a series of 13 regenerative flow compressors in collaboration with FPZ S.P.A company. Our objective was to investigate the flow characteristics within these machines and identify geometric parameters that significantly impact efficiency.

The first phase of our study focused on the experimental and numerical analysis of the E08 family of regenerative flow compressors across four different rotational speeds (1000, 2000, 2990, and 3500 rpm). Our findings revealed that increasing pressure rise led to a drop in efficiency, with circulatory flow exerting a stronger influence on losses. Additionally, our results indicated that unsteady simulations tended to overpredict losses attributed to increased circulatory flow, whereas steady simulations aligned more closely with experimental data, consistent with observations by other researchers.

In the subsequent phase of our study, we simulated 12 different geometries to evaluate their impact on compressor efficiency. To standardize comparisons, we maintained a rotational speed of 2900 rpm and an outer radius of 0.430 mm across all geometries, while varying the depths of the rotor and stator, as well as the inner radius of the compressor. Our analysis revealed that among geometries with constant rotor and stator depths, compressors with smaller inner radii exhibited higher pressure rise but lower efficiency, whereas those with larger inner radii demonstrated higher efficiency but lower pressure rise.

Furthermore, our simulations indicated that increasing the size of the casing resulted in a notable jump in pressure rise at low flow rates, up to a certain threshold beyond which pressure began to decline. Additionally, larger casings exhibited decreased efficiency at high-pressure working points due to flow separation, whereas smaller casings demonstrated improved efficiency. Our findings suggest a limitation on increasing casing depth, beyond which further increments result in decreased pressure ratio. Conversely, an increase in rotor depth led to improved efficiency and higher pressure rise, while maintaining constant outer and inner radii.

In conclusion, our study provides valuable insights into the factors influencing the efficiency of regenerative flow compressors, shedding light on the interplay between geometric parameters and performance characteristics.

CHAPTER 1- Literature review

1 Introduction and background

Before starting, it must be mentioned that in following literature review to give a reader a complete idea of these type of machines principal and how they work in sense of the experimental aspect as well as theoretical aspect, such as model used in different literatures, the concept is expanded a little more than requested with what will be presented by this study later on. Moreover, this approach makes this literature review as a through source of information in a collective which can be used for the possible future works on the subject.

1.1 Working principle

At first a brief description of working principle of machine will be presented in order to help readers to have a clear imagination about how this machine works, since it has a peculiar behavior.
In conventional fluid dynamic compressors and pumps, the predominant direction of flow through the machine is at right angles to the velocity of the blades, whereas in RFC/RFP the predominant direction of flow through the machine is parallel to the velocity of the blades. The term "side channel" comes from the peripheral position of the toroidal channel compared to the impeller shaft. A side channel blower consists of an impeller with blades and a housing with a peripheral toroidal channel without any blades or guidance. Hence, as the flow enters the impeller it is forced to change its direction from mainly axial to circumferential. At the same time centrifugal forces transport the fluid to the outer part of the impeller and there it is discharged into the side channel. This repetitive motion makes the flow follow a helical motion all through the machine to the discharge point at outlet which increases the pressure of the flow constantly by every repetition **Fig. 1**. In another word every time that the flow enters a blade and leaves it the pressure value of the flow increases. A detailed explanation will be explained in the following parts.

1.2 Elements of a Regenerative Turbomachine

The essential elements of a regenerative turbomachine are shown in **Fig. 1**. Typically, they have an impeller, inlet port, discharge port (outlet), stripper, flow passage and a casing. These components' role is discussed and explained detail below:

1.2.1 Impeller

They differ from centrifugal turbomachines because the impeller blades operate in sequence rather than parallel to one another. The toroidal flow pattern, which consists of an annular flow from the intake to the outlet and combined impeller to side-channel circulation, is promoted by the blades on the impeller. Detailed theoretical flow analysis is not easily adaptable to this complex flow regime. The impeller's grooved section is in touch with the fluid. Through centrifugal forces, the impeller moves the fluid radially outward. The fluid is directed into twin vortices around the impeller blade by the surrounding chambers. Near each impeller blade, a very slight pressure rise takes place. To suit specific design requirements, regenerative turbomachines are also created in multistage systems.

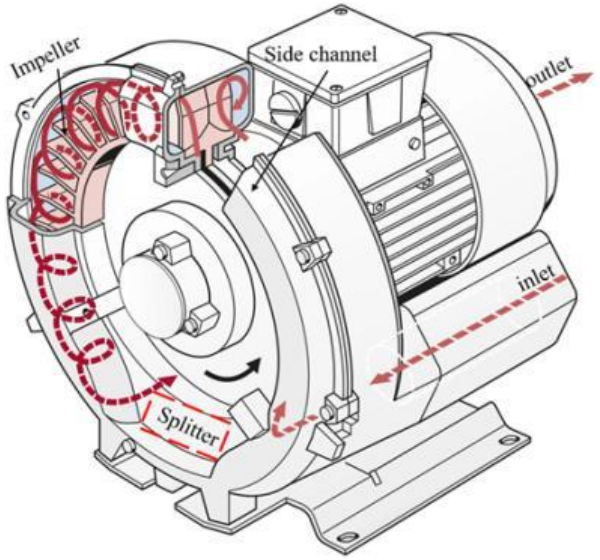

Fig. 1. Flow development in a side channel bower.

1.2.1.1 Classification of Impeller blades

RFC/RFP's impeller can feature blades of various forms. Radial, non-radial, semi-circular, and airfoil blades are a few of the often utilized varieties. In Sreekanth [1], a few illustrations of these blade forms are shown. The airfoil blades on regenerative compressors are typically equipped with a core. The core's function is to direct circulation through the blades and reduce loss brought on by the emergence of vortices at their tips. The core can be fastened to the blades so that it rotates with them, or it can be fastened to the machine's housing. Typically, the blades or vanes are cast into the impeller's face or machined at the edge. The blades can be built in two rows side by side or in a single row.

1.2.2 Inlet and Discharge Ports

The flow channel is joined to the exterior system pipes by inlet and discharge ports. The inlet port, which is shaped to create spiral flow around the annular channel, is where fluid enters the flow channel. The discharge port sends the high-pressure fluid into the pipes. **Fig. 1** depicts the intake and exit ports.

1.2.3 Stripper

The casing clearance is decreased between the inlet and discharge to prevent the high-pressure discharge from entering the low-pressure intake. Only the fluid inside the impeller is permitted to flow through the suction in this area, sometimes referred to as the stripper or septum, the distance between the impeller and the stripper is within a few hundredths of a centimeter.

Leakage from the high-pressure outlet to the low-pressure suction side is prevented by minimizing clearances between the impeller disk and casing. The fluid is compelled to exit through the discharge port by the stripper. The regenerative flow pattern is established and maintained in part as a result of the stripper.

1.2.4 Flow channel

The vanes extend into an annular channel that has a larger cross-sectional area than the impeller vanes along a larger percentage of the perimeter. A raceway or flow channel is present in the casing. The fluid repeatedly passes through the impeller vanes using this annular flow channel. The fluid in the space between the vanes is thrown across the annular channel and out. The fluid in this annular channel is violently mixed, and the angular momentum that the fluid gained during its passage between the vanes is transmitted to it. The mixing process is accompanied by production of a great deal of turbulence, and this implies an undesirable waste of power.

1.3 Turbomachinery

The science of employing working fluids to enhance or decrease pressure using machinery is known as turbomachinery. Turbo literally means "spins or whirls around" in its original sense. The word "turbomachinery" refers to spinning (as opposed to reciprocating) machinery that dynamically alters the motion of one or more rows of moving blades to extract or add energy from fluids. The rotor modifies the fluid's kinetic energy, stagnation pressure, and stagnation enthalpy. This broad description includes

everything from the turbopumps on the main engines of the space shuttle to a traditional Dutch windmill. Aerospace and marine vehicle applications, land propulsion systems, energy applications, hydraulic, gas, and steam turbines, industrial pipelines, and processing machinery including gas, petroleum, and water pumping plants all heavily rely on turbomachinery.

Additional uses for turbomachinery include heart-assist pumps, commercial compressors, and refrigeration facilities.

The type of a turbomachine might vary depending on the application. Through the expansion of a continually flowing fluid to a lower pressure or head, turbines generate power. Pumps are turbomachines that raise the head or pressure of a flowing liquid. Fans are turbomachines that only slightly increase the pressure of a gas that is continually flowing; these turbomachines often have a density ratio across the machine that is less than 1.05, making the gas potentially incompressible. Compressors are turbomachines that increase the pressure of continuously flowing gases with densities greater than 1.05. Pumps and compressors share many common components and working principles. Pumps are typically used to move liquid media, while compressors are used to compress gases.

1.3.1 Classification of Compressors

Shaft power is converted by a compressor into a rise in fluid enthalpy. The fluid, which is frequently a gas, is compressed at low pressure and released at high pressure. A blade assembly is connected to the rotating shaft. The enthalpy is raised as a result of the rotating blades' pressure-increasing force on the gas. Bellows were the first compressors, and blacksmiths utilized them to increase the heat in their furnaces. Simple reciprocating piston-driven machines propelled by a water wheel were the earliest industrial compressors. Due to the virtually endless variety of service requirements, numerous types of compressors are utilized in industry. Before choosing a compressor type for a certain application, some fundamental knowledge on its performance needs should be available. This contains the pressure ratio, the flow rate, the intended efficiency, and maybe other unique properties. Following that, one can evaluate the desired machine type from a variety of possible compressor kinds, as shown in **Fig. 2**. Positive displacement compressors and continuous flow compressors are the two main types of compressors, respectively. In the positive displacement type, a specific volume of air or gas is mechanically decreased and retained in a compression chamber, increasing the pressure therein before being released. With changes in discharge pressure at constant speed, the air flow remains virtually constant. There are two different types of these compressors: reciprocating and rotary. Like bicycle pumps, reciprocating compressors operate reciprocally. A piston that an electric motor drives through a crankshaft and connecting rod reduces the volume of air or gas in the cylinder, compressing it to a greater pressure. While double-acting compressors offer a compression stroke while the piston moves in both directions, single-acting compressors only offer a compression stroke in one direction. Double-acting, water-cooled industrial reciprocating air compressors are large in size.

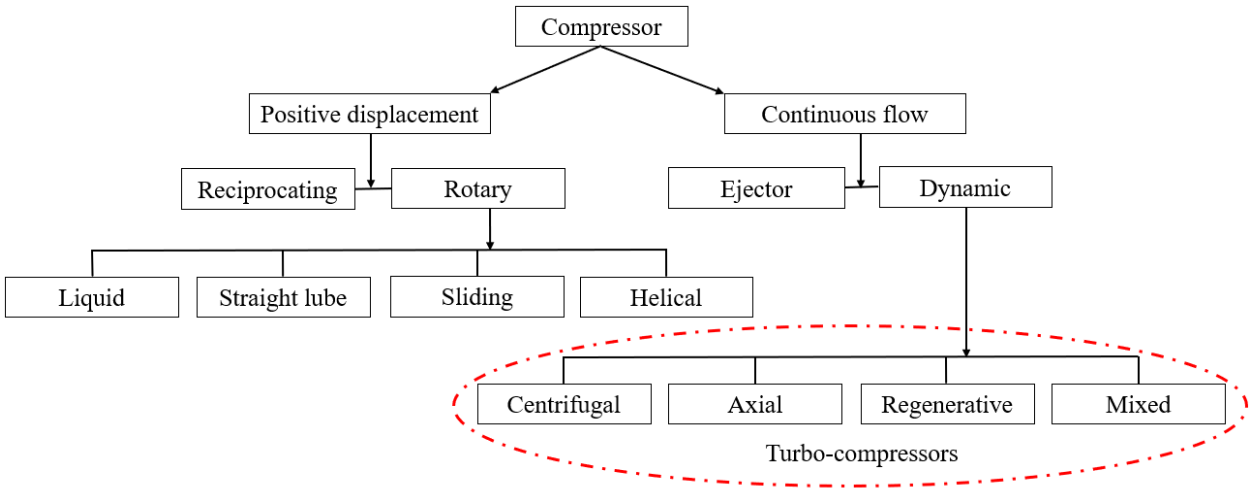

Fig. 2.type of compressors.

The most effective compressors on the market are multistage double-acting machines, which are often bigger, noisier, and more expensive than comparable rotary devices. Sizes for reciprocating compressors range from under 1 horsepower to more than 600 horsepower. The "workhorse" of American industry, rotary compressors have grown in favor. They are most frequently employed in sizes between 30 and 200 horsepower. The helical twin screw kind of rotary compressor (also referred to as a rotary screw or helical lobe) is the most popular type. When male and female screw rotors mesh, air is trapped and moves more slowly to the air discharge point. Rotary screw compressors are inexpensive to buy new, small, light, and simple to maintain. Air- or water-cooled rotary screw compressors are offered in power ranges of 3-600 hp. Straight lobe, liquid piston, and sliding vane rotary compressors are less popular options. In this dissertation, neither reciprocating nor rotary compressors will be further discussed. The idea behind continuous flow compressors is to accelerate the fluid to a high speed and then transform this kinetic energy into potential energy. This potential energy is then converted into an increase in pressure by decelerating the gas through divergent channels. Ejectors and dynamic type compressors are two subcategories of continuous flow compressors. Axial, centrifugal, mixed-type, and regenerative compressors are the different categories of dynamic compressors. Turbocompressor is another name for these four subcategories. Based on the flow path through the machine, they can be further divided into three major groups, which are detailed below.

1.4 Turbocompressor

Based on the type of flow path via the rotor channels, Turbocompressor can be categorized. The compressors are known as axial compressors when the meridional flow route is axial. There are multiple

rows of airfoil cascades in them. Some of the rows (referred to as rotors) are joined to the central shaft and revolve quickly. Stators are other rows that are fixed and do not rotate. Stators are responsible for bringing the flow back parallel to the axis, increasing pressure, and preventing the flow from spiraling around the axis. Radial or centrifugal compressors fall under the second type and have a predominately radial flow pattern.

Deceleration occurs in the diffuser of centrifugal compressors while it occurs in the stator blade passages of axial compressors. The flow leaves the compressor in the axial direction in axial compressors, whereas the flow leaves the compressor in a direction perpendicular to the axis of the rotating shaft in centrifugal compressors. This is a clear distinction between the two types of compressors.
The mixed flow compressors fall under the third classification and have a flow channel that is partially axial and partially radial. Impellers and rotors in mixed flow compressors incorporate the traits of both axial and centrifugal compressors.
The rotodynamic turbomachines known as regenerative flow compressors (RFC) and regenerative flow pumps (RFP) are able to generate high pressure ratios in a single stage. They enable a head that is comparable to multiple centrifugal stages. a single rotor with a similar tip speed yields this result. In a regenerative flow compressor, the fluid rotates helically inside the casing and repeatedly enters the impeller on its way from the inlet to the outlet. This repeated impeller blading on fluid is referred to as "multistaging" and is what gives this particular type of turbomachine its high head per stage characteristic.

The terms peripheral pump and side channel pump are also used to describe regenerative flow pumps. In literature, there are several different types of pumps: vortex, turbine, drag, traction, and tangential. Regenerative turbomachines are characterized by their capacity to produce high heads at low flow rates. They have a very low specific speed and some positive displacement machine traits, like a roots blower, but without lubrication and wear issues. A RFP/RFC has the ability to create far higher heads than any other form of turbomachine with the same tip speed, which is in addition to its self-priming qualities. Another benefit of using a regenerative flow turbomachine as a gas compressor is that there is no surge or stall instability.

1.5 Side channel blowers

Side channel blowers are low-specific-speed turbomachines that present a number of advantages over common centrifugal blowers and compressors. Namely, they are simpler, cheaper, mechanically stronger and do not present instability at low-flow-rate operation, i.e., stall. This rotor-dynamic machine shares some of the characteristics of positive displacement machines capable of producing high heads in a single stage, but without the problems of lubrication and wear. When used, the impeller rotates without touching the

surrounding parts, and so wear-and-tear is avoided, and lubrication is no longer needed. Therefore, side channel blower has found many applications in industry in place of positive displacement machines. The regenerative flow compressor (RFC) and regenerative flow pump (RFP) are turbomachines capable of developing high pressure ratios in a single stage. They are also known by other names, such as peripheral, side channel, turbine, traction, and vortex compressor/pump. Even though the efficiency of RFC/RFP is usually less than 50 per cent based on past design experience, they have found wide applications in automotive and aerospace fuel pumping, booster systems, water supply, agricultural industries, shipping and mining, chemical and food stuffs industries, and regulation of lubrication and filtering.

Side Channel Blowers have many applications: from heavy industry to chemical and environmental sectors. More specific applications of side channel blowers are in operations such as packaging and packing, material lifting and handling, dust and fume extraction, water purification and treatment, subsurface remediation.

This is possible thanks to the special technical features of these blowers:

• Maintenance-free
• No contact among parts
• Low noise level
• No pulsation and no fluid contamination
• Compact in size

A side channel blower can be used in the following sectors:

• Cleaning
• Energy
• Glass
• Medical
• Packaging
• Textile
• Wood
• Chemical-Pharmaceutical
• Electronic
• Food and Beverages
• Graphics
• Metal and Foundry
• Plastics
• Water and Environment

The regenerative compressors are frequently in competition with centrifugal compressors for meeting application requirements. Therefore, it is interesting to mention the relative merits of the two operationally

different compressors being widely used in the industry. Some of the characteristics of both compressors are discussed below:

1. Regenerative compressors give fluid flow both a radial and an axial component, in contrast to centrifugal compressors, which draw fluid from the impeller's center and push it outward radially with no axial component of velocity.

2. Regenerative compressors expose the fluid to the impeller multiple times, whereas centrifugal compressors only expose it once, giving the fluid additional energy.

3. The lack of complicated flow passageways or vane requirements is one of the regenerative type compressors' greatest structural advantages. There is no need for diffusers or scrolls because they are straightforward and simple to machine. Centrifugal compressor impellers can be cast with the outside diameter machined, whereas the regenerative compressor impeller is entirely machined. Regenerative compressors often have more internal components than centrifugal compressors.

4. Due to diffusers and scrolls, centrifugal compressors have a large axial length for each stage and a big overall diameter. As opposed to centrifugal compressors, regenerative compressors have suction and discharge nozzles that are near the periphery, which results in smaller axial and radial dimensions. Regenerative compressors offer significantly higher pressure rise in a smaller compressor design.

5. While centrifugal compressors are by nature more efficient than regenerative compressor types in terms of performance, this may not always be the case. The regenerative compressor is regarded as a low specific speed device, and within its typical range of specific speeds, it performs advantageously in comparison to centrifugal compressors in terms of efficiency.

6. A centrifugal compressor's power requirement grows as flow rate increases, whereas a regenerative compressor's power requirement reduces as flow rate increases. Additionally, there are considerable differences in the two machines' head and flow rate properties.
7. The centrifugal compressor surges occasionally at low flow rates of up to 50% of maximum flow rates. The flow can be stopped in a regenerative compressor without the pressure rising, but there will be a temperature increase. The regenerative compressors offer the benefit of stability since they operate steadily across the flow range (a regenerative compressor will never surge).

8. Compared to centrifugal compressors, stage matching is less crucial and off-design operation is less constrained since regenerative compressors do not spike even at 0% flow.

9. Centrifugal compressors typically require a lot more stages and/or higher rotative speeds. For a given impeller tip speed, regenerative compressors produce heads that are many times higher. Regenerative kinds have head coefficients that have been recorded at or above 5, vs centrifugal forms at or near 0.7 to 0.8. For a centrifugal compressor with radial blades and no pre-rotation, the theoretical head coefficient maximum is 1.0.

10. A centrifugal compressor has a flatter head vs. flow rate graph than a regenerative compressor. A centrifugal compressor lacks the capacity to provide fluid at a variable (desired) flow rate, but a regenerative compressor can. A centrifugal compressor often has a bigger fluid volume than a comparable regenerative compressor.

11. Another distinction between centrifugal and regenerative compressors is that in the former, pressure gain is proportional to the square of the impeller's peripheral velocity, whereas in the latter, the relative velocity to the blades is dependent on the pressure gradient.

12. Regenerative compressor clearances are held to tighter tolerances than centrifugal compressor clearances.

13. Regenerative compressors are quieter than centrifugal compressors and have less wear-related issues.

In contrast to most other turbomachines, the side-channel blower has a disadvantage in that its efficiency is typically less than 50% [2, 3]. This is explained by the fact that the input power is utilized not only for creating head raise but is also used to repeatedly circulate flow through the blades. Raheel [4]. This is mostly because of the work exchange mechanism, which depends on the blending of the channel and rotor flows. The lack of a true blade channel and the poor incidence angle make operating the machine even more difficult [5, 6].

The flow is extremely complex due to inherent unsteadiness and strong circulatory flow. This is why the circulatory flow assumption, which assumes that a helicoidal motion forms between the rotor and side channel, is still used to study the flow using steady, one-dimensional models, such as those by Wilson et al. [7] **Fig. 3**. The fluid in the rotor is centrifuged between the inlet and outlet ports, which are separated by a stripper positioned between them. This causes the fluid to leave the rotor with a high moment of momentum, and even though the mixing is inherently dissipative, it causes a rise in circumferential pressure. The

procedure is then repeated as the circulatory flow repeatedly enters the rotor and combines with the side channel flow. The side channel blower may generate a higher head at low flow rates than any other type of rotor-dynamic machine with the same tip speed thanks to this repeating flow process, which is similar to a multistage effect. This model is physically sound, but the resulting mathematical model uses the balance equations in integral form, necessitating a number of correlations for its closure, such as those for friction losses, leakage flow, rotor inflow incidence and outflow deviation, features of the vortex associated to the circulatory flow, and other aspects like the heat transfer between the flow and the metal parts, for example, see El Hag [8]. Such correlations are the weak link in the model and the main reason why flow forecasts are inaccurate, which has an impact on the machine's design reliability. The shape of the blades and the meridional channel can be altered to create different side channel blower designs.

Numerous authors, including Senoo [9, 10, 11, 12], Iverson [13], Wilson [14], Shimosaka [15], Burton [16], Gessner [17], and Grabow [18], have researched regenerative turbomachines with radial blades. The experimental impact of blade number on regenerative pump performance was reported by Iverson [13]. He examined impellers with 31, 36, and 39 blades and discovered that when the number of blades rose within the studied range, the pump head and efficiency improved as well. The number of blades needed to get the highest head at a particular flow rate was not attained. According to Burton [16], the performance of the pump could be enhanced by adopting a non-radial blade. When employing a blade with a 47° blade angle, the shut-off head coefficient was nearly twice as high as when using a straight blade. Grabow [18] and Hollenberg [19] explored the semi-circular blade Shapes whereas Yamazaki [20, 21, 22] studied non-radial blades. The regenerative compressor with airfoil blades was researched by Sixsmith and Altmann [23], Sixsmith [24], and Abdallah [25]. For both radial and semi-circular blades, Grabow [18] described theoretical and experimental effects of the blade angle. In all scenarios, he tested the pump with various blade angles between 60° and a step size of 20°. Theoretically, he discovered that the optimal shut-off head was achieved for a blade angle between 40° and 55°, however experimental investigation produced an optimal blade angle between 40° and 45°. The ideal range of an airfoil's blade angle, according to Abdallah's theoretical investigation on the impact of blade angle on the shut-Off head, is between 55 and 61 degrees.

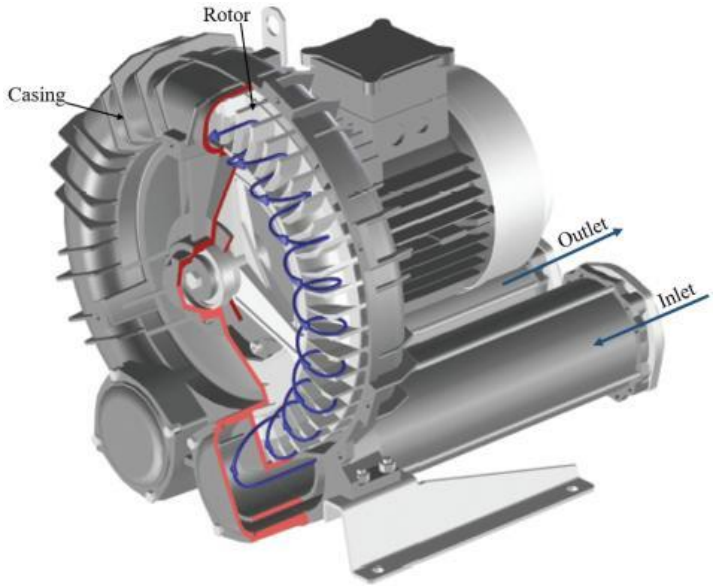

Fig. 3. assembly of a side channel machine.

Fig. 4 depicts a few of the common varieties of side channel blowers. The turbulence and mixing hypothesis and the circulation or liquid filament theory are the two basic hypotheses for how regenerative pumps work. The shearing movements are what cause the head lift, according to the turbulence and mixing theory. According to the circulation or liquid filament hypothesis, momentum generated by the impeller's motion is transferred into the open channel via the circulation. The fluid slows down at this point, transferring momentum to the head. Although ignoring the effects of drag and shear stress, this hypothesis is now widely accepted. Senoo [11] demonstrated the compatibility of the circulation or liquid filament theory with the turbulence and mixing theory, as well as the fact that no one theory can account for all effects.

Many authors have suggested simplified theoretical models for various machines geometries. A turbulence mixing model put forth by Senoo [11] takes into account a turbulent friction force as the pumping mechanism. This idea was put forth on the basis of simulating the internal flow of an impeller with radial blades as Couette-Poiseuille flow in the presence of a negative pressure gradient.

Iverson [13] proposed a viscous model to describe how a radial blade impeller operates. He evaluated the side channel blower's efficiency in terms of the fluid shear stress that the impeller applied. Two shear coefficients and an average impeller velocity were calculated experimentally and included in the derived formulas.

Several flow visualization studies have been conducted by researchers to depict the circulatory (helical) flow pattern. The circulatory flow pattern that is a feature of side channel blowers, however, cannot be clearly explained by any of the two ideas mentioned above [23, 26]. The momentum exchange hypothesis for a radial blade impeller was created by Wilson and colleagues [14], and it can be used to explain helical

flow patterns. This model was chosen by Dewitt [27], Mason [28], and Grabow [26] to estimate the performance of the semicircle blade impeller.

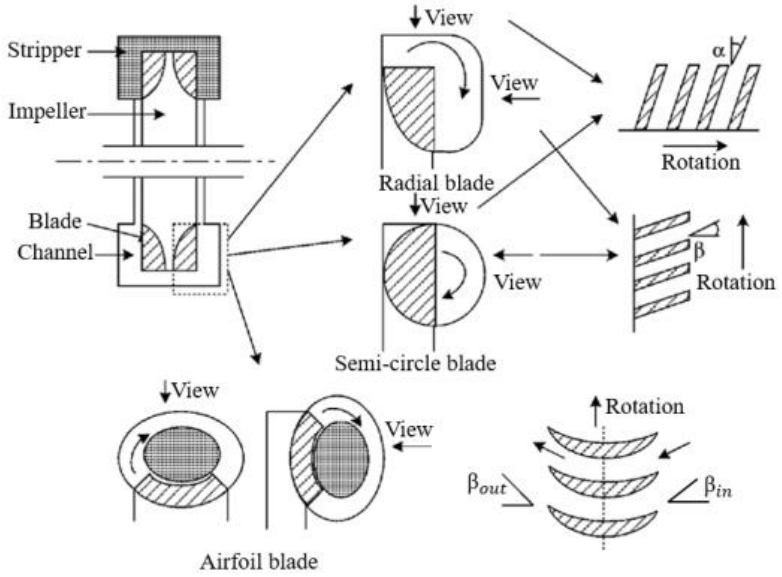

Fig. 4. various type of regenerative machines.

An innovative regenerative flow compressor with aero foil blades was developed by Sixsmith and Altmann [23] and produced greater head rise than any other type of impeller blade. They interpreted the channel's flow slowing as the result of a diffusion process. Whitehead and colleagues [29] proposed a perfect mathematical model based on the supposition that the diffusion process in an RFC suffers no loss. These writers employed geometry akin to that of Sixsmith and Altmann [23], but they made no recommendations for design principles. After reviewing every theory for a side channel blower, Senoo [10] came to the conclusion that the models mentioned above are all compatible. Aside from the theory described by Whitehead and colleagues [29], all the models, in the authors' opinion, can only be applied for the range where flow is fully developed, even though the aforementioned theories do explain some aspects of flow in a side channel blower. In contrast, a side channel blower has a developing area that comes before the beginning of the fully formed area. The performance of a side channel blower, according to the authors, is significantly influenced by the emerging region. The development zone of a side channel blower's flow behavior has not received much attention in the past. Senoo [12] conducted experimental research on several inlet area shapes to examine the impact of the developing region on performance. He came to the conclusion that using a bigger channel area in the input portion of a pump can result in increased head rise and efficiency and has the added benefit of reducing cavitations.

After researching the RFP, Badami [30] proposed a fresh layout. In his study, Badami compared theoretical and experimental data using the momentum exchange theory developed by Wilson and colleagues [7]. However, in order to find the unknown coefficients needed to estimate the performance, Badami's study required extensive experimental backing.

According to earlier studies, a side channel blower has an internal flow pattern that is helical and that repeatedly passes through the blade via the impeller. According to the helical flow pattern, it enters the blade by the channel close to the blade root (incoming flow) and exits the blade through the channel close to the blade tip (outgoing flow). In order to sustain the tangential head rise, the angular momentum of the outgoing flow is lost in the channel after being augmented by the action of the blade as it passes through the blades. According to experimental findings for the head distribution along the channel, the physical operating range of a blower is divided into five areas, as indicated in **Fig. *5***. These regions are inlet, acceleration, linear, deceleration, and exit region [8, 12].

In most cases, the entrance and exit regions' sizes are calculated geometrically. The diameters of the acceleration and linear regions vary depending on flow rates if the deceleration zone can be disregarded due to its minimal impact. Wilson et al. [14] made the assumption that the circulation velocity and head elevation would be constant throughout the channel. To depict the three-dimensional fluid motion inside the regenerative pump, they developed a simplified model. His model, however, did not take into account the effects of changing channel area or fluctuating circulation velocity through expanding channel area. An revised model was then proposed in order to account for variables that Wilson did not take into account, such as head lift brought on by changes in channel area and variations in circulation velocity in the acceleration region.

Pressure variation of the fluid as it circulates through the machine for several flow rates is shown in **Fig. 6**. These curves suggest five regions in the pump operation, which are also marked in **Fig. 5**.

- Inlet region (A): The flow experiences some pressure loss through the inlet region.
- Acceleration region (A-B): The flow enters the working section of machine with a velocity and pressure dependent largely on the inlet region.
- Linear region (B-C): The pressure gradient is constant as indicated in the diagram. This region is referred to as the working section of the machine where the flow pattern is fully developed.
- Deceleration region (C-D): In this region, a deceleration occurs, and the kinetic energy of the circulatory velocity is changed as pressure rises. Therefore, there is a little pressure rise as shown in **Fig. 6**.
- Outlet region (D): A loss similar to that at the inlet region occurs at the outlet region.

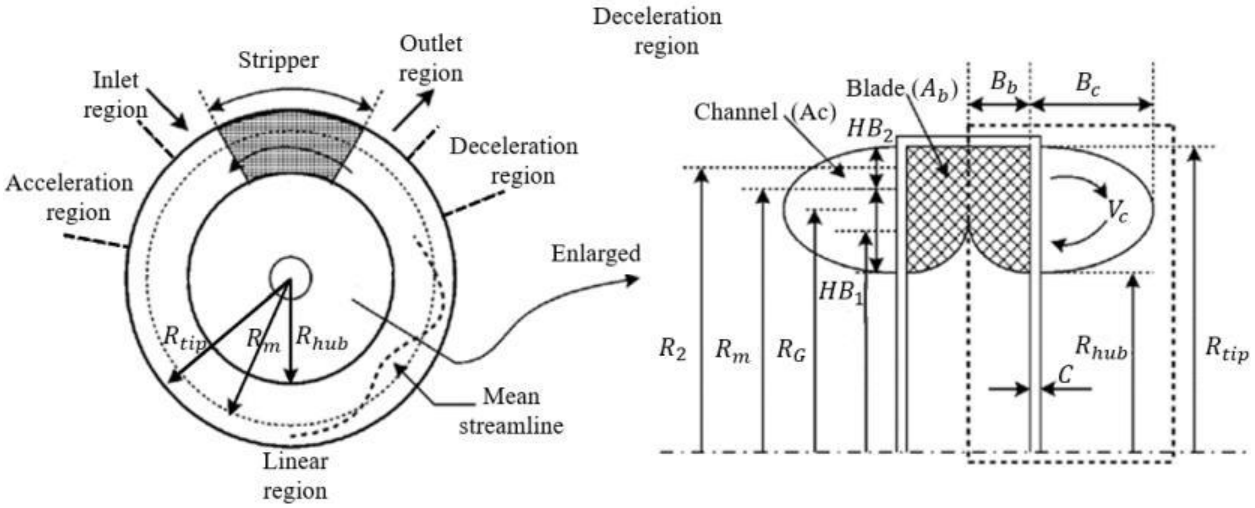

Fig. 5. Schematic drawing and geometric symbols for a regenerative machine.

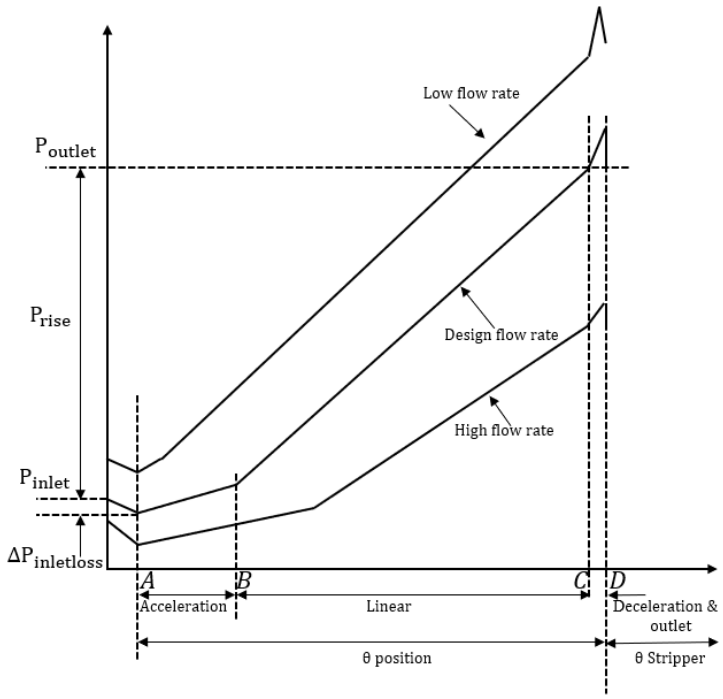

Fig. 6. Tangential pressure variation in a regenerative turbomachine [25].

Given the unique design and operation mechanism of RFC/RFP, which allows them to generate high pressures and deliver reliable performance in challenging environments, a wide variety of applications call for this kind of equipment, however, their low efficiency have been their Achillis heel which comes from the fact that their internal flow is incredibly intricate and not fully understood to this point.

To address the latter, Ritter [31] and Schmiedchen [32] made a first attempt to investigate the flow behavior in these machines. Both articles assess performance curves (versus V) and define impeller and side channel efficiency. Data on the work coefficient Ψ=ΔP/ (ρ. U^2) (precise definition of Ψ is given below) for various side channel machine designs may be found in Schmiedchen's study. Ritter and Schmiedchen's work are summarized and given an overview by Pfleiderer [33]. They started their investigation into the flow inside

side channel machines using two competing theories. The first theory is based on the notion that turbulent shear stress is used to transmit momentum from the impeller into the side channel. For instance, this hypothesis was used by both Iversen [13] and Weinig [34]. The other definition of the flow inside side channel pumps is a circular flow, as previously mentioned. For instance, Senoo's work [35] is built on this premise. Today, we know that the side channel pump has a strong circulation flow, and that the behavior of the machine is controlled by this flow (details are given below). A good review of the literature without CFD data is given by Grabow [36]. The first attempts at dimensionalizing side channel machines were undertaken by Schmiedchen [32]. Surek [37], outlines a more complex design procedure. Surek [38] presented a number of important details regarding pressure oscillations in side-channel compressors, the impact of blade shape on the gradient of side channel machines' performance curves, and other subjects. The conclusion of [39] was that the characteristic curves of side channel could be converted from 1500 rpm to 3000 rpm using the similarity laws from the centrifugal blowers/pump theory. The analysis of CFD findings shows that the circulating flow is so powerful that it exceeds the side channel machine's discharged volume for the majority of all operational locations [40, 41]. When the machine is working near to zero head, the circulating flow is modest; nevertheless, when throttled, it becomes quite forceful.

Regenerative pumps, despite their subpar efficiency, can often be a more effective alternative to other (centrifugal) pumps, Quail and colleagues [42]. Due to the fluids being pumped at a low velocity, small centrifugal pumps are notoriously inefficient. The moving fluid has a fair amount of friction with the impeller and the walls of the pump chamber because of their low ratio of enclosed volume to interior surface. As a result, the fluid only passing through the pump once, this has a substantial impact on the head rise that is created. Contrarily, the regenerative pump impeller makes several interactions with the fluid in a single-stage configuration, resulting in higher heads than any other pump type with a comparable tip speed. Existing computational models struggle to accurately depict the intricate flow field inside the pump and necessitate substantial experimental adjustment, Nejadrajabali and colleagues [43]. In the areas of biomedical pumping, water treatment, boiler feed, brine circulation, coolant pumping, condensate return, aero-/auto fuel pumps, sump service (clear water), car washers, refrigeration, refineries, and marine (potable water) applications, regenerative pumps demonstrate advantages over other pumps. The pump can also be used to pump caustic fluids, viscous fluids, hot/volatile liquids, and chemicals.

Most of the existing literature can be broken down into broad areas of regenerative turbomachine research:

1) Experimental work
2) Theoretical Models
3) Loss categorization
4) CFD Analysis

Which will be explained in more detail in the following.

1.6 Experimental Work

The initial researchers on regenerative turbomachines were interested in investigating the implications of different geometry on the design of regenerative turbomachines over a broad range. The experimental work entailed changing the side channel's shape, the blade profiles, and the ratios of the blading to its coverage over the side channel. These experiments yielded a wealth of knowledge, but it was still impossible to determine the ideal proportions for a standard regenerative turbomachinery design. In regenerative turbomachines, Bartles attempted to experimentally examine the precise flow process. In the same pump case, he examined three rotors. The first rotor was a smooth disc without any grooves or vanes, the second had grooves removed, leaving only the standard radial vanes, and the third had the standard radial vanes as well as additional vanes that were normal to them. He suggested that if the first rotor pumped, it must be as a result of a smooth metal disc's drag, which is viscous. If the second rotor pumps, it may be because of the centrifugal forces acting on the fluid as it travels through helical patterns within and outside of the impeller, or it may be because of the shearing stresses of viscous and turbulent drag. As any potential radial flow was substantially inhibited by the cross blades, it would demonstrate that the shearing stresses are the main force generating the pumping if the third rotor produced pumping. If it failed to pump or was substantially rendered useless, it suggests that the pumping was mostly generated by centrifugal force because the cross blades' ability to shear the radial blades was minimal. Wilson's regenerative theory of pumping mechanism in these turbomachines was supported by his discovery that the pump would only function when the impeller design permitted circulatory motion and centrifugal pumping. Crewdson also looked at how the circulation or centrifugal pumping affected the transmission of enthalpies in a regenerative pump. To separate the side channel into two sections, he soldered a thin brass strip down the middle of it. As a result, any circulatory flow in the channel that is primarily radially inward would be significantly impacted and may have been divided into two: one in the lower section of the channel and one in the top part. It was difficult to assess the impact of this configuration on the fluid motion inside the impeller. However, it was suggested that although being significantly reduced, the circulatory flow was not entirely stopped since centrifugal forces persisted even after the channel was divided in two. The performance curves led to the conclusion that the effectiveness of the pumping was significantly decreased by the drop in circulatory flow. Pfleiderer detailed early experimental work from Germany and Japan (before to 1949), in which variations in impeller and side channel geometry were investigated for their impact on machine performance curves. Additionally, he provided a simplified design method based on this and the experimental data that was available at the time, as well as a one-dimensional momentum analysis for the head. A regenerative pump having two channel diameters 5 centimeters and 3.125 centimeters and an impeller with 40 centimeter, and 20 blades each was the subject of an experimental study by Mason [39]. He contrasted theoretical studies of the fluid dynamic mechanism of regenerative pumps with experimental performance characteristics. He attempted to link empirical parameters to pump geometry, but no clear

connection could be made. A new intake for a regenerative pump was created by Bicard [44] using a model of the fluid dynamic process in the inlet region as a basis. By extending the linear region of the channel and subsequently the head across the channel, he was able to make some improvements to the inlet design. Senoo [12] conducted an experimental investigation into the effects of a regenerative pump's suction port location. He proved that the fluid enters the pumping tube too far upstream, where the impeller action is not fully realized, when the inlet port is too close to the barrier. Thus, in order to retain the incoming flow, there must be a pressure difference between the input port and the entrance zone. When the discharge flow rate is large, this pressure drop results in a significant energy loss because the required acceleration is substantial. He claimed that by strategically placing the intake port downstream of the barrier, fluid could enter the pump route in an area where the impeller effect was reasonably established, greatly enhancing pump performance. He identified 65° as the ideal angle for the design he was thinking of between the barrier and the inlet port. However, there was no correlation between this value and any other design factors. Shimosaka and Yamazaki [45] looked at the effects of changing the clearances, impeller, and channel sizes. After fixing some of the dimensions, they discovered how changing the others would affect the pump's performance. They discovered that it was impossible to create a complete strategy for the performance prediction due to the multiple variables involved. They came to the conclusion that methodical experimentation can be used to determine the dimensions of a high efficiency pump.

There is a scarcity of design information since there is so little information available on gases as the working fluids in regenerative turbomachines. Mechanical Technology Incorporated, Massachusetts Institute of Technology, the Los Alamos Scientific Laboratory, Compair Ltd. of Ipswich, and the Oak Ridge National Laboratory (ORNL) are among the organizations that have conducted some gas experiments; however, the majority of their work dealt with relatively low Mach numbers. Many factors that affect performance, such as flow channel geometry, impeller blade geometry, nozzle design, radial and axial clearances, and multistaging, require performance data that takes compressibility effects into account. The gas-cooled reactor designs that were being researched at ORNL were intended to use the regenerative machine as a light gas compressor and circulator. The Oak Ridge Gaseous Diffusion Plant investigated the regenerative compressor's performance characteristics on gases with molecular weights ranging from 4 to 400 and speeds ranging from 5000 to 14000 rpm. In a study that was published, Cates [46] described the test results of the regenerative compressor with several gases that ranged in molecular weight from 4 to 400. He provided broad features in Mach numbers that went all the way into the range of compressible operation. With the range of gases, the regenerative compressor performed satisfactorily without surging or unstable operation. At such a high Mach number, compressibility effects are believed to begin to manifest. Based on an ideal isentropic process between suction and discharge pressure, Cates derived the compressor efficiency. This efficiency was described as follows:

$$\eta_s = \frac{H'_{OD} - H_{OD}}{H_{OD} - H_{OS}} \tag{1}$$

where H_{OD} , H_{OS} were average total enthalpies at discharge and suction respectively and H'_{OD} was total enthalpy at discharge total pressure along the isentropic path. He treated the test gases as perfect gases with C_p and γ evaluated at an average of the suction and discharge temperatures. The isentropic efficiency can be rewritten as:

$$\eta_s = \frac{C_p\left(T_1' - T_1\right)}{C_p\left(T_1 - T_2\right)} \times 100 = \frac{T_1\left[\left(\frac{p_{out}}{p_{in}}\right)^{\frac{\gamma-1}{\gamma}} - 1\right]}{\left(T_2 - T_1\right)} \times 100 \tag{2}$$

Efficiency was plotted with specific mass flow rate for several test gases. It was observed that values of η_s greater than 50% were obtained under certain conditions. As the Mach number increased, efficiency generally declined. Furthermore, data collected on air at 15, 40, and 70 kPa showed that efficiency decreased with a rise in pressure level, suggesting that pressure level or Reynolds number may have an impact on efficiency. In general, the heavier gases demonstrated poorer efficiency when evaluated at the same Mach number. Also, when the tip Mach number was greater than 1.0, very low efficiency was observed. The performance of compressor on the various gases in terms of ψ - λ curves is Shown in **Fig. 7** with approximate efficiency contours included. The head coefficient ψ and flow coefficient λ were defined as:

$$\psi = \frac{gH}{U_2^2} \tag{3}$$

$$\lambda = \frac{Q_s}{U_2 A_c} \tag{4}$$

where H is developed adiabatic head, Q_s , is suction volume flow rate and A_c is cross sectional area of open channel. It must be noted from ***Fig. 7*** that at small flows, the efficiency was lower, and the delivery head was also found to be reduced. The logarithmic plot of the head coefficient as a function of tip Mach number is given in ***Fig. 8*** for three values of flow coefficient. When compressibility effects started to play a role,

the was practically constant for a given flow at low Mach values, but it went off quickly beyond that. Changes in flow channel geometry's implications on compressor performance were also observed by Cates. At various Mach number values, the consequences of the geometry alterations were quite variable. Also displayed in ***Fig. 9*** is Cates' presentation of the impact of impeller-to-casing clearances on pressure ratio. In order to reduce cross leakage, regenerative compressors have been defined in the literature as machines that need modest clearances at the stripping section and sides between the revolving impeller and the stationary casing. The results of Cates' experiments showed that, most likely as a result of this impeller's high carry overflow characteristic, increasing impeller-to-casing clearances had no impact on performance. Additionally, as shown in **Fig. 10**, he provided a brief comparison of six regenerative compressors that had been examined by independent groups. In his research, Hollenberg [29] looked at regenerative turbomachines that used both water and air as operating fluids. He researched three devices with two different geometries each, and he created a non-dimensional correlation between pressure and flow and driving torque. Experiments using information from geographically dispersed studies were used to confirm this. He prepared a research of maximal effectiveness as a function of particular speed using this knowledge. The governing parameter was discovered to be a single loss coefficient. He discovered that extending the distance between the impeller and the stripper had a negative impact on the optimal head and maximum efficiency.

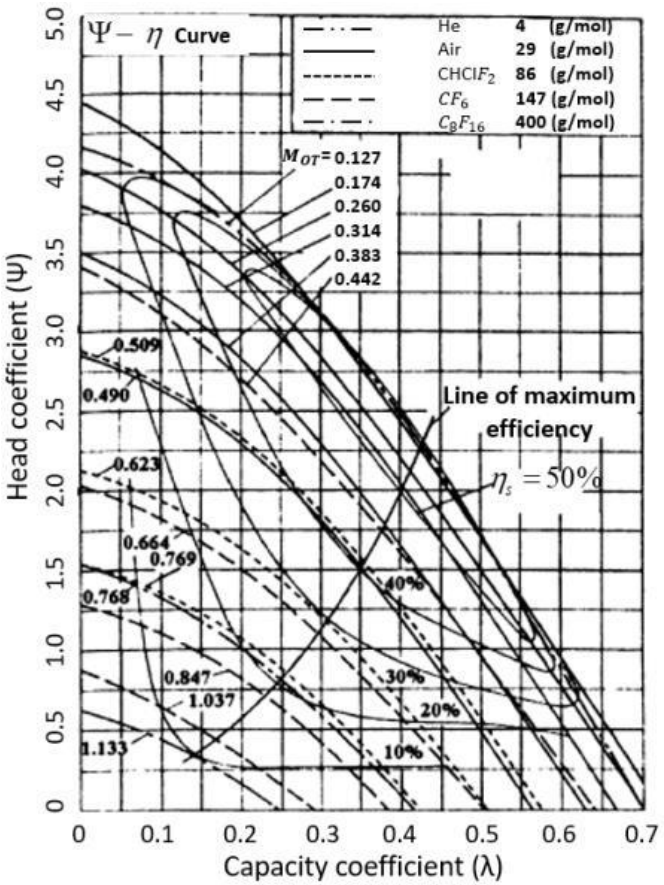

Fig. 7. Head coefficient of ORGDP-1 regenerative compressor [46].

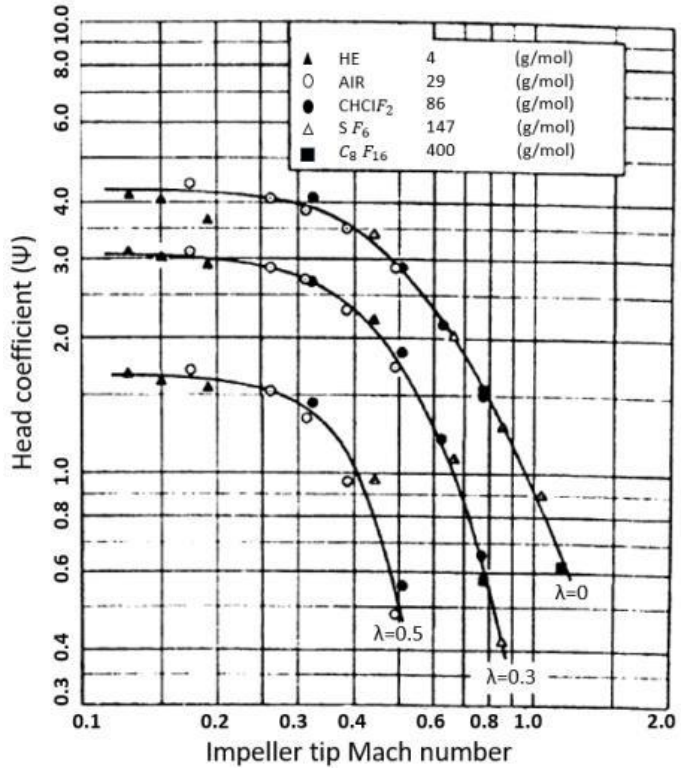

Fig. 8. Head coefficient dependence on impeller Mach number [46].

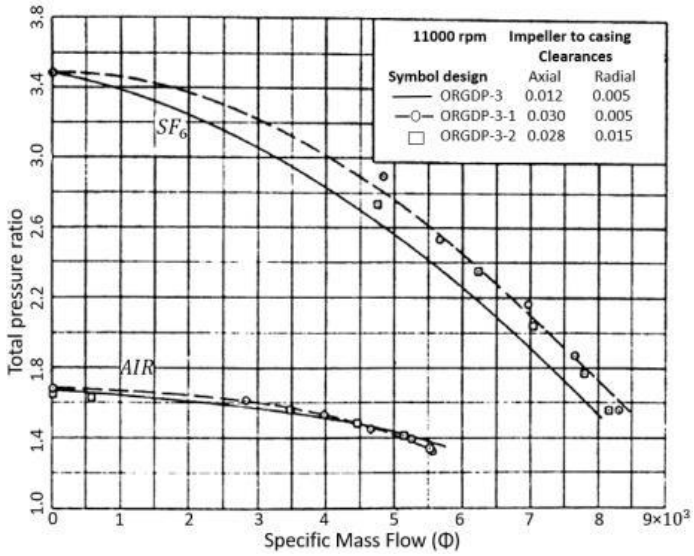

Fig. 9. Influence of clearances on pressure ratio [47].

He also came to the conclusion that higher specific speeds might be used to achieve improved efficiency. Using various impeller blade designs, numerous other writers have examined the impact of impeller clearance in the regenerative pump. While Hollenberg [48, 49] reported on the experimental effects in the case of semi-circular blades, Senoo [10] reported on the theoretical and experimental impacts of clearance in the case of radial blades. Senoo [11] created a theoretical model to investigate how clearance affects the effectiveness of the pump. Using a pump with radial blades, he conducted a number of experimental studies.

He experimented to clarify the effect of the clearance and then compared the results to his theoretical predictions. He altered the pump clearance eight to ten times, from 0.04 mm to 0.36 mm. He discovered that the pump head significantly depends on the pump clearance value. Using an experimental pump with radial blades, he conducted a number of tests. He eight to ten times varied the pump clearance from 0.04 mm to 0.36 mm, defined the effect of the clearance experimentally, and then compared his theoretical findings to the experimental data. The value of pump clearance, he discovered, has a significant impact on the pump head. Additionally, he established the impact of Reynolds number on a conventional regenerative pump in another work. Sixsmith [23] analyzed the effect of the stripper and proposed that the performance of the regenerative pump might be enhanced if the solid stripper were modified to form a row of stationary blades, allowing flow between the blades to continue in a toroidal path rather than just a peripheral path. This advice was utilized by Abdallah [25] in his thesis, which examined RFC for airfoil blades. By pumping air through two regenerative compressors with airfoil blades, Sixsmith and Altmann [23] evaluated them. 250 liters per second at a pressure of 2 atm are produced by the MKl regenerative compressor, which can operate at speeds of up to 10,000 rpm. It had an impeller of 300 mm diameter with a Single row of blades. The performance of MKl compressor is given in ***Fig. 11***.

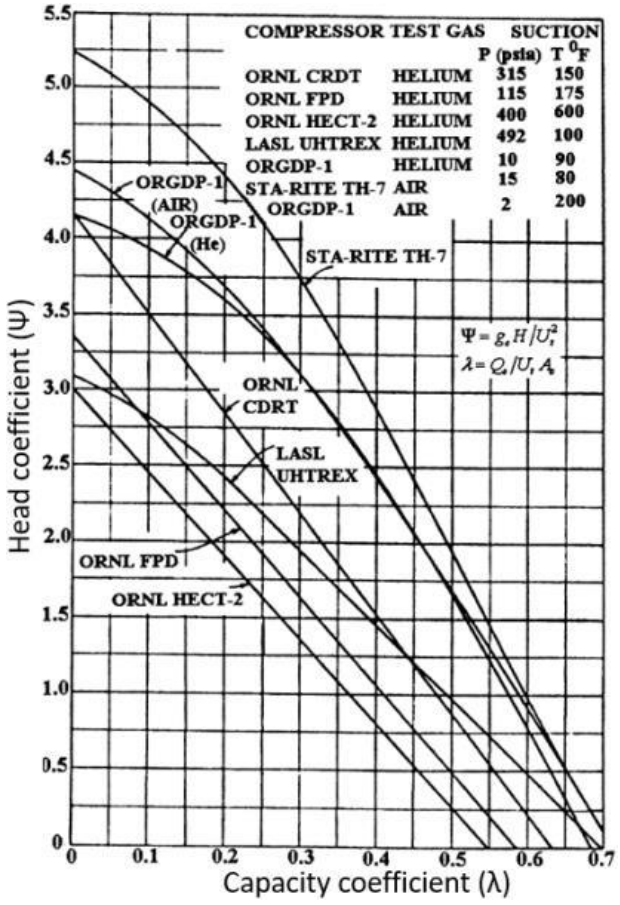

Fig. 10. Comparison of several regenerative compressors [47].

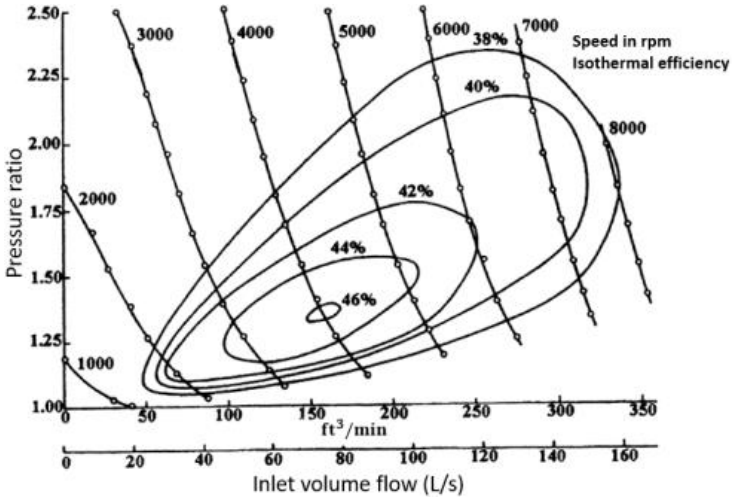

Fig. 11. Performance of MK1 compressor [23].

The efficiency was maintained under a variety of operating circumstances, and the characteristics were similar to those of a positive displacement compressor. The compressor could be run from maximum flow to zero flow without surging or stalling since the torque and back pressure were virtually directly proportional. Additionally, the authors tested a second MK2 regenerative compressor with a similar basic design but two rows of blades. ***Fig. 12*** displays the MK2 RFC performance curves The main improvements over the first compressor's performance were an increased peak efficiency of 52%, a lower pressure ratio at which this efficiency occurred, a gentler slope to the pressure-volume curves, a lower efficiency at high pressure ratios, and a large volume flow at low pressure, or roughly 2.5 times more than before. Making the blading symmetric allowed the scientists to evaluate the MK2 regenerative compressor, and ***Fig. 13*** illustrates the enhanced performance characteristics.

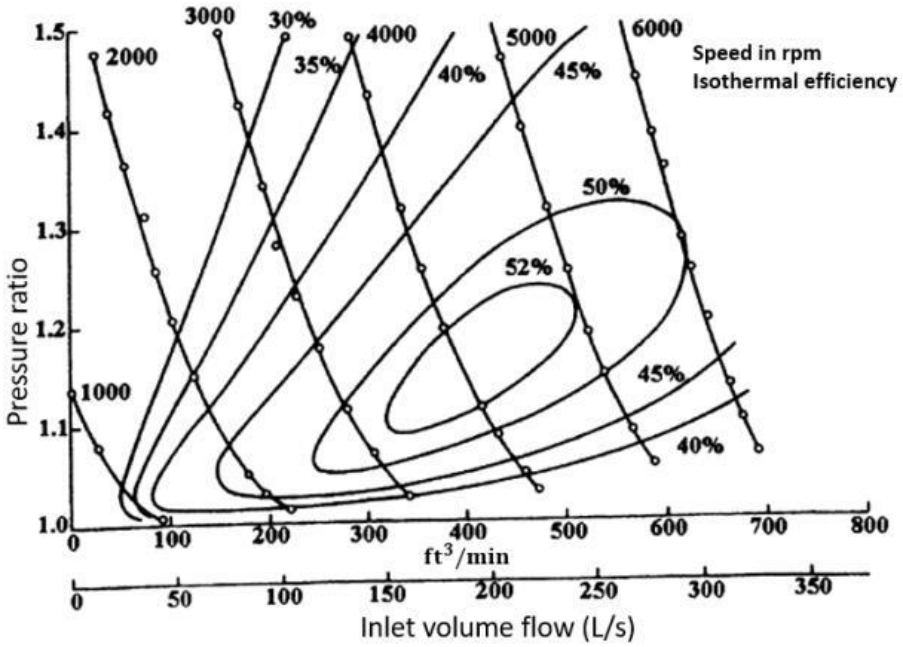

Fig. 12. Performance of MK2 compressor with not symetrical blading [23].

When compared to ***Fig. 12***, the gain in efficiency was particularly marked at high pressure ratios. For example, at 4000 rpm, the efficiency increased by 10 percent at a pressure ratio of 1.5. Four stages and a total pressure ratio of 10.521 were produced by the experimental helium regenerative compressor built by Sixsmith and Watson [50]. The stripper seal and rotor had a 0.5 mm clearance during the tests. A pressure ratio of 1.3 for single Stage was achieved with volumetric flow rate of 0.14 $\frac{m^3}{s}$ yielding a maximum isothermal efficiency of 31%. Further testing carried out on reduced clearance of 0.25 mm yielded a pressure ratio of 1.3 at volumetric flow rate of 0.31 $\frac{m^3}{s}$ with a maximum isothermal efficiency of 42%.

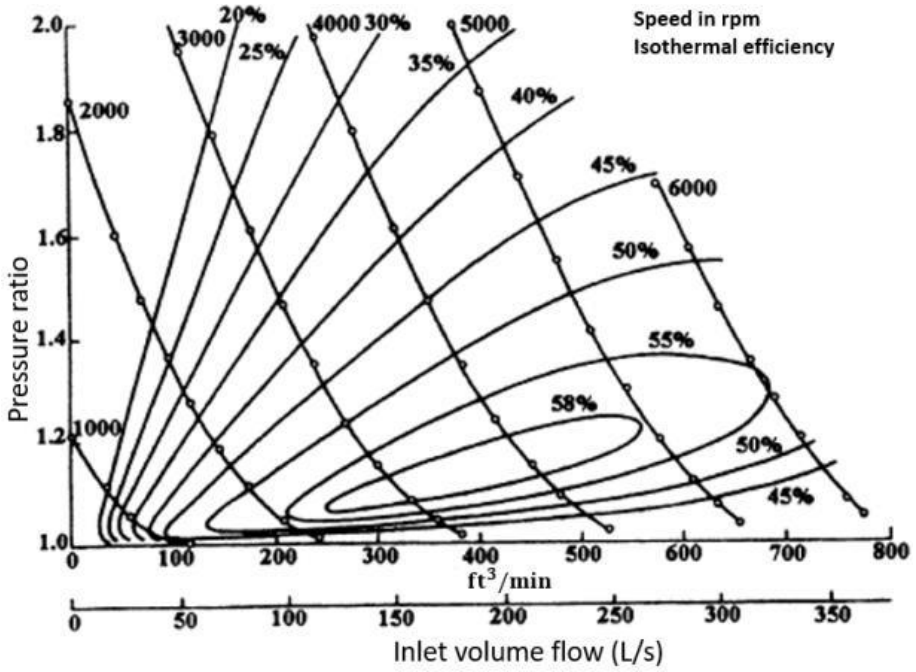

Fig. 13. Performance of MK2 compressor with Symmetric blading [23].

A regenerative compressor with aerodynamically curved blades was created by Swift et al. [51] primarily for cryogenic helium systems. Test results showed that at a flow rate of 12 g/s, a pressure ratio of 1.5 was achieved with estimated isothermal efficiencies of 30%. In order to support the design of the prototype machine, the authors created a compressor performance prediction model. The model included significant performance and loss mechanisms that connected machine geometry to pressure rise, flow rate, and speed. Blade angles, inlet and exit port sizes, internal clearances, and other basic geometric parameters were ranked according to importance in the model used to predict performance. In the model, significant loss mechanisms were included. A UHTREX gas bearing regenerative blower created by Mechanical Technology Incorporated for Los Alamos Scientific Laboratory's performance curve was described by Crowe [52]. Because the research of unclad fuel elements resulted in highly radioactive system contamination, this blower design was chosen for use in the Ultra High Temperature Reactor Experiment (UHTREX). ***Fig. 14*** shows the pressure rise versus flow rate curve and ***Fig. 15*** gives overall efficiency versus flow coefficient curve for the regenerative blower.

Although this blower could generate a pressure rise of 200 kPa at the intended flow rate and temperature, its total efficiency was only around 10% under those circumstances. Gessner [17] used a four-stage regenerative compressor to compress helium gas in the creation of a very durable, long-lasting cryogenic refrigerator for space vehicle utilization. Due to its capacity to generate high pressure ratio at a low flow rate with a compact overall machine size, RFC has an advantage. Oil-free operation and immunity from stall or surge instability are further benefits. These features are beneficial for compressors designed to be used in compact, closed-cycle helium refrigerators.

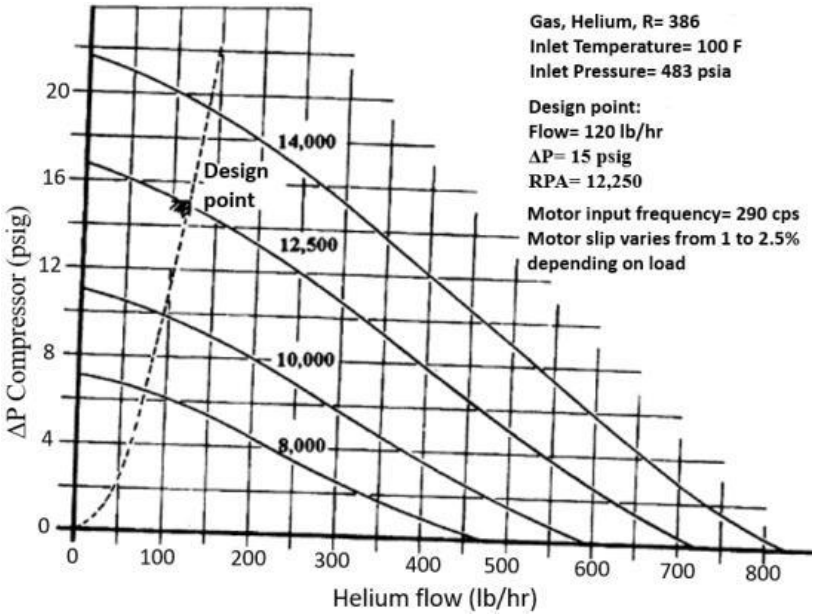

Fig. 14. Pressure rise VS. flow curve for UHTREX gas cleanup system regenerative compressor [52].

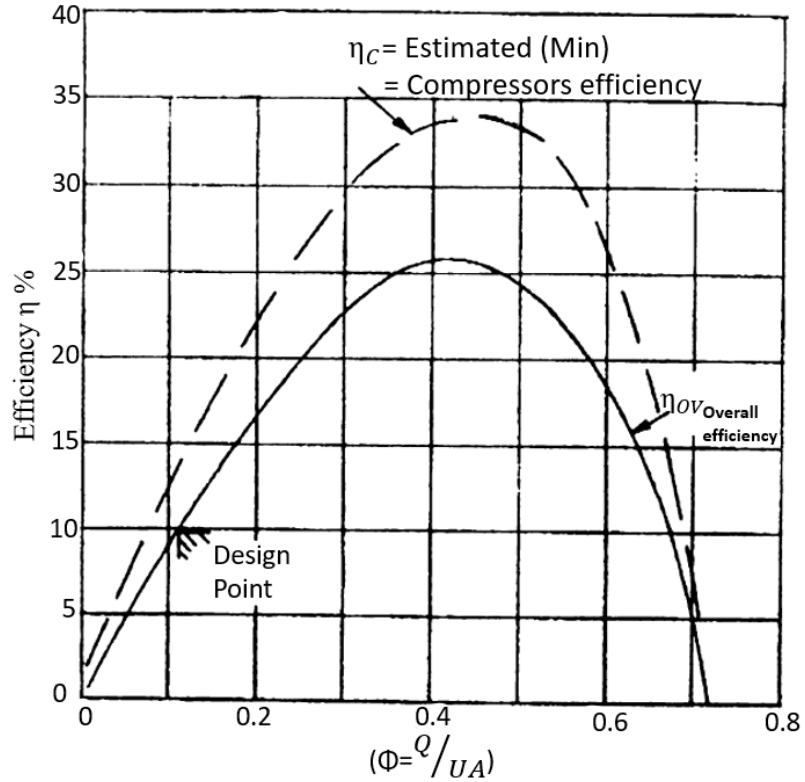

Fig. 15. Overall efficiency curve for UHTREX gas cleanup system regenerative compressor [52].

1.7 Theoretical Models

After the Second World War, some researchers made an effort to create logical explanations for the kind of flow that evolved inside a regenerative turbomachine. The flow in regenerative turbomachinery has been attempted to be described using a variety of theoretical models. As an illustration, the top scholars Crewdson

[53] and Iverson [13] proposed that the crucial flow mechanism was drag caused by the impeller on the stationary fluid in the Side channel. Iverson proposed a viscous performance model. He evaluated the regenerative pump's efficiency in terms of the fluid shear stresses the impeller imparted. The performance equations were derived by considering a linear system with a linear motion of rough surface as shown in **Fig. *16***.A force balance on the fluid in the horizontal flow channel was applied to derive performance equations. Two shear coefficients and an average impeller velocity were calculated experimentally and included in the derived formulas. The pump's output head, power, and efficiency were as follows:

$$gH = \frac{C_i a_i U^2}{2A}\left[\left(1-\frac{Q}{UA}\right)^2 - \frac{C_c a_c}{C_i a_i}\left(\frac{Q}{UA}\right)^2\right] \quad (5)$$

$$P = \frac{C_i a_i \rho U^3}{2}\left(1-\frac{Q}{UA}\right)^2 \quad (6)$$

$$\eta = \frac{\rho Q g H}{P} = \frac{Q}{UA}\left[1-\frac{C_c a_c}{C_i a_i}\left(\frac{\frac{Q}{UA}}{1-\frac{Q}{UA}}\right)^2\right] \quad (7)$$

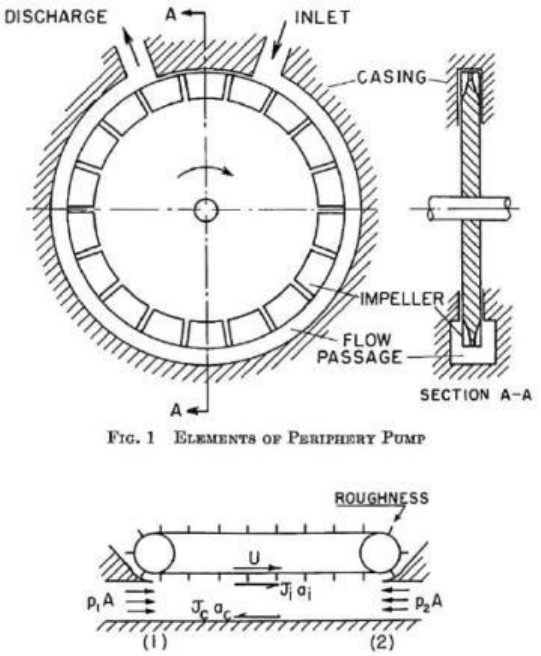

FIG. 1 ELEMENTS OF PERIPHERY PUMP

Fig. 16. Simplified Periphery pump for force analysis [13].

The shapes of the head, power, and efficiency curves as a function of flow were predicted as Shown in ***Fig. 17***. It was demonstrated that the flow area and impeller roughness were related to the shear coefficients and pump performance. This resulted in a concave form and an increase in pressure with a decrease in flow velocity. As a result, losses are likely to blame for the estimated maximum flow rate being about 23% greater than what was actually discovered. The test curves reported in Iverson [13] were found to be in fair agreement with the projected performance curve forms. This hypothesis led to some explanations of the

observed performance, but it was only partially successful in elucidating all of its components. Due to the uncertain magnitudes of the Shear coefficients and effective vane velocity, Iverson's method cannot be used to forecast the performance of any particular pump shape, but it does offer a straightforward illustration of how regenerative pumps operate.

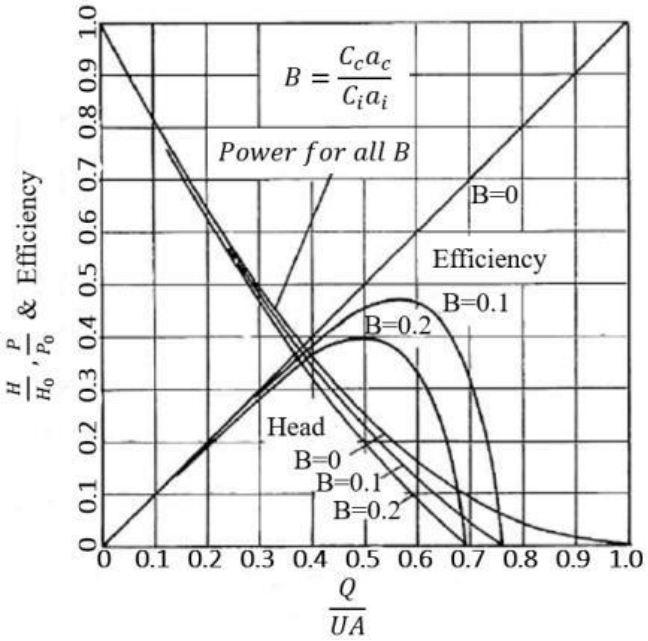

Fig. 17. Performance characteristics of regenerative compressor [13].

Balje [54] used a condensed method similar to Iverson to study the regenerative turbomachines. Based on the experiment, he came to the conclusion that a regenerative turbine has an optimal efficiency of 35%, compared to regenerative pumps' lower efficiency. Balje's theory made it possible to forecast regenerative turbomachine performance fairly for compressible and incompressible media while taking design geometries' effects on performance range and peak efficiency into account. Wright disapproved with the views put out by Iverson and Balje, claiming that they ignored the blade shape, which is crucial [13]. In his analysis of Iverson's work, Wright put up a competing idea that relies on a momentum transfer between the fluid in the channel and the blade row. Wright's significant discovery was that if the blades were given an appropriate backward curvature, it could be possible to increase the pump rpm without raising the shutdown pressure rise. Thus, he discovered that the same pressure rise could be achieved by speeding up the device and curving the blades backwards, proving the inadequateness of a solely viscous Iverson and Balje model. By taking into account a helical flow, Wilson, Santalo, and Oelrich [7] proposed a hypothesis of regenerative pump operation. They calculated various loss allowances and provided experimental confirmation of their findings. According to Wilson's theory, fluid picks up angular momentum in the impeller and transfers it to the fluid in the casing channel, which is traveling more slowly. Re-entering the impeller, the fluid has less angular momentum. The torque applied to the fluid by the impeller determines the rate of change of angular momentum. Based on a study of the hypothesis, just three empirical constants

were needed to express pump performance over the whole working range. Wilson [7]'s fundamental model sought to depict the phenomenon in a linear zone, as seen in Figure 2.10. He used fluid dynamic equations to arbitrary control volumes of the pump while making a number of assumptions.

The entire pump flow was characterized by the tangential velocities V_t, and circulatory velocity V_c, along a mean streamline. The overall head rise, net power input and efficiency of the pump were given as:

$$gH = \frac{\Delta p}{\rho} = \frac{Q_c}{Q_s}\left(\sigma U_2^2 - \alpha U_1^2\right) - K_t\left(\frac{Q}{\left(2r_2\right)^2}\right)^2 \tag{8}$$

$$P = \rho Q_s\left[gH + K_t\left(\frac{Q}{(2r_2)^2}\right)^2\right] \tag{9}$$

$$\eta = \frac{\rho QgH}{P} = \frac{\frac{Q}{Q_s}}{1 + \frac{K_t Q^2}{gH\left(2r_2\right)^4}} \tag{10}$$

Wilson examined and documented the STA-RITE TH 7 regenerative pump's dimensionless performance characteristics [7]. With air as the working fluid, the experimental flow versus head graphs were obtained at seven different speeds. Excellent agreement was found when comparing the calculated and experimental performance curves. Qualitatively, Wilson's relations accounted for the majority of the observed flow phenomena, but they could only be used to forecast the head-flow characteristics in the pump's linear domain. His model, which made the incompressible flow assumption, was unable to forecast the performance of compressors that produced high pressure ratios. Wilson's model also failed to account for the relationship between losses and geometrical and aerodynamical characteristics. The design's most noteworthy feature was how it could characterize the performance of the regenerative pump across the course of its working range using just three performance metrics. Burton [55] used a test device with Perspex walls to record the fluid flow process that Wilson's idea was founded on. Small electrically charged beads were dropped into the stream, and their motion was photographed. Burton offered an experimental and theoretical investigation of regenerative turbines and pumps. His research produced formulas for the performance of turbomachines over their whole operating range using empirical constants. The theoretical equations' coefficients were chosen to provide the greatest possible overall fit to the outcomes of their experiments. The features discovered by Wilson [7] were comparable to those discovered by Whitehead [56], despite the fact that both writers utilized geometrically very different devices. Therefore, it was impossible to directly compare their efforts. Whitehead conducted an experimental investigation into the Reavell RC5O regenerative compressor's performance. He discovered that at a particular speed of 0.05, aerodynamic efficiency reached a maximum of 44%. At maximum speed, the efficiency dropped to 30%

due to severe mechanical losses. In his work, a theoretical model of internal fluid dynamics was developed, presuming that the blades were not stuck, and that circulation was zero at the machine's inlet. Since the blades were stalled the majority of the time, the model's assumptions were flawed. The predictions and the outcomes of the experiment did not agree well. Whitehead also discovered that although Reynolds number impacts were determined to be minimal, Mach number effects had a minimal impact on performance. Simplified theoretical models for regenerative pumps with various blade configurations have been described by numerous authors. Both radial and semicircular blades have a theoretical model that was created by Grabow [26]. Grabow's model was expanded by Abdallah [25] in order to create a theoretical representation of the regenerative compressor with airfoil blades. The inlet effect, which was not considered in most theories, was included in this model. There was good agreement between the theoretical and experimental pump performance. Theoretical models were created by Wilson et al. [7], Burton [55], and Abdallah [25] to correlate the machine performance based on the recirculating flow pattern. But all of these approaches have two fundamental flaws that greatly restrict how they may be used as design tools. The first of these is that they include loss coefficients that were obtained empirically and are not based on geometrical or aerodynamic factors. Therefore, they cannot be used to evaluate designs that significantly deviate from those on which the models are based because they provide no indication of how the design might be improved to reduce the losses.

The second flaw is that they are inaccurate for compressible flow in RFC since they are primarily beneficial for incompressible pump flow. As a result, these models are unable to offer any design recommendations. A theoretical analysis of regenerative pumps was created by El Hag [7]. He derived flow equations for regenerative turbomachines, which showed that in order to apply the well-known Euler equation for the head across rotor dynamic machines to regenerative turbomachines, it needs to be supplemented with an additional component that accounts for the tangential pressure gradient. Thus, the tangential flow displacements in the rotor must be calculated in order to calculate head rise. He defined a portion of the pump's circumference for his investigation, and it was predicated that the tangential pressure gradient was nearly constant. This part described the flow in a way that, when the laws of fluid mechanics were applied to it, the resulting flow equations could be solved numerically using a computer. The flow in the linear part of these devices could be precisely calculated because to the flow equations he developed in his research. He calculated the fluid head difference between any two positions 1 and 2 at the same impeller streamline by:

$$\Delta\left(gH\right)=\left(U_2V_{\theta 2}-U_1V_{\theta 1}\right)+\frac{1}{\rho}\frac{\partial p}{\partial\theta}\Delta\theta-gH_L \qquad (11)$$

The first term on the RHS of equation 7 is the familiar Euler's head. The second term is the energy added to the fluid because of its angular displacement $(\theta_2 - \theta_1)$ in a field in which there is a tangential energy gradient $\partial H / \partial \theta$. E1 Hag [22] showed the variation of fluid energy along a flow cycle on energy gH - angular displacement (θ) plane as shown in **Fig. *18***.He considered flow along a streamline, which starts just inside the impeller, passes through the impeller exit, goes through the channel, and reaches just inside of the impeller for next circulation. The losses experienced by this streamline were compared with the ideal flow cycle as shown in **Fig. *18***. In **Fig. *18***, the actual flow cycle is indicated by 123.3 and the ideal cycle is represented by path 145. The increase in the fluid specific energy is given by:

$$\Delta(gH)_a = (gH_3 - gH_3) \qquad (12)$$

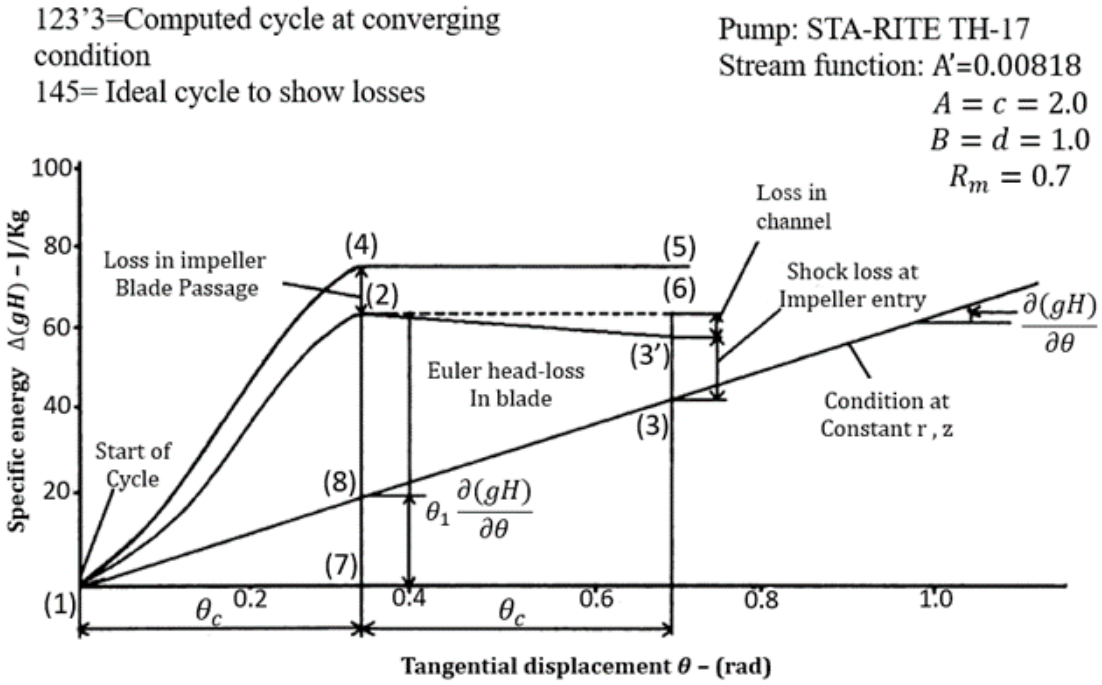

Fig. 18. Typical flow cycle along a streamline [7].

El Hag's analysis lacked the empirically ascertained empirical variables that Wilson [49] required from tests on the pumps in order to be determined. However, where suitable in the research, well-established loss empirical characteristics such as the friction loss factors of flows in conduits were employed to estimate losses. If the shape and size of the impeller, the dimensions of the channel, the number of blades, the stripper angle, and the clearances are known, the proposed method can predict the performance of a given pump. However, El-Hag's approach is likewise restricted to regenerative pumps. Regenerative pumps and blowers were the subject of an experimental and theoretical research by Hollenberg [48], who then revealed the factors affecting their effectiveness. He showed a relationship between torque, pressure, and flow rate that

was only reliant on one experimental factor. The diversity in efficiency-Specific speed characteristics of regenerative turbomachines along the range of their likely configurations was examined using this correlation. It was demonstrated that the greatest efficiency depends on the friction head coefficient ratio and the radius ratio parameter. Theoretical methods to the design of regenerative pumps were covered by Kupryashin [57]. Due to the analytically indeterminate coefficients present in the performance curve equations, both methodologies used by Wilson and Iverson were reviewed and found to be inappropriate for application in practical calculations. Due to its encouragement of the secondary circulation, he advocated the circular radial segment as being the most advantageous. Pump efficiency near 50% were demonstrated by experimental data. Jakubowski et al.'s approach [58] was more theoretical. In a toroidal container, they examined the rotating flow of an incompressible, non-viscous fluid. The model could only be used to a limited extent due to the laborious nature of the underlying mathematics and the simplifications required to arrive at a solution. Schively [59] used a one-dimensional flow model to theoretically solve the flow inside a regenerative pump. All major variables in his model were given as functions of just the radius. He separated the vortex chamber's flow into three sections and examined each region's flow separately using Navier Stoke's equations and momentum balance. Bullough [60] also conducted theoretical and practical research into the operation of a straightforward regenerative pump, but the model was unable to forecast the operation of any particular pump design. The disparities between the viscous and momentum exchange theories, according to Senoo [10], can be explained by differences in the assumptions they make. His work covered theories that were created for incompressible flow. At that point, it became clear from the experimental data that none of these hypotheses could account for all the effects that geometry had on performance. Even if we are now interested in extending the theories and designs into compressible flow range, this is still the case. There aren't many theories about how compressible fluid flows in regenerative turbomachines in the literature. Burton [61] made an attempt in this regard and published a Simplified theory that considered the effects of compressibility and area change in regenerative turbomachines. He made the assumption that shear stress between the impeller and the fluid in the casing is how energy is exchanged. Any radial flow components were disregarded. A linear control volume was subjected to the continuity, momentum, and energy equations, and differential equations were produced. In Burton [61], the following differential equations were derived:

Continuity:

$$\frac{d\rho}{\rho} = -\frac{d\left(AV_m\right)}{AV_m + A_R U_p} \tag{13}$$

Momentum:

$$\frac{dp}{\rho}=\frac{R_p\left(2r_2-2r_0+2b+t\right)}{2Ag}f_R\left[\left(U_p-V_m\right)^2-\lambda V_m^2\right]d\theta+\frac{A_R U_p V_m}{Ag}\frac{d\rho}{\rho}-\frac{V_m}{g}dV_m \tag{14}$$

Where,

$$\lambda=\frac{f_c}{f_R}\frac{2b_1+2b2-t}{2h+t} \tag{15}$$

Energy:

$$\frac{dp}{\rho}=C_p\left(1+\frac{AV_m}{A_R U_p}\right)dT+\frac{AV_m}{A_R U_p}\frac{V_m}{g}dV_m+\frac{1}{2g}\left(U_p^2-V_m^2\right)\frac{d\rho}{\rho}-\frac{R_p\left(2r_2-2r_1+2b+t\right)}{2gA_R}f_R(U_p-V_m)^2d\theta \tag{16}$$

The equation of state can also be used for gases showing behavior close to perfect gas.

$$p=\rho RT \tag{17}$$

If the speed, gas, and compressor shape are known, the equations published by Burton are a set of formulae for figuring out how well a compressor will work. The shear stress theory, which was empirically shown to be unable to explain the fluid motion inside regenerative turbomachines, was also the foundation of Burton's model.

It is not surprising that most designs of regenerative turbomachines remained a fairly simple geometrical layout with simple vanes either machined or cast into the impeller given the lack of design knowledge in regenerative turbomachinery. However, Sixsmith and Altmann [23] demonstrated that the performance may be significantly enhanced by including an airfoil blade and a core in the flow channel to guide the circulating flow. They replaced the radial vanes by blades with an airfoil section as shown in **Fig. *19***. The blades were made to convey fluid motion with the least amount of turbulence and friction possible. They were made to turn the fluid via a specific angle, ideally one of approximately 90 degrees. The annular channel featured a core to help direct the fluid in a way that minimizes fluid loss as it circulates through the blading. Additionally, the core served as a shroud to lessen losses brought on by the development of vortices at the blade tips. According to one blade passage, the enthalpy transfer caused by the action of the blades on the impeller was:

$$\Delta H_0 = \omega\left(r_2 w_2 \sin\beta_2 + r_0 w_1 \sin\beta_1\right) \tag{18}$$

The mass flow rate through the blading was estimated by:

$$\dot{M}_B = 2\pi\left(1-F_s\right) r_0 L_1 \rho_1 W_1 \cos\beta_1 \tag{19}$$

The forward mass flow rate through the flow channel was estimated by:

$$\dot{M}_A = \frac{\rho_M A_c}{2}(U_1 + U_2 + W_2 \sin\beta_2 - W_1 \sin\beta_1) \tag{20}$$

The number of times fluid passes through the blades N was Obtained by dividing the mass flow rate through the blading by the mass flow rate through the annular channel, i.e.

$$N = \frac{4\pi\left(1-F_s\right) r_0 L_1 \rho_1 W_1 \cos\beta}{\rho_M A_c (U_1 + U_2 + W_2 \sin\beta_2 - W_1 \sin\beta_1)} \tag{21}$$

The pressure ratio was related to the enthalpy of a Stream of gas being compressed from H1, to H2 in the form of the following equation:

$$\dot{M}\left(H_2 - H_1\right) = \frac{\dot{M} C_p T_1}{\eta}\left\{\left(\frac{p_2}{p_1}\right)^{\left(\frac{\gamma-1}{\gamma}\right)} - 1\right\} \tag{22}$$

Relationship between the inlet velocity with respect to the blades, the pressure gradient in the annular channel and the geometry of the annular channel was given as:

$$\frac{1}{2}\rho W_1^2 = \frac{\left(P_2 - P_1\right) S}{L\left(1 + \frac{\rho_1 L_1}{\rho_2 L_2}\right)\left(\frac{\rho_1 L_1 \sin\beta_2 \cos^2\beta_1}{\rho_2 L_2 \cos\beta_2} + \sin\beta_1 \cos\beta_1\right)} \tag{23}$$

S is the circulation distance of a blade's trailing and leading edges measured perpendicular to the blade's motion. The authors' intriguing conclusion was that the pressure gradient depends on the fluid's velocity in relation to the blades rather than the blades' own velocity. In contrast, and more accurately, the velocity with respect to the blades is what is affected by the pressure gradient. This is one key distinction between a centrifugal and regenerative compressor. The pressure increase in a centrifugal compressor is proportional

to the square of the impeller's peripheral velocity. Regenerative compressors frequently operate in a manner similar to positive-displacement equipment like a roots blower.

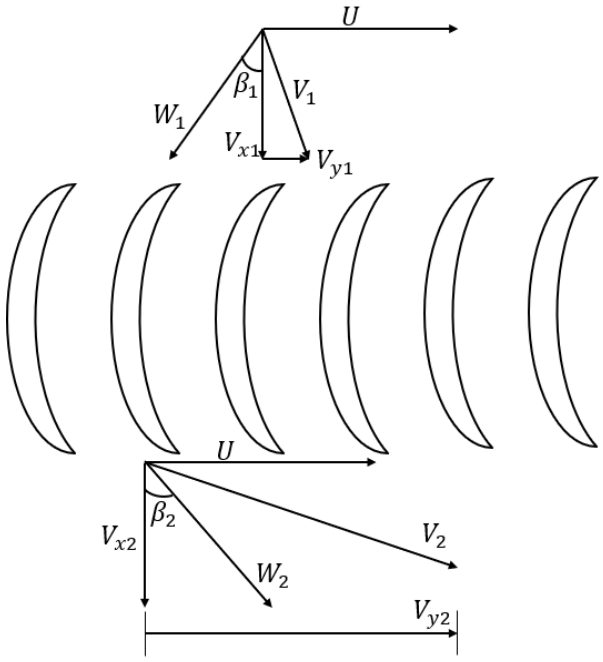

Fig. 19. Velocity diagram for compressor blades [23].

The pressure difference across the ports and the torque are almost directly related. To verify the theoretical findings, Sixsmith and Altmann [23] built two regenerative compressors with aerodynamic blading. When compared to Wilson [7]'s test on a regenerative compressor that used radial blades, the efficiency was significantly higher. To demonstrate the benefits of airfoil blade RFC design over solely radial blade RFC design, these authors published a performance comparison, as shown in **Table 1**.

These non-dimensional factors, which include the particular speed, pressure ratio, and specific mass flow rate as specified below, are crucial in the analysis of RFC.

Specific speed $$N_s = \frac{\sqrt{Q\omega}}{H^{3/4}} \quad (24)$$

pressure ratio $$\Pi = P_{out} / P_{in} \quad (25)$$

specific mass flow rate $$\Phi = \frac{\dot{m}}{4r_2^2 P_{in}} \sqrt{\frac{RT_{in}}{\gamma}} \quad (26)$$

Table 1. Performance Comparison at 4000 rpm and pressure ratio of 1.17.

Performance	Formula	Wilson	Sixsmith & Altman	Ratio
Efficiency	$\frac{\dot{m}RT \ln \frac{P_2}{P_1}}{Shaft\ Power}$	45%	58%	1.29
Specific Speed	$\frac{nQ^{1/2}}{(gH)^{3/4}}$	0.244	0.220	0.90
Head Coefficient	$\frac{gH}{U^2}$	1.5	4.2	2.8
Flow Coefficient	$\frac{Q}{D^2U}$	0.014	0.044	3.14

1.8 Loss categorization

It is thought that more than 40% of the input power in a regenerative turbomachine is consumed in overcoming losses. The regenerative pump Operation is affected by different types of losses including:

- Losses due to slip
- Hydraulic losses in the circulation process between impeller and free channel
- Shock losses at the Rotor inlet
- Peripheral friction loss in the flow channel
- Inlet and outlet losses
- Leakage between the impeller face and the pump casing
- Leakage between through the stripper

To have a better understanding of how these losses affect the performance of the machine, each of these losses will be explained in brevity alongside with their correlations which are acquired by other scholars to calculate these losses, at the end of this section.

The biggest cause of efficiency loss, according to Sixsmith and Altmann [23], is slip. In the presence of losses from turbulence, fluid friction, and blade drag, the slip loss is the flow rate required to maintain circulation through the annular channel down the pressure gradient. By far the biggest loss is the slip loss, thus efforts to increase efficiency should focus on minimizing it. These authors noted that, in addition to slippage, there are other kinds of leakage losses and carryover losses of pressurized gas between the blades as they go through the stripper. Leakage through the clearances from the high-pressure zone to the low-pressure section of the annular channel decreased the flow rate the compressor delivered. Estimates of these leakage losses were made using a 4500 rpm compressor and a 2.0 as pressure ratio. According to reports, a 0.25 mm gap between the rotor's faces and the case allows for a 4% leakage rate. A leakage rate of roughly 3% was permitted with a gap of 0.305 mm between the impeller's profiled edge and the stripper. In the stripper, there was a 3% leakage rate past the edges and tips of the blades. In the stripper, there was a 3% leakage rate past the edges and tips of the blades. The stripper was found to transport a small but

considerable portion of the compressed gas from the high-pressure area, which expanded down to the intake pressure as the blade pockets between the blades opened into the annular channel at the inlet end. This represents an efficiency loss and is typically referred to as carryover loss. The stripper seal is completely passive when a regenerative compressor uses an incompressible fluid, with the exception of a little amount of leakage. However, the tiny seal will play a significant role in machine performance in compressible flow circumstances. Large amounts of compressible fluid near the exit port are sucked through the seal and combined with the fluid entering the machine in a very irreversible manner. As the Mach number rises, this mixing process limits the pressure ratio. The machine's total efficiency is significantly decreased by the seal. In order to cut down on slip losses, Sixsmith and Altmann replaced the standard straight radial vanes on the rotor with aerodynamic blading and altered the annular channel. To encourage vortex circulation and the least amount of turbulence, they suggested an annular channel with a circular cross section. To achieve a smooth entry to the blades, they recommended that the blade angles be created to match fluid angles. The angles are influenced by how quickly the velocity's circulation component varies in relation to a streamline's radius. The actual vortex should fall between a free vortex and a vortex with constant linear velocity when the effects of fluid friction are taken into account. Due to the tangent of the inlet and outlet angles being proportional to the square of radius, this resulted in blading, in which the deflection rises with radius. The use of this style of blading increased regenerative turbomachinery performance and broadened its applicability.

In order to cut down on slip losses, Sixsmith and Altmann replaced the standard straight radial vanes on the rotor with aerodynamic blading and altered the annular channel. To encourage vortex circulation and the least amount of turbulence, they suggested an annular channel with a circular cross section. To achieve a smooth entry to the blades, they recommended that the blade angles be created to match fluid angles. The angles are influenced by how quickly the velocity's circulation component varies in relation to a streamline's radius. The actual vortex should fall between a free vortex and a vortex with constant linear velocity when the effects of fluid friction are taken into account. Due to the tangent of the inlet and outlet angles being proportional to the square of radius, this resulted in blading, in which the deflection rises with radius. The use of this style of blading increased regenerative turbomachinery performance and broadened its applicability.

By removing some of the compressed gas going through the stripper and refeeding it back into the annular channel at an intermediate pressure, Burton [16] suggested that the carryover loss may be decreased. Thus, the stripper carryover gas would be made to expand some of its energy inducing the incoming supply rather of being ineffectively deposited near the suction.

This idea is further explored in this dissertation by employing decompression ducts to feed high pressure flow entrapped in the stripper blades to various locations in the flow channel.

1.8.1 Losses due to slip

In regenerative turbomachines, the tangential pressure gradient significantly raises the slip factor. Any time there is a pressure difference between any two adjacent blades of an impeller, there is a tendency for a secondary circulation to occur around each blade, which leads the fluid to exit the impeller to divert from its intended course and go counterclockwise to the positive direction of rotation. As a result, the fluid's exit tangential velocity is lower than what the velocity triangle predicts based on the outlet blade angle. A slip factor is typically provided to account for the decrease in the ideal tangential velocity; it is defined as the ratio between the actual tangential velocity and the one derived under the assumption that. Blade angle and flow angle are the same. Due to its direct impact on energy transfer, the slip factor is one of the essential pieces of design information. Several techniques have been created by various researchers to evaluate the impact of slide. The contributions from Stodola, Busemann, Fergusons, and Stantiz are noteworthy. These writers, along with others, did, however, offer techniques for situations in which there is essentially no tangential energy gradient. Therefore, the formulations proposed by these writers do not apply to regenerative turbomachines, where the creation of tangential pressure gradient is the only goal. Both the flow angle and the blade angle are the same. Because it directly affects how energy is transferred, the slip factor is one of the most important pieces of design information. Various researchers have devised a variety of techniques for determining the impact of slide. The contributions of Stodola, Busemann, Fergusons, and Stantiz deserve special attention. However, in situations when there is essentially no tangential energy gradient, these writers and others have produced solutions. As a result, the formulations proposed by these authors do not apply to regenerative turbomachines whose only goal is to create tangential pressure gradient.

$$\sigma = f\left(r_2, \omega, \beta_2, Z, W_2, \frac{\partial H}{\partial \theta}\right) \tag{27}$$

El-Hag extended the expression proposed by Stodola and proposed a slip factor correlation given below for computing a first order estimate of the slip factor in regenerative turbomachines.

$$\sigma = 1 - \frac{U_2 \pi \sin \beta_2}{V_{\theta 2} Z}\left[1 + 2\left(\frac{\omega r_2}{W_2}\right)\frac{\psi}{\theta_p}\right] \tag{28}$$

1.8.2 Hydraulic losses in the circulation process

Circulatory head losses have two contributions.

- Head loss of circulatory velocity through the impeller region is referred as gH_{cb}
- Head loss of circulatory velocity through the channel region is referred as gH_{cc}.

The sum of these two head losses is the total circulatory head loss given as:

$$gH_c = gH_{cb} + gH_{cc} \quad (29)$$

Circulatory head losses arise from many sources. Following sources of circulatory head loss is quantified:

1.8.2.1 Channel turning losses (K_t)

The fluid turning 180 degrees through the channel is what causes these losses. The flow pattern resembles that of a 180° turn without guide vanes. The following equation can be used to simulate channel turning losses.

$$\Delta P = \frac{1}{2}\rho K_t V_c^2 \quad (30)$$

where K_t is channel turning loss coefficient and V_c is the circulatory velocity.

1.8.2.2 Channel and Blade Mixing Losses

Fluid enters the channel after making a 90° turn through the blade. Channel mixing loss occurs as a result of the mixing of the flowing fluid with the incoming stream of flow. Additionally, this mixing causes a loss known as blade mixing loss to occur in the blade channel.

The mixing losses experienced in the side branch (flow leaving the blade and heading into the channel) are quantified by two non-dimensional geometric and aerodynamic characteristics, which are:

$$C_1 = \frac{Q_c}{Q}, \quad C_2 = \frac{A_c}{A_{circulation}} \quad (31)$$

Where,

Q_c is the circulatory flow through one blade passage.

Q is the flow through the channel.

$A_{circulation}$ is the area through which flow circulates from blade towards channel.

A_c is the channel through flow area.

The mixing losses which occur at the exit of blade region when flow takes 90° turn and mixes with the incoming stream of through flow can be simulated by introducing a loss coefficient K_s given by:

$$K_s = \frac{\left(1+\left(C_1C_2\right)^2 - 2\left(1-C_1\right)^2 - 1.41C_2C_1^2\right)}{\left(C_1C_2\right)^2} \quad (32)$$

Blade mixing losses can be determined from:

$$\Delta P_s = \frac{1}{2}\rho K_s V_c^2 \qquad (33)$$

Mixing losses in the peripheral branch (through flow in the channel) result in pressure drop in the peripheral direction and they can be simulated by introducing a loss coefficient K_{ch} given by:

$$K_{ch} = \frac{1-\left(1-C_1\right)^2 - 1.41C_2C_1^2}{\left(1-C_1\right)^2} \qquad (34)$$

Channel mixing losses are determined from:

$$\Delta P_{ch} = \frac{1}{2}\rho K_{ch} V_{\theta m}^2 \qquad (35)$$

Thus, the mixing losses are correlated to aerodynamic parameter C_1 and geometric parameter C_2 .

1.8.2.3 Sudden expansion (K_{se})

This loss is caused by the increase in flow area when fluid flows from blades to channel. Sudden expansion loss coefficient is related to blade blockage factor given as:

$$K_{se} = \left(\frac{BF}{1-BF}\right)^2 \qquad (36)$$

Sudden expansion loss can be quantified by:

$$\Delta P_{se} = \frac{1}{2}\rho K_{se} V_c^2 \qquad (37)$$

Consequently, model for the circulatory head loss can be arranged as follows:

$$gH_c = \frac{1}{2}K_t V_c^2 + \frac{1}{2}K_s V_c^2 + \frac{1}{2}K_{ch} V_{\theta m}^2 + \frac{1}{2}K_{se} V_c^2 \qquad (38)$$

1.8.3 Shock loss

When fluid enters the blades, the discrepancy between the flow angle and the blade angle results in shock or incidence losses. A shock loss parameter was developed by Wilson [7] to measure such losses. With various geometric and aerodynamic characteristics, he associated shock loss. Nevertheless, Wilson's concept was based on the geometry of a rectangular channel. **Fig. 20**depicts the channel dimensions and form that Wilson employed for his shock loss model. Wilson connected the throughflow rate to a given shape and a shock loss parameter. Wilson [7] made the following relational suggestion.

$$Q = \frac{1}{2}\left(\frac{r_2}{r_G}\right) Q_s \left(K_1\sigma + \frac{r_1^2}{r_2^2} K_2\alpha \right) \tag{39}$$

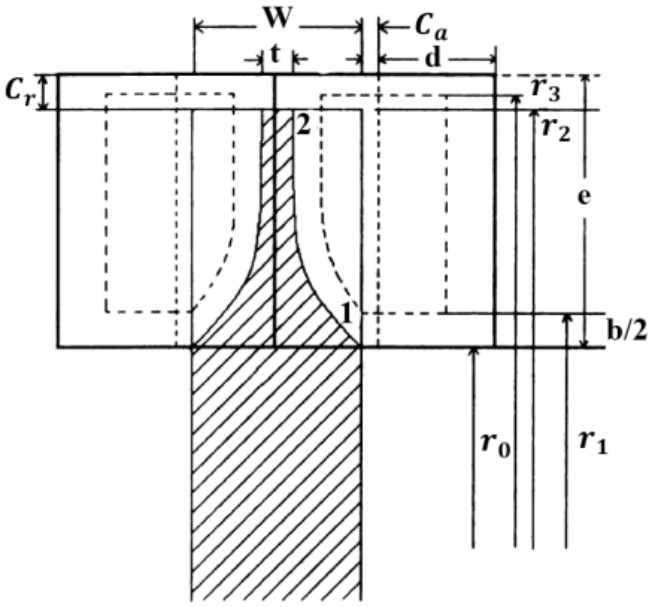

Fig. 20.channel shape used to introduce shock loss model by [69].

where, $Q_s = r_G A_c \omega$ denotes the flow associated with solid body rotation and K_1, K_2 and K_3 are dimensionless coefficients depending only on the geometry of the open channel. These coefficients are given as:

$$K_3 = \frac{r_2}{r_G}\left[\frac{(A_3+A_4)^2}{A_c^2} - \frac{(A_1+A_2)}{A_c^2} + \frac{cA_1A_2}{r_3A_c^2} - \frac{1}{3r_1d}\left(A_3 + A_4 - bd\frac{r_3}{r_1} \right) \right]$$

$$K_1 = K_3 + 2\frac{(A_1+A_2)}{A_c} - \frac{cA_2}{r_3A_c} - \frac{cA_1}{2r_2A_c} \tag{40}$$

$$K_2 = -K_3 + \frac{2r_2(A_3+A_4)}{r_1A_c} - \frac{A_3^2r_2}{3A_cr_1^2d}\left(5 - 2\frac{r_3}{r_1}\right)$$

Where,

$$A_1 = \frac{bC_r}{2},\ \mathrm{A}_2 = \left(\frac{b+d}{2}\right)C_r,\ \mathrm{A}_3 = \left(r_3 - r_1\right)d,$$
$$A_4 = \frac{bd}{2},\ \mathrm{A}=\mathrm{A}_1 + A_2 + A_3 + A_4 \qquad (41)$$

1.8.3.1 Peripheral friction loss in the flow channel

Head losses caused by channel friction are referred as tangential head losses (Peripheral friction loss) and denoted by dgH_L. They involve the channel curvature effect and can be determined by applying the classic pipe-loss formula:

$$dgH_L = \frac{\lambda_f V_{\theta m}^2 dX_G}{2D_h} \qquad (42)$$

Where,

$$\lambda_f = \lambda_0\left(1 + 0.075\,\mathrm{Re}^{0.25}\left(\frac{D_h}{2r_2}\right)^{0.5}\right) \qquad (43)$$

λ_0 is defined for straight channel as:

$$\lambda_0 = 0.316\,\mathrm{Re}^{-0.25} \qquad (44)$$

where Re is given based on hydraulic diameter as:

$$\mathrm{Re} = \frac{D_h V_{\theta m}}{\nu} \qquad (45)$$

1.8.3.2 Losses in Ports

Losses in inlet and discharge ports can be estimated by:

Inlet Port:

$$\Delta P_{in} = \frac{1}{2}\rho K_{in} V_{in}^2 \qquad (46)$$

Outlet port:

$$\Delta P_{out} = \frac{1}{2}\rho K_{out} V_{out}^2 \tag{47}$$

The two loss coefficients K_{in} and K_{out} need to be correlated with the nozzle geometries and flow rates to study the effect of inlet and discharge ports on performance. These losses cause obstructions in the intake and outlet flow, which lowers the machines' overall capacity to generate pressure.

1.8.3.3 Leakage Losses

Total leakage flow rate can be estimated by the following equation suggested by El-Hag [8].

$$Q_{leakage} = \frac{\omega r_2}{2}\left(c_r b + \frac{c_a r_2}{2}\right) + 2C_D \omega r_2 \sqrt{\frac{2\frac{d\psi}{d\theta}}{Z_s}\left(c_r\left(b + c_a\right) + c_a\left(r_2 - r_0\right)\right)} \tag{48}$$

1.9 CFD Work

In the past few years, computational fluid dynamics (CFD) has been extensively employed for the flow study of various turbomachines. The computational approaches appear to be very appealing to be applied to RFC/RFP because they offer a chance to calculate the flow in order to predict the likely effects of design modifications and in the hope of gaining a clearer understanding of some of the losses given that the flow field in these machines is very complicated and CFD simulation seems to have a not only an answer for these complicated flows but only provides a cheap instrument to produce results in regard to. The flow is extremely complex due to intrinsic unsteadiness and significant three-dimensionality. For this reason, steady, one-dimensional models that are based on the circulatory flow assumption, such as [62], are still used to study the flow.

1.10 Objective of research

As it demonstrated above, in many applications, regenerative turbomachines are desirable because of their small size, great dependability, and low noise. Hence, an in-depth knowledge of regenerative compressors may tap into their great hidden potential for tasks demanding high head and low flow rates were they shine the most. Moreover, they are a formidable rival to centrifugal turbomachines in low specific speed applications due to their higher efficiency at low specific speeds. To enhance their functionality and increase their appeal to industry, RFC/RFP must undergo research and design improvements.

To that end, the goal of the current study is to increase the efficiency of regenerative turbomachines by studying the flow development inside the machine and improving existing designs. Moreover, the flow in this study is considered to be air which is improving novelty of the study since almost all the predecessor studies used water as a working fluid. The industry has expressed interest in replacing the traditional designs of regenerative turbomachines with improved designs as a result of the development of commercial software and enhanced manufacturing techniques over the past few years. There are no trustworthy theoretical models that use geometric parameters as input to predict the performance of regenerative turbomachines. To predict performance, the majority of the theoretical models now in use require considerable experimental evidence. As a result, changing the design to enhance performance is difficult. The majority of academics used experimental analysis to investigate how different geometric and aerodynamic characteristics affected performance. Experimentation always costs a lot of money and takes a lot of time. In order to forecast how current regenerative turbomachines will operate, current research's goal is to explore the consequences of geometrical modifications using experimental and CFD methods. Extensive sensitivity analysis is carried out once the performance is predicted to determine whether design changes can increase performance. This thesis develops certain design criteria that might be very helpful to designers and engineers that work with regenerative turbomachinery. Prototype models cannot be created until proposed design changes have been validated using CFD. Unsteady CFD analysis on regenerative turbomachines using commercially available CFD software is not well supported by the literature, and there are even less studies that used incompressible flow as the fluid in these machines. This study is being done in collaboration with FPZ S.P.A., Milan. Therefore, experimental data on FPZ's RFC is examined to learn more about the compressor's performance traits and validation data.

To that end since in this study the flow is intrinsically unsteady and the geometry is very complicated, the first step of the work will aim at determining a suitable computational setup in terms of mesh size and refinement, computational scheme for the unsteady flow, and choosing turbulence modelling. Comparisons with steady computations are also worthy, as the circulatory flow model is based on such an assumption. Then, the effect of relevant geometrical quantities and operation parameters will be investigated. This constitutes the core of the present work and will be performed on computations on a test matrix which includes:

geometrical parameters size of both rotor and side channel in the meridional plane.

2 Geometries (base E08)

This works stems from a collaboration with the PFZ S.P.A company which is established in Milan, Italy. This work started with analyzing a single geometry, namely E08, which some experimental data were at disposal. For this study a CFD simulation for five different working points and four rotational speeds (1000, 2000, 2990, 3500 rpm) were used. Moreover, 12 geometries which have small differences in blade width and depth are simulated with rotation speed of 2900 to understand which geometry parameter has the most effect on the efficiency of the machine. These geometries will be introduced after E08 geometry later on.

2.1 Basic Geometry (E08-3500 rpm)

In this section, the geometrical properties, and the general characteristic of the machine for the E08 geometry will be presented. **Fig. 21**. shows the studied side channel blower, which includes a rotor, casing, inlet, outlet, and stripper. The casing and rotor have internal diameters of 0.3096 m and outer diameter of 0.436 m, and 52 evenly spaced blades. The overall specification of the RFC is shown in **Table 2** for the E08 geometry. It must be mentioned that for our work we simulated the half of the machine due to the symmetry.

Table 2. side channel blower specification (E08)

Diameter	0.436	[m]
Radius	0.218	[m]
Rotational Velocity	3550	[rpm]
Inner Diameter	0.3096	[m]
Number of blades	52	
Inlet Area	0.009184	[m^2]

The casing is a half tube without any fins or guides(unlike other turbomachines), and the rotor is a circular disk which has 52 closed equal blades, also there is a splitter which located between inlet and outlet that separates the relatively hot and high-pressure outgoing flow from the cold and low-pressure inlet flow.
In order to prepare the geometry and initiate the simulation procedure, it was necessary to remove trivial parts of the geometry and layers to optimize the process running time and number of mesh cells. The logic behind that was to consider only parts that have direct contact with the working flow and not exterior parts, for example parts like outer protective casing layers or the shaft hub etc. To achieve that, the geometry was stripped down using an open source CAD software and only the rotor, casing, inlet, outlet, and splitter were left. Then, the 0.3 mm gap between the rotor and the casing was closed using CAD software to create a closed space geometry. Then the cleaned geometry was imported into the CFD software (STARCCM+

2021 v4) for meshing process and simulation. However, since the imported geometry was concluded of 2000 segments, it was necessary to patch them together to create the two region of rotor and stator and then close the free edges on these regions, all these process for each geometry took at least one week. In **Fig. *21*** the initial geometry and the cleaned geometry is shown in different views. As shown the upper part of figure is dedicated to raw geometry (before cleaning) in rear, front and isometric view, and the bottom row is in the same view order as top but, for the cleaned geometry. After importing the geometry into the STARCCM+, two region created namely rotor and stator which includes: inlet, outlet, stripper, and casing, then an interface was created between rotor and stator to distinguish the rotating and fixed domains for the CFD software. Then the final check was done using repair toll of the STARCCM+ to make sure there were no free edges or open spaces on the geometry before meshing process.

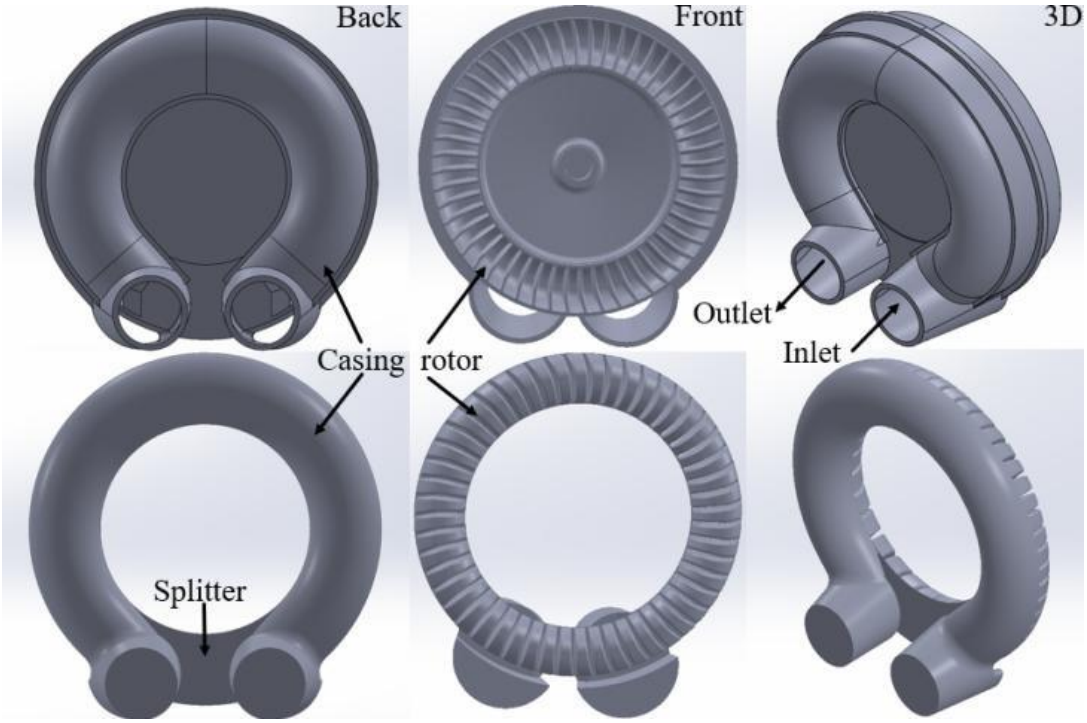

Fig. 21. initial geometry (top) and cleaned geometry (bottom).

2.2 Experimental results

The experimental results reported in this section are for 4 different rotational speed of 1000, 2000, 2990, and 3500 rpm and all has been done by FPZ spa. ***Fig. 22*** shows the characteristic curves of the E08 geometry based on the experimental results. It shows that by moving from high Φ working point (P1) the pressure is at the lowest value for each rotational speed and by moving toward low Φ the pressure value increases and reaches at its maximum value in P5 for all rotational speed curves.

An interesting fact about the characteristic curves provided is that all four characteristic curves for four different rotational speeds are collapsing on each other while it was expected that each rotational speed create a separate curve. Since we know that the density could change so this phenomenon could be resulted from the high losses and temperature increase too much which goes beyond adiabatic transformation rate at the same pressure level, and this is keeping density constant.

Moreover, ***Fig. 24*** depicts the efficiency of E08 Geometry against Φ for all rotational speed based on experimental measured data. As it can be seen by increasing the rotational speed, the pressure increases, however the efficiency of the machine decreases, which is a character of these machines as it will be discussed in depth on following chapters. Another interesting fact about the characteristic curves graph is that curves in all rotational speed collapsing on each other. Since we know that the density could change so this phenomenon could be resulted from the high losses due recirculating flow and too much temperature increases which goes beyond adiabatic transformation rate at the same pressure level, and this is keeping density constant. To explain better the phenomenon, it can be seen that the machine, at 3500, achieve 1.4 beta however, the density variation is less than pressure variation but the curve scales on 1000 rpm case which gives similar effect to constant density case by moving toward temperature increase in the machine ***Table 3***. This can be explained by the fact that the inlet temperature is at ambient temperature for a short period of time and after that inlet temperature will be affected considerably by hot recirculating flow coming from outlet and mixed with the inlet hence real inlet temperature increasing, and this high temperature in inlet and losses leading to reduction in density variation in which similarity theory holds for constant density in these machines.

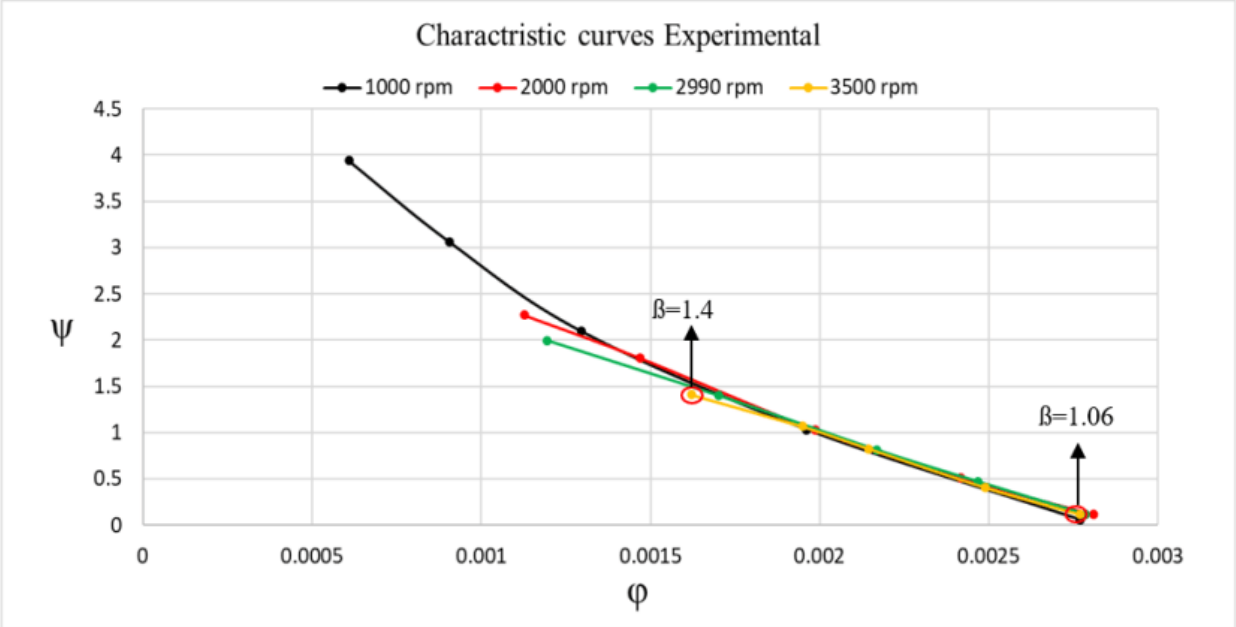

Fig. 22. Experimental characteristic curves of the E08 geometry for 4 different rotating speed.

The effect of recirculating flow on temperature of the inlet flow is demonstrated in **Fig. *23***, which suggests that the inlet flow temperature is not constant as it sets in boundary condition and gets affected considerably by the hotter recirculating flow. Moreover, it must be considered too that by moving toward higher pressure working points the amount of recirculatory flow increases while the inlet flow decreases which results in an even hotter recirculatory flow coming and mixing with inlet flow. This to a great extent justifies why all characteristic curves are scaling on 1000 rpm machine.

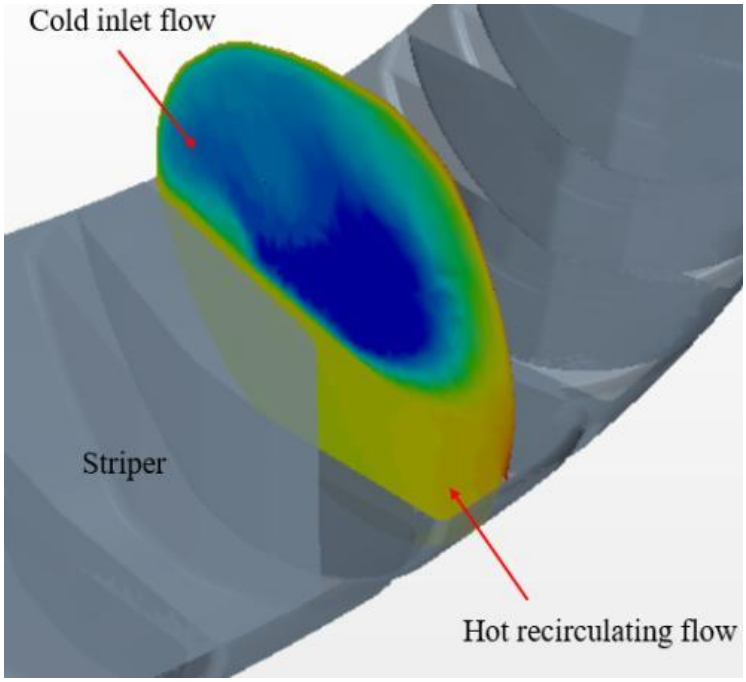

Fig. 23. Hot recirculating flow mixing with cold inlet flow.

Table 3. density ratio, and recirculatory mass flow for 3500 rpm regarding beta change.

Working points	Recirculatory mass flow (Kg/s)	Density ratio	Beta (Pout/Pin)
P1	0.078	1.03	1.06
P2	0.082	1.07	1.13
P3	0.086	1.13	1.24
P4	0.087	1.14	1.30
P5	0.088	1.15	1.42

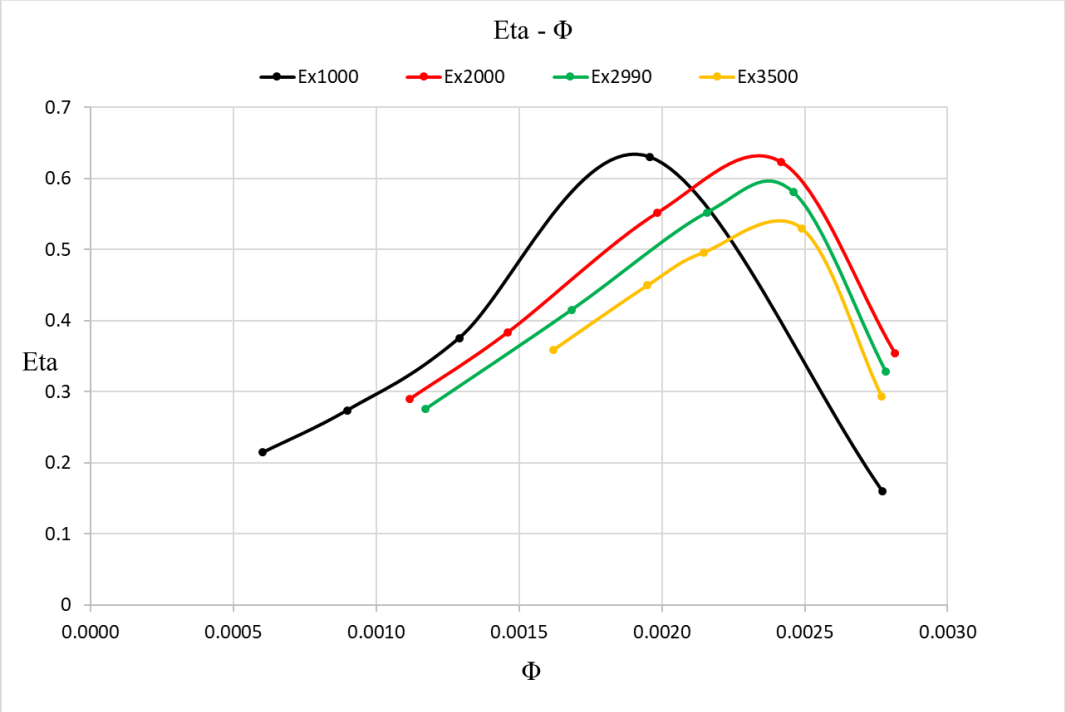

Fig. 24. Efficiency of the E08 geometry in four rotational speed.

Ther information provided in the **Table 4**, showing the experimental pressure results for all rotational speeds ranging from 1000, 2000,2990, and 3500 rpm at all five working points, which also measured and provided by F.P.Z spa to be used as the data validator for the upcoming simulation data in this study. These data suggesting that by increasing the rotational speed while all other parameters are kept constant, the pressure keeps increasing constantly at each working points.

Table 4. Experimental pressure for all five working points and four rotational speed.

E08	P1	P2	P3	P4	P5
	Pressure (Pa)	**Pressure (Pa)**	**Pressure (Pa)**	**Pressure (Pa)**	**Pressure (Pa)**
1000 (RPM)	136	2527	5109	7448	9519
2000 (RPM)	1144	5050	8573	17526	21922
2990 (RPM)	2625	10167	17408	29620	41691
3500 (RPM)	3492	12439	25211	32362	42400

3 Numerical setup

Computational Fluid Dynamics (CFD) can give insight into fluid flow aspects, which cannot be obtained analytically or experimentally. Improvements in performance by decreasing losses are possible with CFD studies. Also, costly fabrication of prototypes can be made after ascertaining convincing performance using CFD models. With the advent of high-speed computing, applications of CFD have become very popular in engineering design and analysis. Since the working and flow pattern is not properly understood in regenerative flow machines, one has to resort to either experimental or CFD studies for flow visualization. Experimental flow visualization has been attempted by using transparent casing, The simple and cheap technique which is not suitable for colorless gases like air. Therefore, it becomes mandatory to opt for CFD techniques in order to visualize the flow.

3.1 Mesh setup

As mentioned earlier, after cleaning the geometry there was a 0.3 mm open gap between rotor and casing which in each domain (rotor and casing) is 0.15, which created difficulty to mesh it accurately and the height of this regions on each side was smaller than the base size (4 mm) dedicated to the geometry, so for those gaps the customized mesh was used to get an accurate results. Another problem during meshing process was the fact that the E08 geometry was very complex with lots of 90 degree blade angels and sharp edges which made it a challenging task to achieve a high quality mesh all around the geometry, to address that different tools such as Feature curves was applied to increase the quality of mesh through the geometry.

Fig. 25 shows the shape of the E08 geometry rotor which is partially radial and partially curved inward. This shape of blades seems to have a positive effect on the efficiency of the machine, but it makes the simulation and meshing process a challenging task.

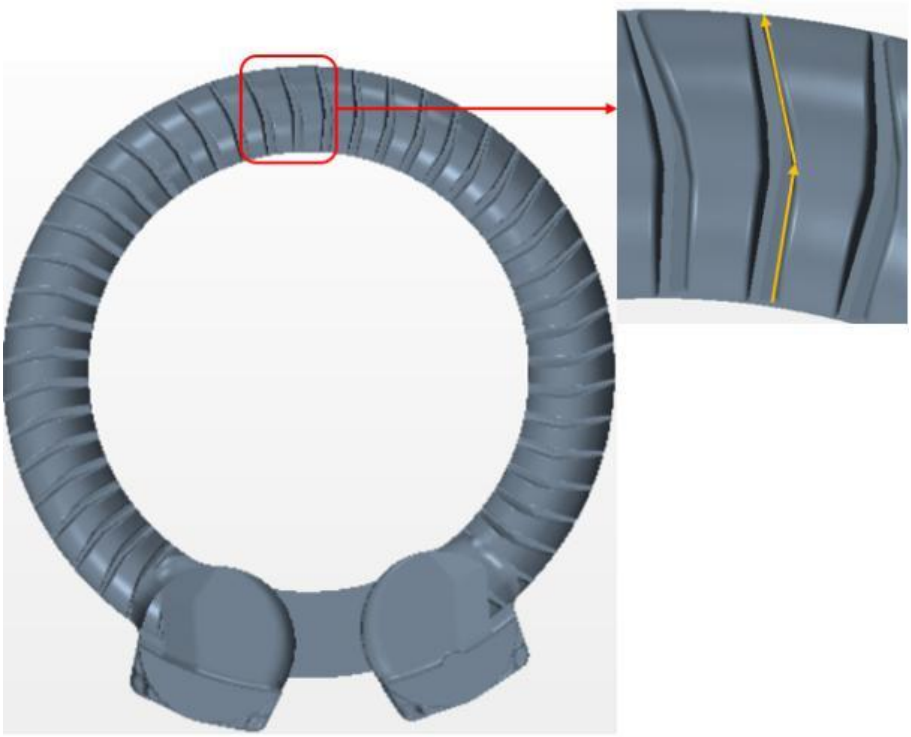

Fig. 25. the shape of blades in E08 geometry.

The mesh models used in this study was set as follows:

- Prism layer Mesher, to solve accurately boundary layer effect. Prism layers allow the solver to resolve near wall flow accurately, which is critical in determining not only the forces and heat transfer on walls, but also flow features such as separation. Separation in turn affects integral results such as drag, or pressure drop.

    - The polyhedral mesh type was selected since Polyhedral meshes provide a balanced solution for complex mesh generation problems. They are relatively easy and efficient to build, requiring no more surface preparation than the equivalent tetrahedral mesh. They also contain fewer cells than a tetrahedral mesh for a given starting surface.
    - Surface remesher, in order to improve the overall quality of an existing surface and optimize it for the volume mesh models, the surface remesher can be used to retriangulate the surface.

In **Fig. 26** the meshed geometry is shown indicating the rotor mesh, a cylindrical section in Z orientation and the prism layers. The above-mentioned mesh consists of 8 prism layers and a 4-millimetre base size which results in 6.3 million cells.

With the chosen turbulence model, which be explained further ahead, in this study at the maximum flow rate simulated, the average y+ is about 1.3 with a peak value of about 5 near the walls which is satisfied the range described in STAR CCM+ manual in order to accurately solve the near wall flow.

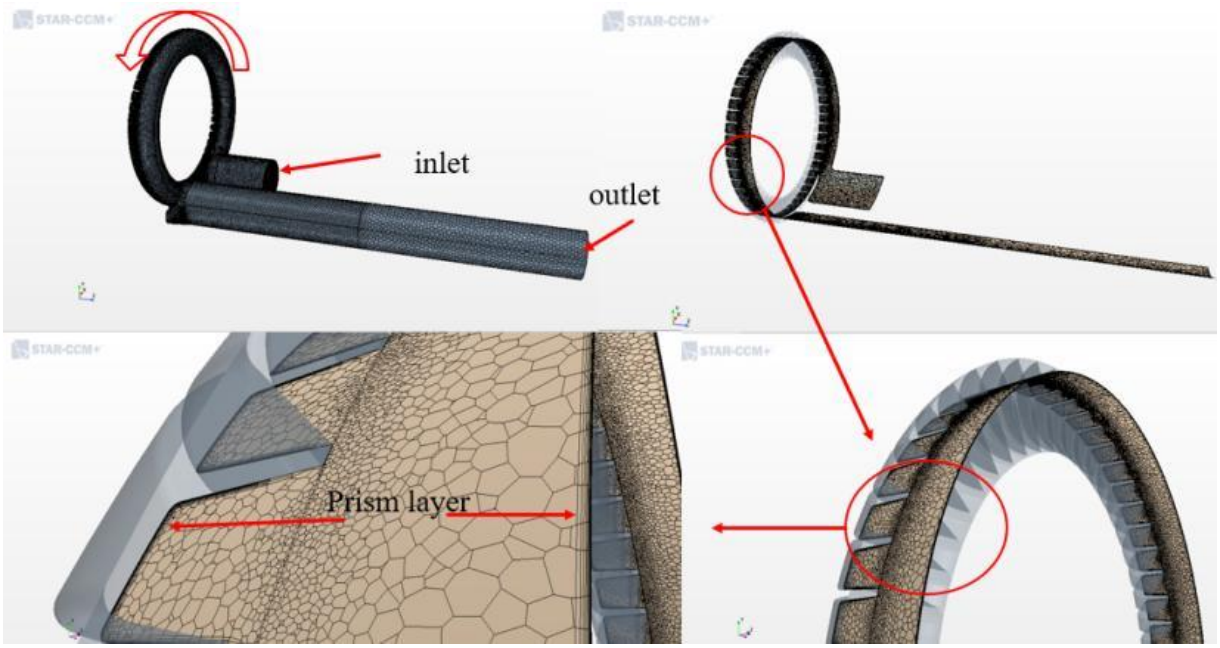

Fig. 26. Generated polyhedral mesh with prism layer close to the wall of the machine.

3.2 Mesh sensitivity

The mesh sensitivity analysis has been based on the steady simulation only, then it is useful just to consider the variations in the pressure rise. In the range between 3 million and 7.6 million of cells. This variation of cells controlled by modifying number of prism layers, base size, and the surface growth rate. To this end these variables are explained as follows:

- Base size: The Base Size is a characteristic dimension of the model that can be set before using any relative values. As general examples, the base size can be set to the diameter of an inlet, the length of the fluid volume, or a size that is convenient for scaling other values.
- Prism layer: The prism layer mesh model is used with a core volume mesh to generate orthogonal prismatic cells next to wall surfaces or boundaries. This layer of cells is necessary to improve the accuracy of the flow solution. In this case prism layers were 3, 5, 8, 12, 20.
- Surface growth rate: can be specified on a part or part surface to control the triangle growth rate on those surfaces. The minimum and maximum value of the surface growth rate in STARCCM+ are 1.1 and 1.6 respectively, hence in this case the chosen range were 1.1, 1.3, and 1.5.

The two computational domains, stator, and rotor, were discretized with a hybrid mesh, using prismatic elements near the walls and tetrahedral elements for the domain. A mesh of 6,300,000 cells was required to obtain grid independence and numerical convergence of the solution in a reasonable computation time. This set up was selected after running the simulations for a wide range of mesh cells from 5 to 12 million, but difference in results after 6 million mesh cells was negligible so 6.3 million mesh cells was chosen. The difference in pressure rise is limited to less than 1000 Pa hence, the mesh setting with 6.3 million cells considered as the final and most reliable setting for the rest of the simulations **Fig. 27**. Given the fact that E08 geometry is very complicated, especially in rotor part, is seems necessary to validate the generated mesh, using mesh sensitivity analysis, with another method. Since having the experimental results as an reliable source of validation, at the next step, to validate the simulated data with experimental results, the above-mentioned 6.3 million mesh applied for all variation of E08 geometry STD and Unstd simulation for the five working points. This method of validation with experimental results gave enough assurance that the chosen mesh is reliable enough to be used for simulation and the acquired results considered valid. **Fig. 28** shows the comparison of characteristic curves of the four E08 variants between experimental results and simulations (STD and Unstd) for five working points, which suggests that the mesh with 6.3 million cells is reliable enough to be used for the simulation since the simulations results were in acceptable range of 1000 Pa difference in respect to experimental data .

The differences between experimental and simulation results could be due to the overestimation of losses by the simulation and therefore difference in pressure rise at low flow rate working points (P4, P5). This difference will be discussed more in detail in this study.

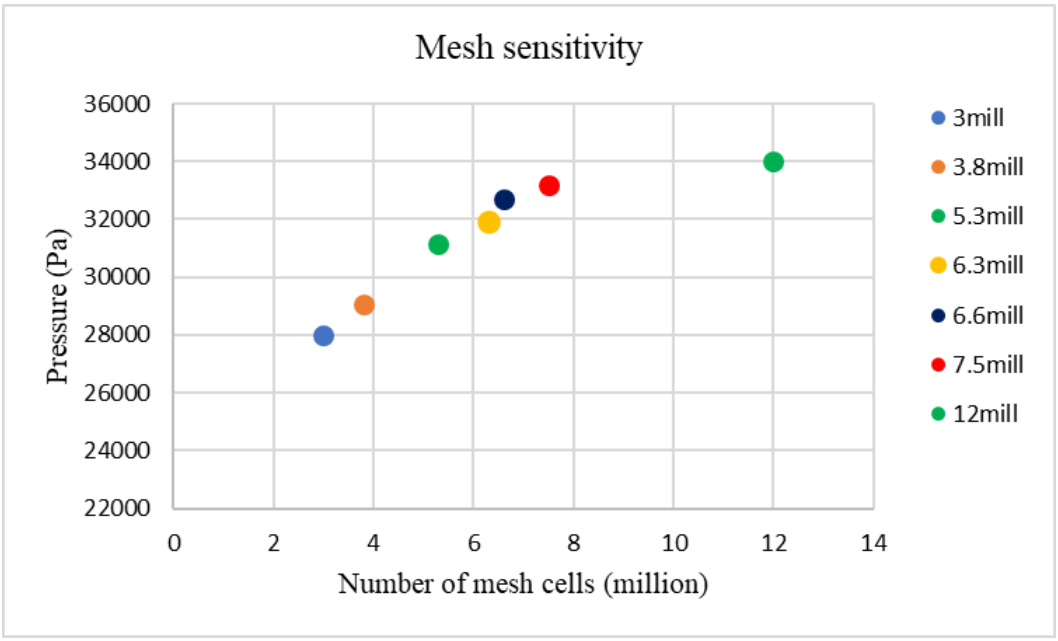

Fig. 27. Mesh sensitivity analysis.

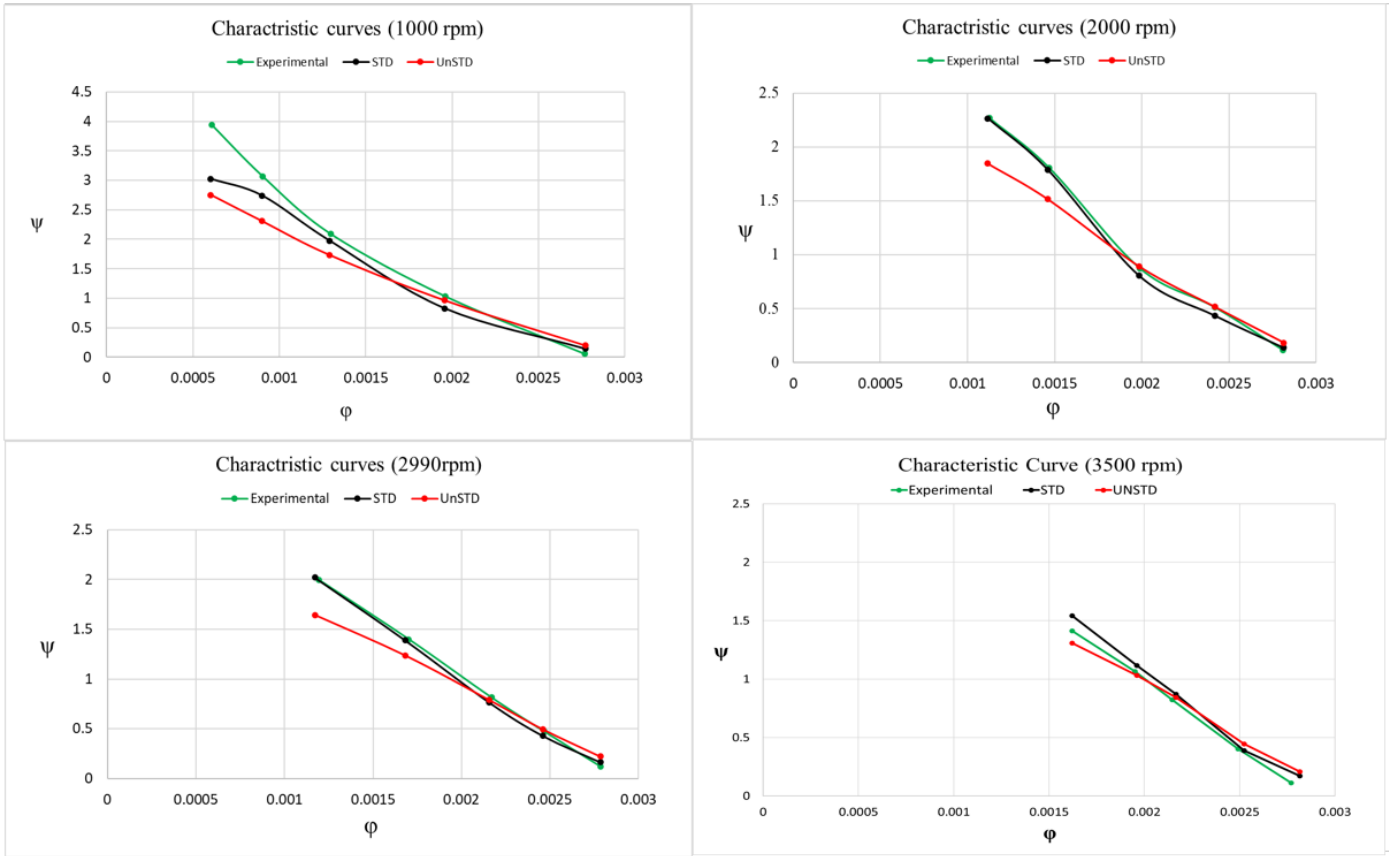

Fig. 28. Comparison of characteristic curves of simulation results with measured experimental results.

3.3 Physics Model

The following setup is used to simulation model:

- 3D
- Unsteady flow.
- Ideal gas
- Turbulent
- URANS_SST (Menter) K-Omega
- All y+ Wall Treatment
- compressible fluid
- All processes are adiabatic
- Velocity inlet
- Pressure outlet

The CFD campaign was carried out using the Star CCM+® v2020.1.1 solver. Second-order accurate discretization was used in time and space. The realizable k- ω SST model was used as turbulence closure in conjunction with the Menter-Lechner and all y+ wall treatment, turbulence intensity, and viscosity ratios were kept constant as default [63, 64,65]. The selected turbulence closure demonstrated to be reliable for the prediction of performance of regenerative machines, as shown by Quail *et al.* [42]. It worth mentioning that the almost all the literature existed about this subject, which are not much, were conducted unsteady simulation used k-ω SST as turbulence model and only when a steady simulation approach was studied k-ε turbulence model were used. Moreover, one advantage of the K-Omega model over the K-Epsilon model is its improved performance for boundary layers under adverse pressure gradients [41, 63, 65, 66] which makes it more suitable to use for this study and type of machines.

The walls were considered as adiabatic, the velocity inlet was imposed at the inlet duct as boundary conditions, while the outlet pressure was set at the outlet boundary condition. Also, The Coupled Flow model solves the conservation equations for mass, momentum, and energy simultaneously, one advantage of the latter formulation is its robustness for solving flows with dominant source terms, such as rotation. Another advantage of the coupled solver is that CPU time scales linearly with cell count; in other words, the convergence rate does not deteriorate as the mesh is refined.

The segregated flow model invokes the segregated solver which solves each of the momentum equations in turn, one for each dimension. This model has its roots in constant-density flows. Although it can handle mildly compressible flows and low Rayleigh number natural convection, it is not suitable for shock-capturing, high Mach number applications. At the outlet boundaries, the computational domain is extended

to obtain a fully developed velocity profile, also for avoiding the formation of flow recirculation on the outlet section due to the presence of residual swirl under some operating conditions.

As was mentioned earlier, geometry consists of two regions in this simulation, the rotor, and the stator. The latter one includes the inlet, outlet, casing, and the splitter **Fig. 29**. The rotational speeds of the rotor were 1000, and 3500 rpm, and the velocity inlet was 6.572 (m/s). At the beginning, to have a better range of simulation 1000 rpm was chosen for the rotational speed. For that rotation, the maximum pressure rise was 10000 Pa, and the maximum temperature rise measured was 26˚. The segregated numerical scheme was selected since the measured quantities are not high enough to effect compressibility of the air.

However, simulation done for 3500 rpm rotational speed, showed 42400 Pa pressure rise, and 80˚ temperature rise since in these conditions the compressibility effect not negligible the coupled numerical scheme was applied for the simulation.

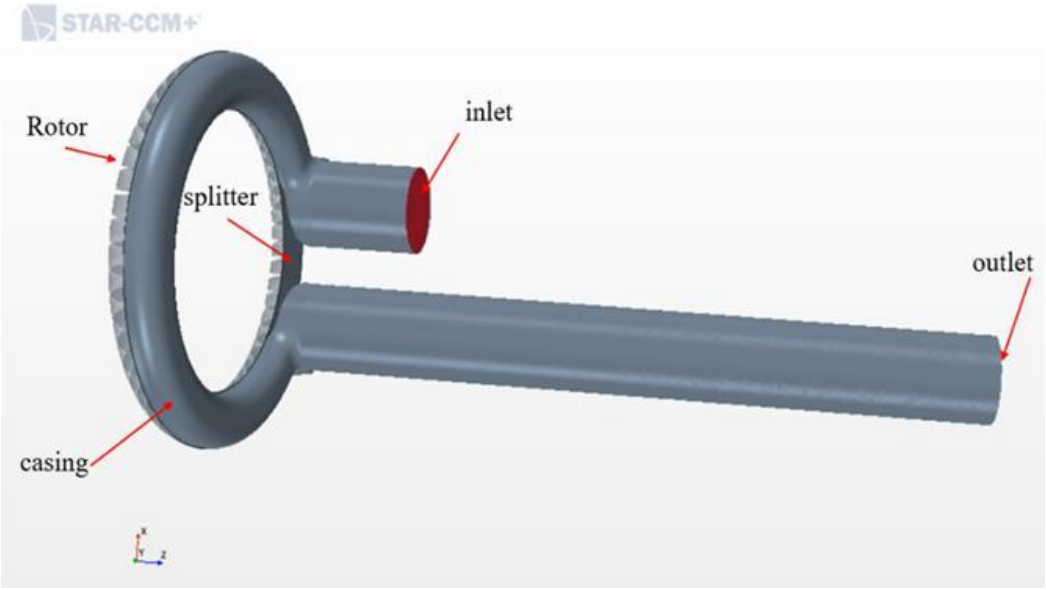

Fig. 29. Rotor and stator (casing, splitter, inlet, and outlet) regions.

For this geometry, five working points are considered at the same rotational speed which were based on the real working condition of the side channel blower. Under such conditions, both steady and unsteady CFD simulations were performed to evaluate the influence of unsteadiness on performance prediction. The changing parameter between these five working points is volume flow rate, which is controlled by velocity of the flow in the inlet. Since the simulation results will be evaluated with the experimental results these inlet velocities are exact values that are used for experimental setup **Table 5**.

Table 5. Inlet boundary conditions.

Working points / values	**1**	**2**	**3**	**4**	**5**	
V inlet	9.38	8.41	7.21	6.53	5.40	[m/s]
volume flow rate	310	278	238.5	216	178.5	[m^3/h]
Mass flow rate	0.0997	0.0894	0.0767	0.0695	0.0574	[kg/s]

3.3.1 Design Point

Design point refers to the point where RFC is desired to operate at. The design point which is selected yields the best combination of efficiency and pressure rise for this geometry. For E08-3500.the design point was provided by the company using experimental tests.

3.4 Physical schemes and settings:

For initializing the simulation Steady state conditions were considered in the simulation and a compressible ideal gas with constant specific heat was assumed. the ‘‘Frozen-Rotor’’ technique was considered as the most appropriate because it permits one to obtain satisfying turbomachine performance results, in terms of pressure ratio, mass flow rate and efficiency, without risks of instability or of an excessive calculation time [63]. The Frozen Rotor technique treats the flow from one component to the next by changing the reference frame while maintaining the relative position of the components. This technique offers the advantage of being robust and it uses less computer resources than the other frame change models. Then after the convergence of steady simulation, turbulence modeled changed to unsteady simulation to simulate the realistic results.

For the unsteady simulations, the “sliding mesh” approach was used. A time step corresponding to 1/40 of the vane periodicity (360°/ (n blades×30)) was selected. Such time step is equivalent to 0.23° of the impeller rotation and, according to the works of Fleder and Böhle [63] and Nejadrajabali et al. [43] (that used respectively ≈0.9° and 1°), is low enough to ensure an appropriate resolution of the unsteady phenomena.

4 Results

4.1 E08 (reference geometry 3500 rpm)

- Different Working points results comparison:
- Pressure and temperature graphs unsteady- experimental.
- Characteristic curves unsteady- experimental.
- Efficiency curves unsteady- experimental.
- Data driven from interface for ceding points.
- Choosing 5 blades throughout the theta position.
- Streamlines characteristics and averaged integral values of the flow.
- Compering length of the streamlines and describing the cause of it.
- Temperature distribution in meridional section close to inlet and outlet.
- Changing pattern of circulatory and tangential velocity from inlet to outlet.
- Mass flow rate difference inlet and outlet.
- Separation growth in regards volumetric flow rate (or regarding working points)
- Showing the same trend for other E08 rotational speeds in characteristic curves and pressure Vs Volumetric flow rate.

In this section the results of the reference (E08) geometry such as efficiency, characteristic curves, pressure, temperature, circular, and tangential velocity contours will be presented and discussed to have a better understanding how the flow is developing in a RFC. It must be mentioned that the STD results are also included here, alongside the experimental measurements and UNSTD results since after through investigation it seems that the STD simulation results are closer to experimental data.

Fig. *30* compares the efficiency of the E08 geometry in five different working points using the experimental and simulation results. The results show that the simulated efficiency follows closely the results of the experiments, besides the first working point (low pressure). The disparity between the simulated value and the experimental results appears to be attributed to the side effects of assumption of adiabatic process and not considering the effect of leakage flow at the stripper.

As it shown in **Fig. *30*** with increase of the volumetric flow rate going from Φ=0.00162 to Φ=0.0025 (P5 to P1) the efficiency increases and after that efficiency drops. or in other word the maximum efficiency happens in lower pressure (P2), and the minimum efficiency happens at the highest pressure (P5), it must

be mentioned the efficiency of the P1 is the lowest, but this working point is very close to the choking point so safely can be said the minimum efficiency is happening at P5. The primary reason for that is the increased number of circulations through the impeller blades at a low flow rate and consequently producing very high pressures in RFCs. However, these large number of circulations through the blades require a high amount of power draw which is the reason why RFCs have a high-pressure ratio at low flow rates, but very low efficiency. This is an interesting difference between regenerative compressors and centrifugal compressors in power coefficient. Centrifugal compressors draw more power at higher flow rates, however regenerative compressors draw more power at low flow rates.

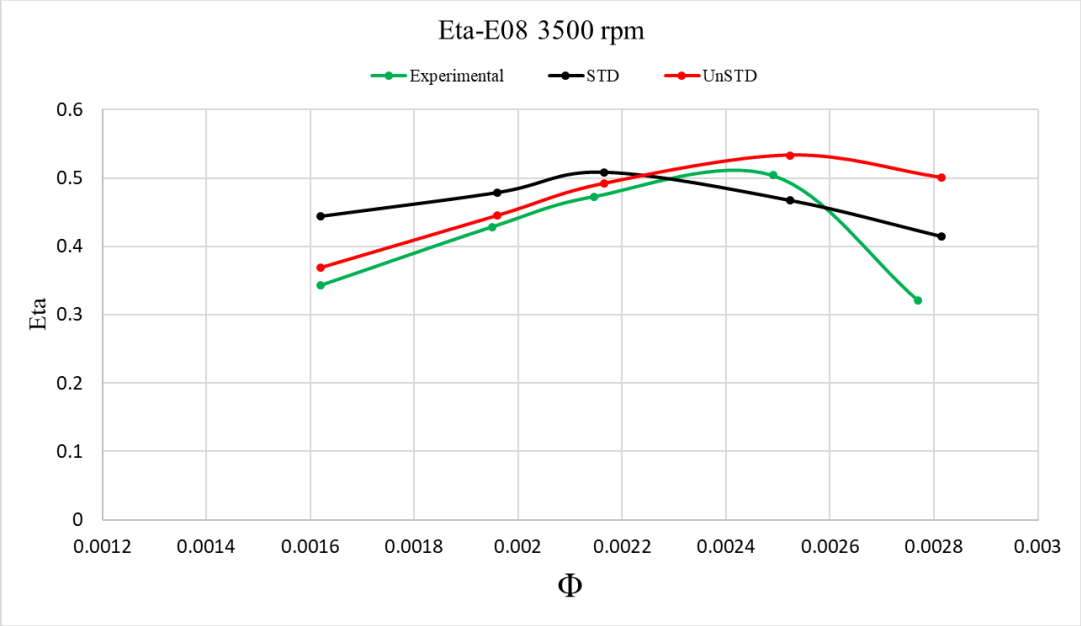

Fig. 30. Efficiency comparisons of experimental and numerical results

Fig. *31* shows the characteristic curve of the E08 geometry, and how close the simulation results in low pressure (high flow rates) but deviates at last working point in highest pressure working points (lowest flow rate). This coherency between unsteady results with experimental results showed that the turbulent model was able to almost in all working point simulate the results close to the real condition. Moreover, it is worth mentioning that the machine in the real practice was designed to work at the working point of 4 (design point), and for that point the simulated results were in the acceptable range. In the other hand, it is evident that the STD simulation is produced closer results with experimental measurements in respect to unsteady simulation, however it must be mentioned that the STD simulation does not take in to account circulatory flow which directly effects the temperature and pressure of the inlet flow and obviously output of the machine, having said that, this problem will be addressed and explained later.

Fig. *32* shows the characteristic curves and efficiency graphs together to put in perspective the reverse relation of the efficiency and pressure rise in these machines. Also **Fig. *33*** shows the pressure rise result for each working point for simulation and experiment to show the coherence of the simulation results with

experimental. And as it brought to attention above, the steady simulation results are closer to the experimental data in all the working points except P5, while unsteady simulation starts to drift away at P4 and continues to P5, this latter phenomenon in unsteady simulation could be the result of presence of separation and/or overestimation of losses. However, the deviation of unsteady results from the experiment is not that high and can be used for post processing of the acquired data.

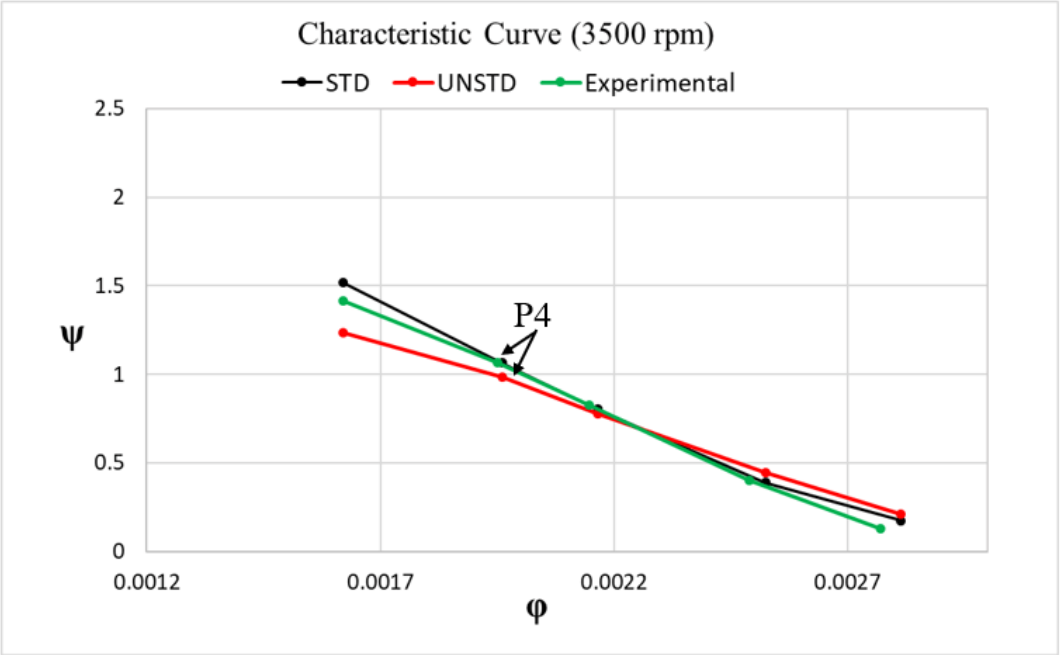

Fig. 31. Characteristic curves of experimental and numerical results.

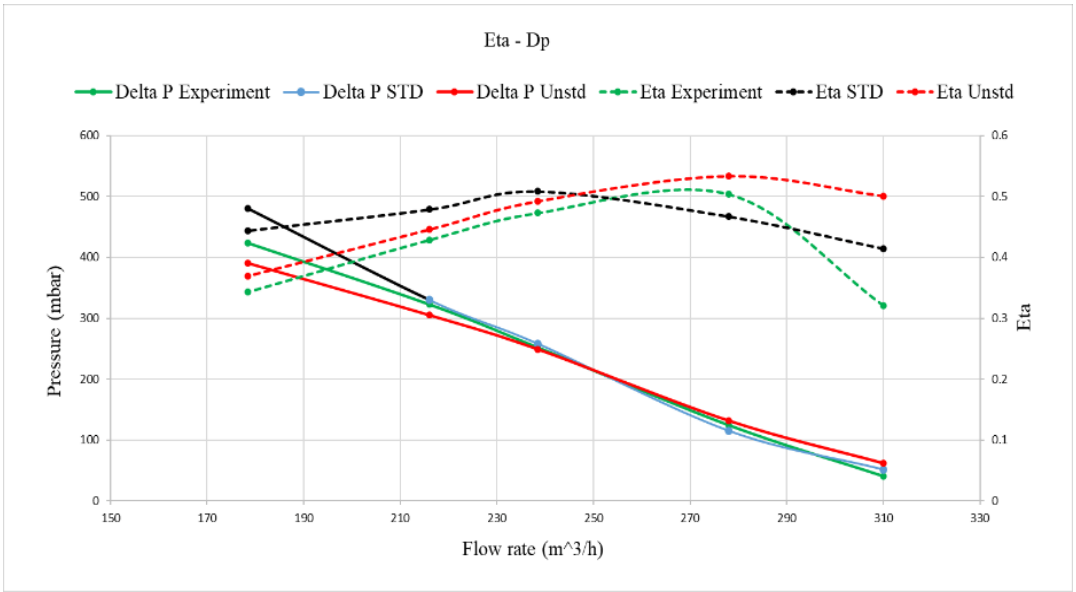

Fig. 32. Pressure rises and efficiency of the machine for five different working points, experimental and simulation.

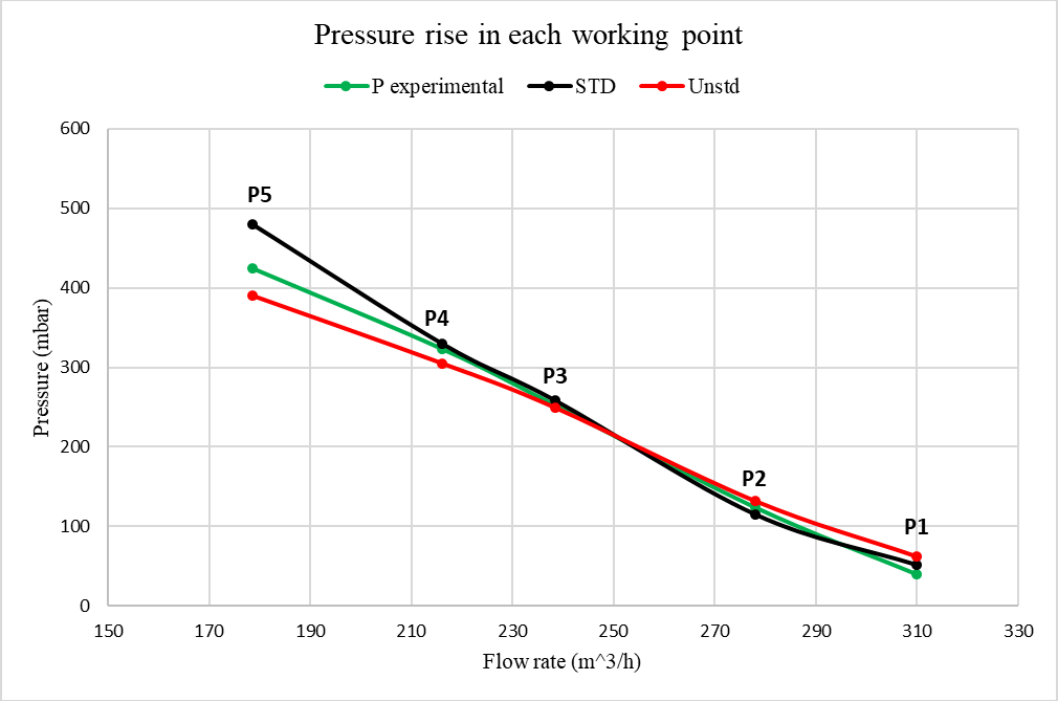

Fig. 33. Experimental and numerical pressure rise in different working points.

It was discovered that a very small but significant portion of the compressed gas was transported through the stripper from the high-pressure area and expanded down to the intake pressure as the blade pockets between the blades opened into the annular channel at the inlet end. This represents an efficiency loss and is sometimes referred to as carryover loss. The stripper seal is completely passive when a regenerative compressor uses an incompressible fluid, with the exception of a little amount of carryover. However, the tiny seal will play a significant role in machine performance in compressible flow circumstances. Large amounts of compressible fluid (low flow rate working points) close to the exit port are taken past the seal and mixed with the fluid entering the machine in a very irreversible process. As the rotation speed increases, this mixing process limits the pressure ratio. The machine's total efficiency is significantly decreased by the seal. [19] suggested that the carryover loss may be decreased by taking some of the compressed gas going through the stripper and sending it back into the annular channel at a middle pressure. Thus, the stripper carryover gas would be made to expand some of its energy inducing the incoming supply rather of being ineffectively deposited near the suction.

As is demonstrated so far, the flow in these type of machine are very complex and smallest changes can affect the efficiency of the machine hence, to have a better understanding of how flow evolves from inlet to outlet, some of the flow characteristics needed to be plotted. To that end, four meridional sections were created near the inlet and four meridional sections near the outlet to study different flow characteristics. In ***Fig. 34***, ***Fig. 35***, ***Fig. 36***, ***Fig. 37*** the circulatory velocity is depicted for 3500, 2990, 2000, and 1000 rpm, respectively on these meridional sections for 5 working points. It can be seen from ***Fig. 34*** that the circulatory velocity near the inlet initially for all working points are weak and starting to develop around

the outer edge of the meridional sections. However, by moving toward the outlet the circulatory velocity gets stronger by passing each blade and is fully developed near the outlet port, which is at its maximum value of 41, 52, 75, 81, and 88 m/s starting from P1 to P5 respectively. Also, on the sections close to the outlet it is shown that the circulatory velocity is very strong in almost all the areas of the last sections except the center of sections. These increase of circulatory velocity near the outlet port has a direct relation with pressure rise in the machine. Another phenomenon is the zero velocity region in the middle of the sections which gets more concentrated moving toward outlet. This can be explained by the fact that the flow leaving blade at higher radius have a high circulatory velocity and when in turn backs in to the blade at the lower radius has low circulatory velocity so in enter of the section there is always zero velocity regions which getting smaller as the pressure values getting higher.

The same trend of increase of circulatory velocity from P1 to P5 for other rotational speeds were also true in a sense that the for 2990, as it showed in ***Fig. 35***, the circulatory velocity increasing from inlet to outlet for all working points with starting value of 33 m/s for P1 and 38 m/s for P2, and54 m/s for P3, and 65 m/s for P4 , and 75 m/s for P5.

For 2000 rpm, ***Fig. 36*** the maximum circulatory velocity observed at P5 with value of 68 m/s as the same working points in the two higher rotational speeds. Meanwhile, in the second runner up the maximum circulatory velocity was 59 m/s recorded at P4 followed by P3 with maximum value of 42 m/s. the last two working points values were 32 m/s, and 19 m/s for P2 and P1 respectively.

Fig. 37 shows the circulatory velocity for 1000 rpm rotational speed in which the maximum circulatory velocity registered on P5 (lowest mass flow), like in other rotational speeds, with value of 39 m/s and maximum of 33 m/s while for the other three working points the maximum values recorded 25 m/s, 19 m/s, and 9 m/s for P3, P2, and P1 respectively and all these maximum values, like other rotational speeds, happened at the meridional sections close to the outlet port.

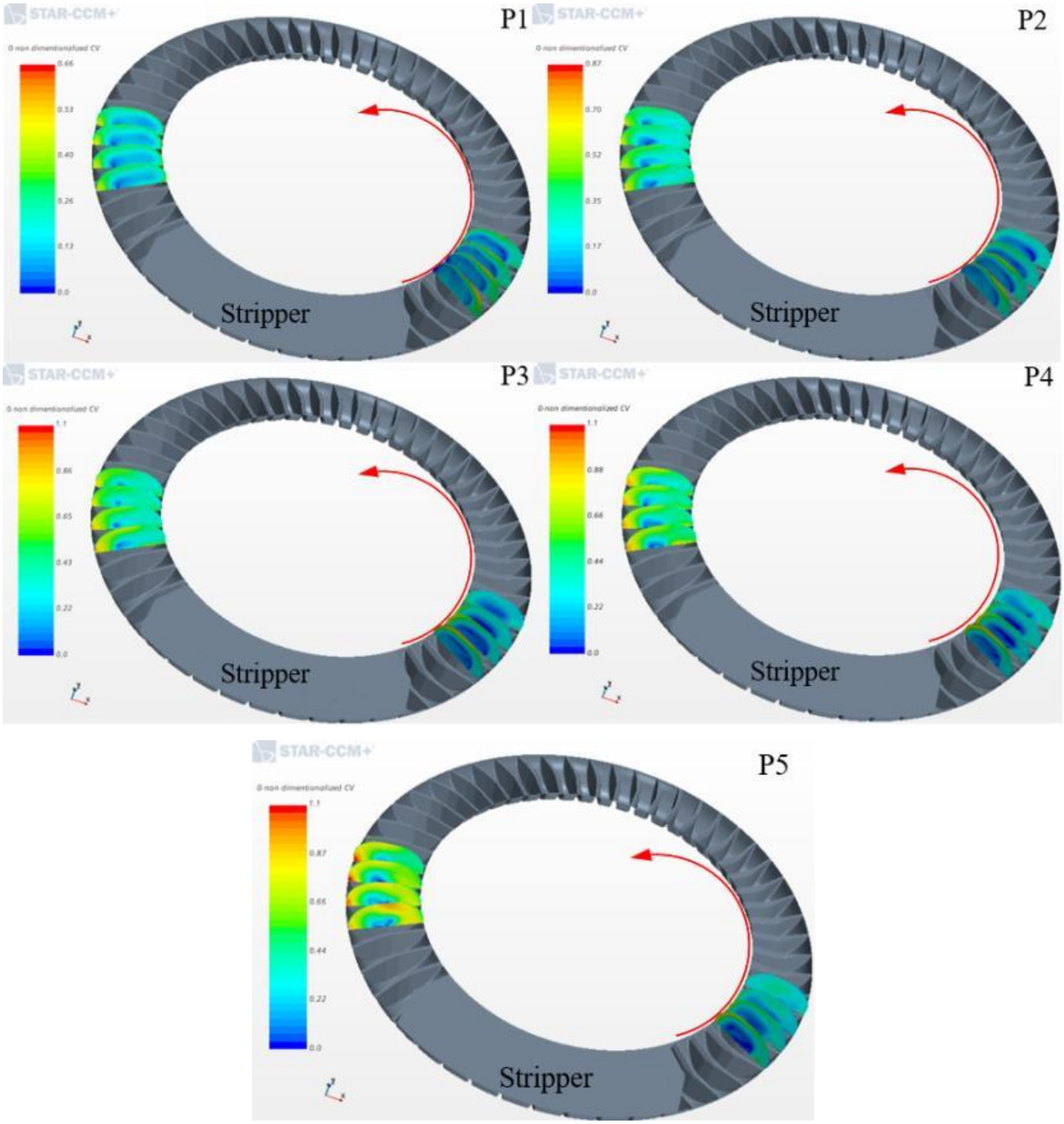

Fig. 34. Circulatory velocity development from inlet to outlet at 3500 rpm for five working points.

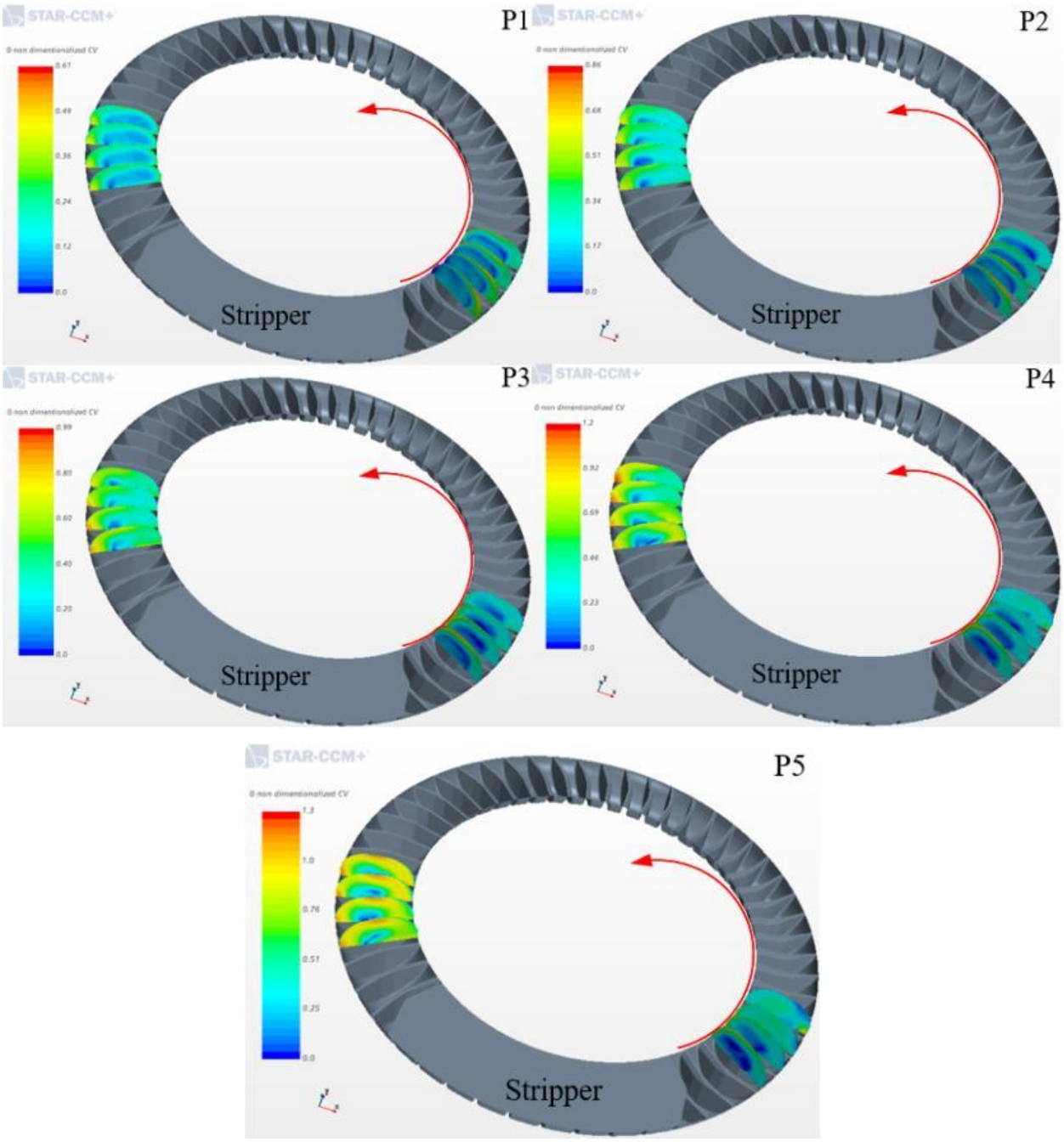

Fig. 35. Circulatory velocity development from inlet to outlet at 2990 rpm for five working points.

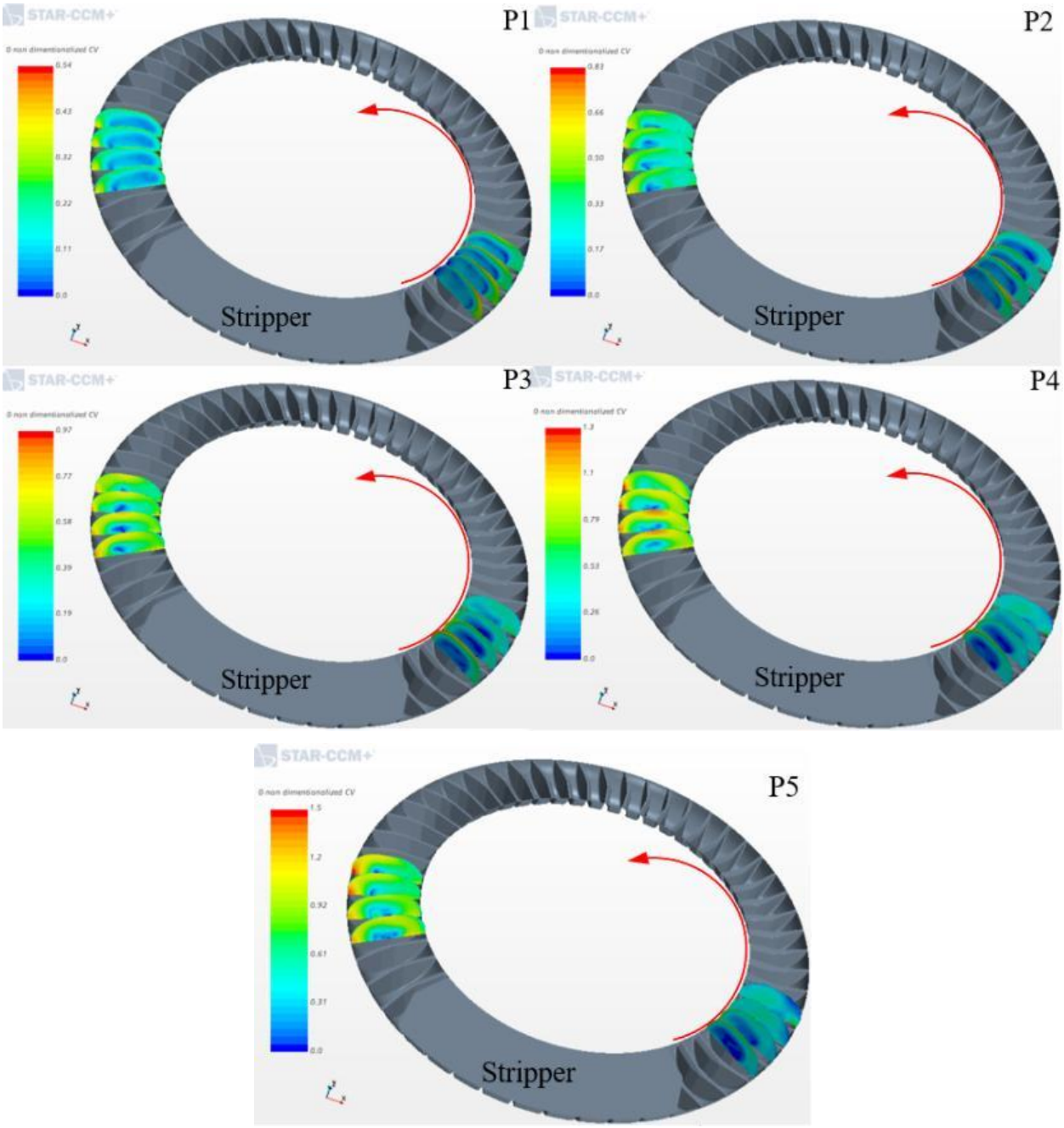

Fig. 36. Circulatory velocity development from inlet to outlet at 2000 rpm for five working points.

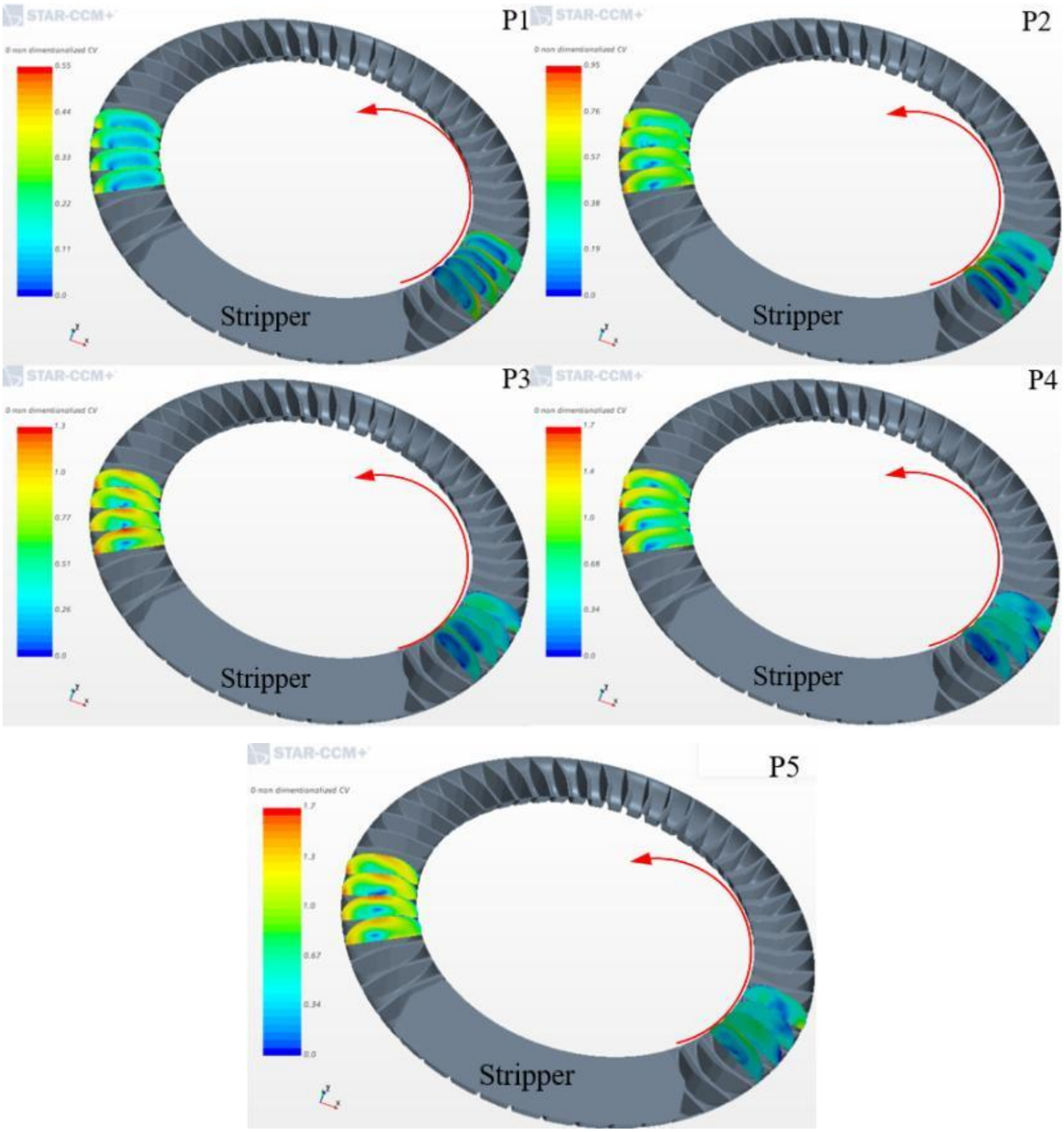

Fig. 37. Circulatory velocity development from inlet to outlet at 1000 rpm for five working points.

After showing the circulatory velocity in all rotational speeds it is worth to show the effect of the similarity phenomenon, for circulatory velocity at Φ=0.002 for all four rotational speeds. As it can be seen from **Fig. *38*** the circulatory velocity in all for rotational speed follows a same trend in which from inlet to outlet circulatory velocity increases and the zero velocity region gets concentrated on the middle section of the blades. In all four rotational speeds the non dimentionalized circulatory velocity are in the same range and showing the same character when the Φ is same in all rotational speeds, it must note that the small differences in the figures are due to fact that they are instantaneous figures so they can be a little different, but the average values are the same.

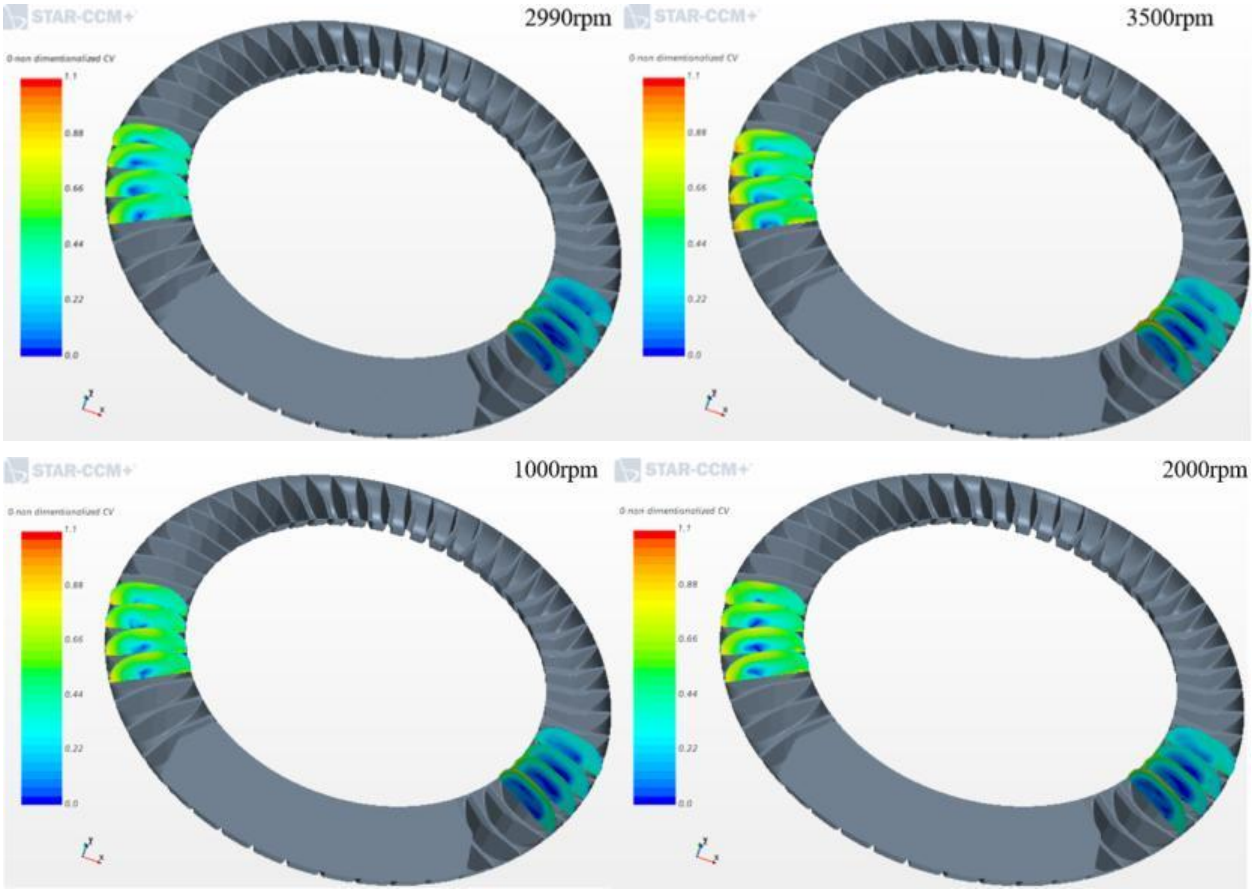

Fig. 38. Similarity effect for the circulatory velocity at the same Φ=0.002 in all four rotational speed.

Moreover, in ***Fig. 39***, ***Fig. 41***, ***Fig. 43***, ***Fig. 45*** where the tangential velocity is depicted on the same meridional sections for 3500, 2990, 2000, and 1000 rpm, respectively in which the section near the inlet, the exact opposite trend in respect to the circulatory velocity happened in the way that, in sections close to the inlet the tangential velocity value are at their highest value at each working point, whereas by moving toward the outlet the magnitude of it diminishes to its minimum for each working point. These decrease of the tangential velocity could be due to the tangential adverse pressure gradient along the casing from inlet to outlet which creates the separation and flow starts to move backward, another reason lies in the fact that by moving toward outlet the amount of the flow in a section at the rotor increases however, in the casing part decreases which suggests that a part of tangential velocity decrease happens at casing.

In ***Fig. 39*** for 3500 rpm, the Tangential velocity in sections close to the inlet has no blue region (negative value) in none of the five working points. Also, at P1 there is no negative value in the sections close to the outlet too. This could be happened for the fact that the advert pressure gradient is not strong enough to push the flow in the opposite direction, yet which makes sense since the pressure increase in the P1 at 3500 rpm is 6000 Kpa. Meanwhile, the maximum tangential velocity value registered at 91 m/s close to inlet section for the P1.

On the other hand, from P2 onward, the blue region (negative value) starts to grow in a way that at P2 the reaches to -9 m/s close to outlet whereas at P3 and P4 reaches to -31 m/s and at P5 reaches to -52 m/s as expected since in this working points the maximum pressure in the outlet registered at 39000 Kpa. This graph suggests that with increase of the pressure (decrease of flow rate going from P1 to P5) the tangential velocity decreases due to the separation which at end results in loss in efficiency of the machine. In ***Fig. 40*** it is shown that separation growing as the pressure rises in the machine. At P1 there is no separation since the adverse pressure gradient is not strong enough to reverse the flow the however , there is a small separation at inlet which is result of coinciding inlet flow and recirculatory flow. By moving toward higher pressure working points separation zones start to develop, mostly appearing in low to mid radius where the flow seems to start to get pressurized. Also, some separation also appeared on the casing surface due to the skin friction and losses.

In section close to the outlet where the circulatory velocity is stronger in outer radius so middle section has lower pressure, and separation region is bigger.

At 2990 rpm the value of tangential velocity decreased by moving from inlet to outlet for all five working points. the blue region does not exist in P1 and maximum Tangential velocity for this working point registered at 75 m/s in sections close to the inlet. However, the negative tangential velocity started to develop from P2 and continued to get bigger as the flowrate decreased (moving toward P5). The negative value of the -10 m/s and -24 m/s registered for P2 and P3 respectively and other two negative values arrive at -36 and -61while the former value registered for P4 and the later for P5. These trend suggest that with increase of the pressure the tangential velocity decrease due to develop of the separation **Fig. *41***. More over the same trend of separation at 3500 rpm is reoccurred here too in which the higher the pressure are the stronger the separation becomes **Fig. *42***.

Fig. 43 and ***Fig. 45*** showing the tangential velocity at 2000, and 1000 rpm which like trend in previous rotational speeds, the tangential velocity decreases by moving from the sections close to inlet to sections close to outlet in all working points. Also my moving toward higher pressure working points the separation also grow which can be seen from ***Fig. 44***, and ***Fig. 46***in which the former represents the 2000 rpm and the latter represents 1000 rpm.

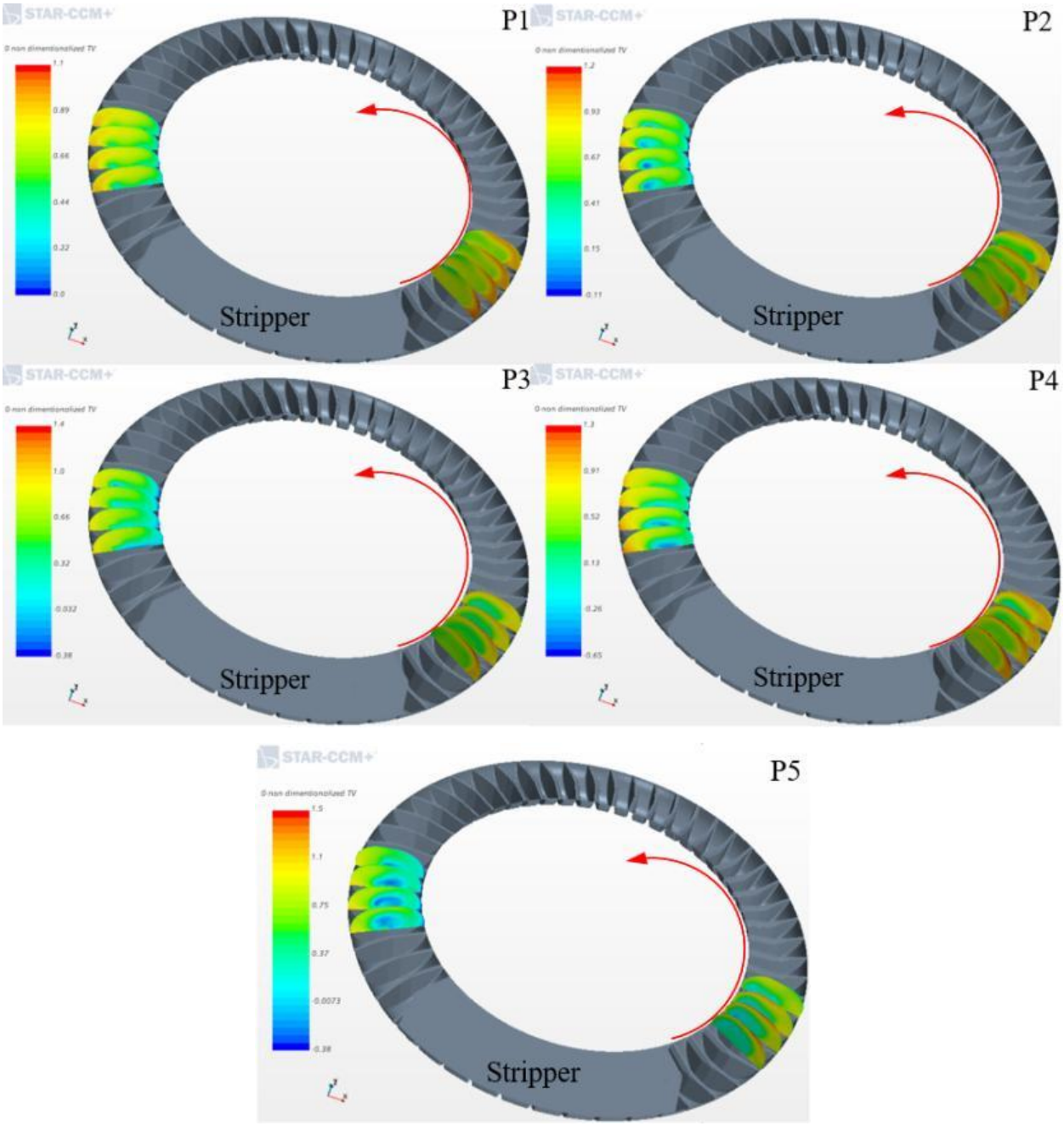

Fig. 39. Tangential velocity development from inlet to outlet at 3500 rpm for five working points.

Fig. 40. separation zone in five working points at 3500 rotational speed.

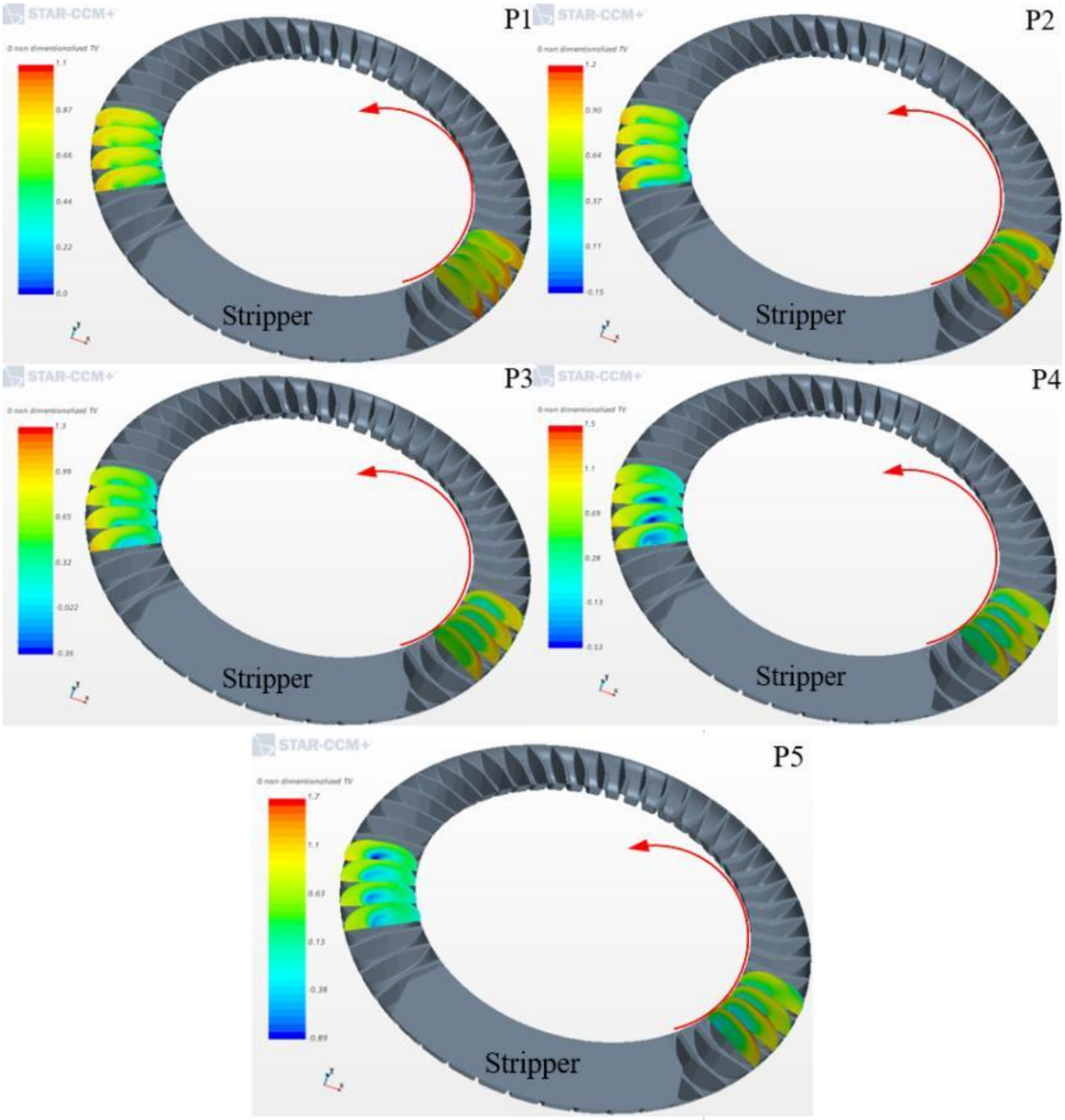

Fig. 41. Tangential velocity development from inlet to outlet at 2990 rpm for five working points.

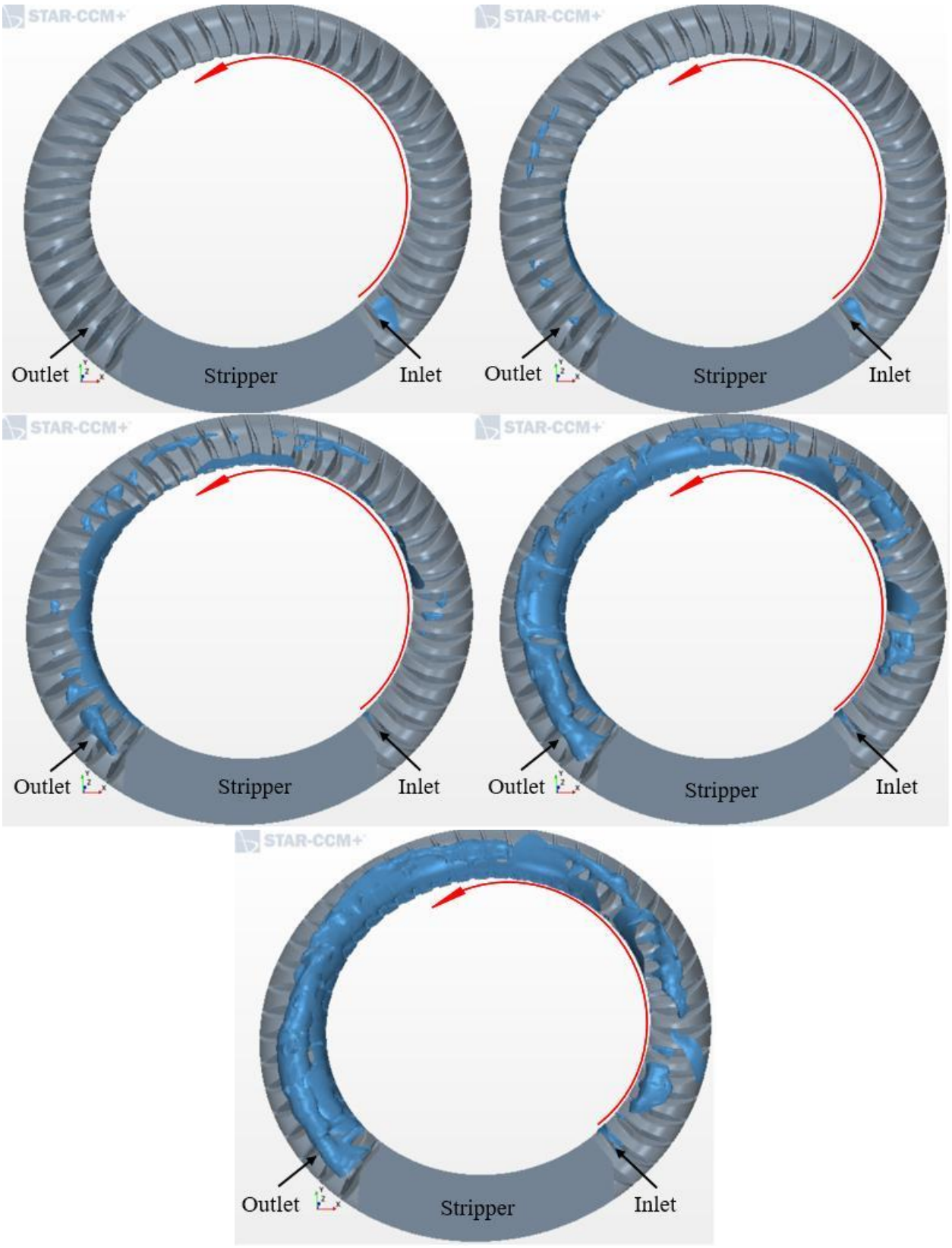

Fig. 42. separation zone in five working points at 2990 rotational speed.

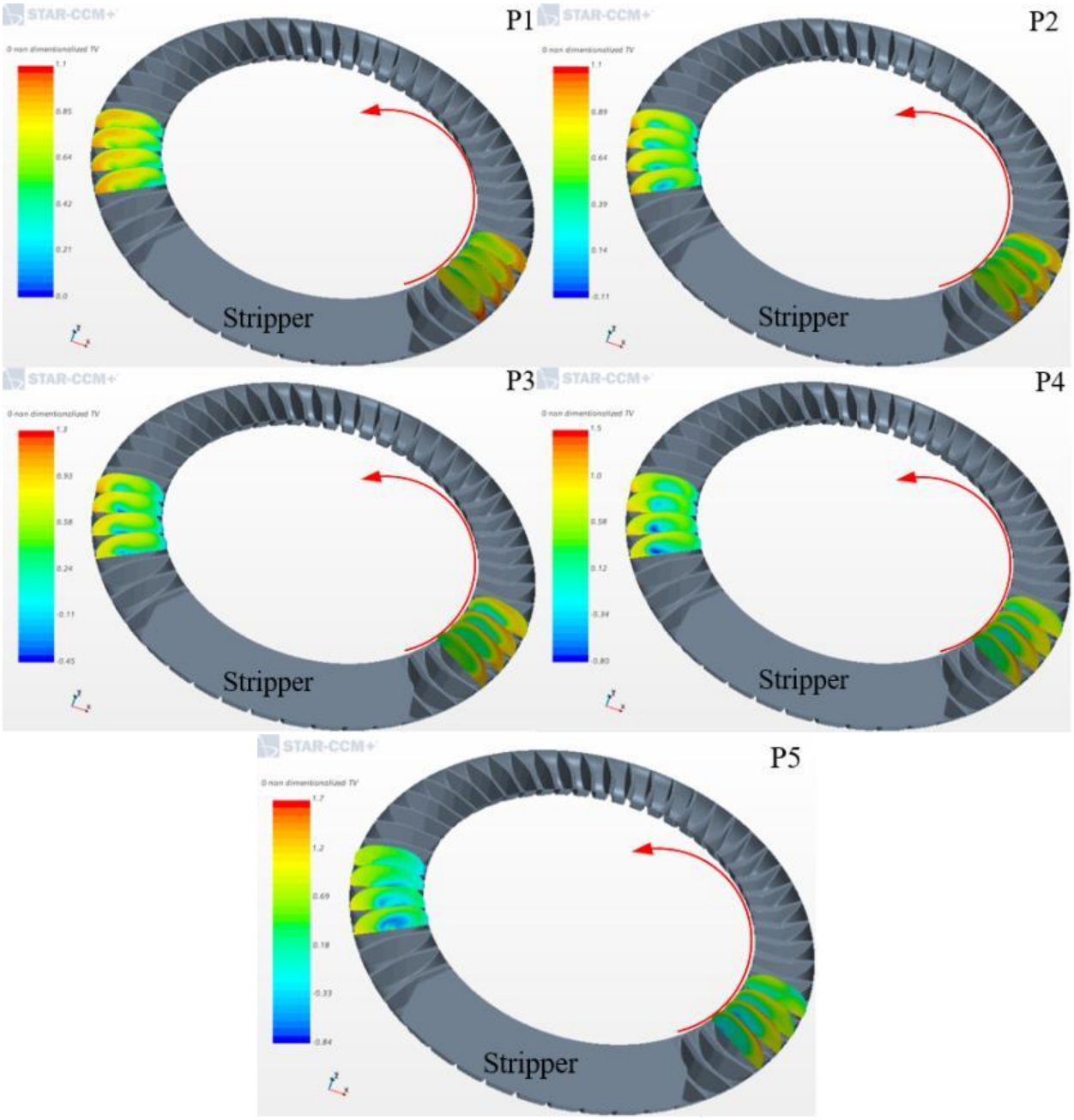

Fig. 43. Tangential velocity development from inlet to outlet at 2000 rpm for five working points.

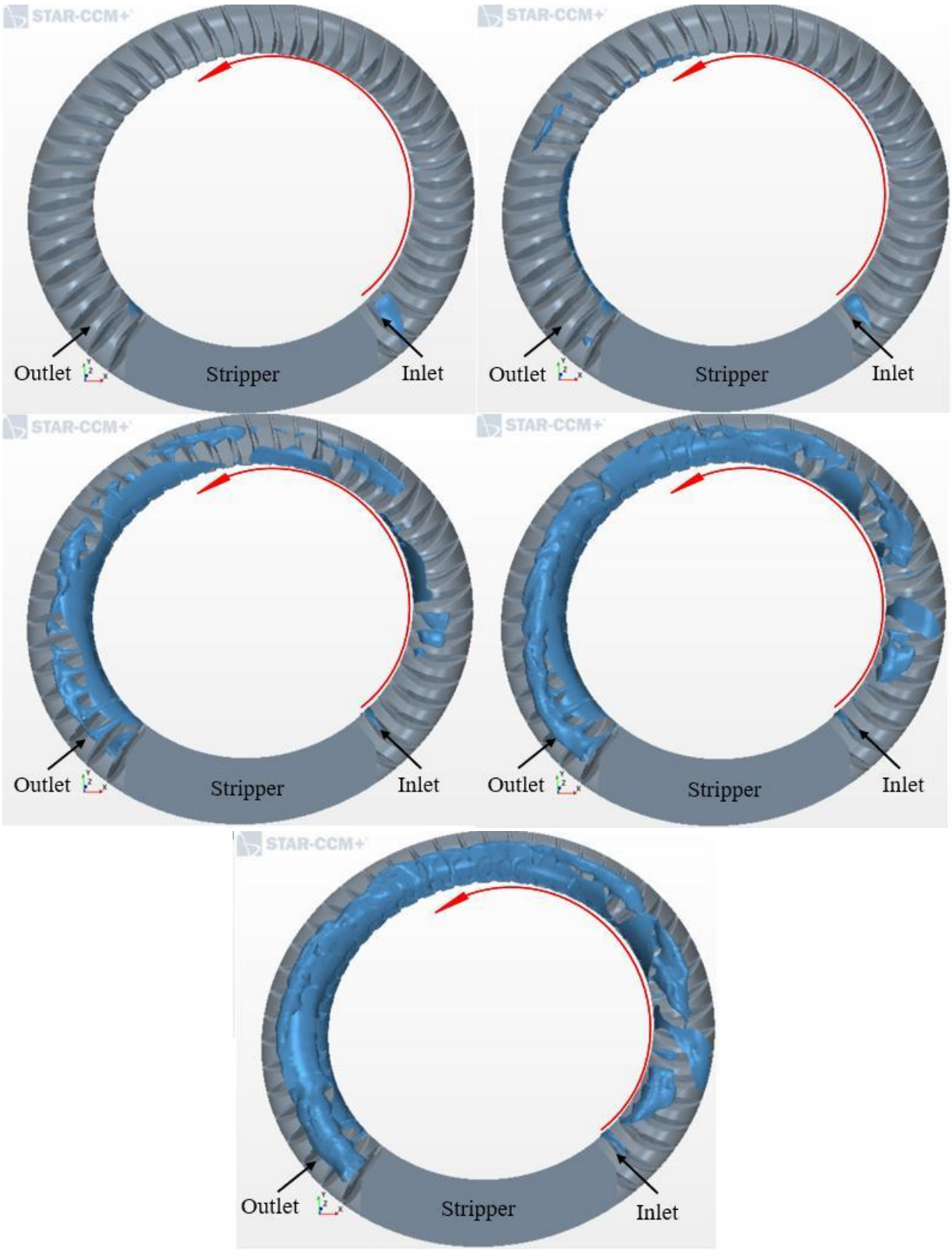

Fig. 44. separation zone in five working points at 2000 rotational speed.

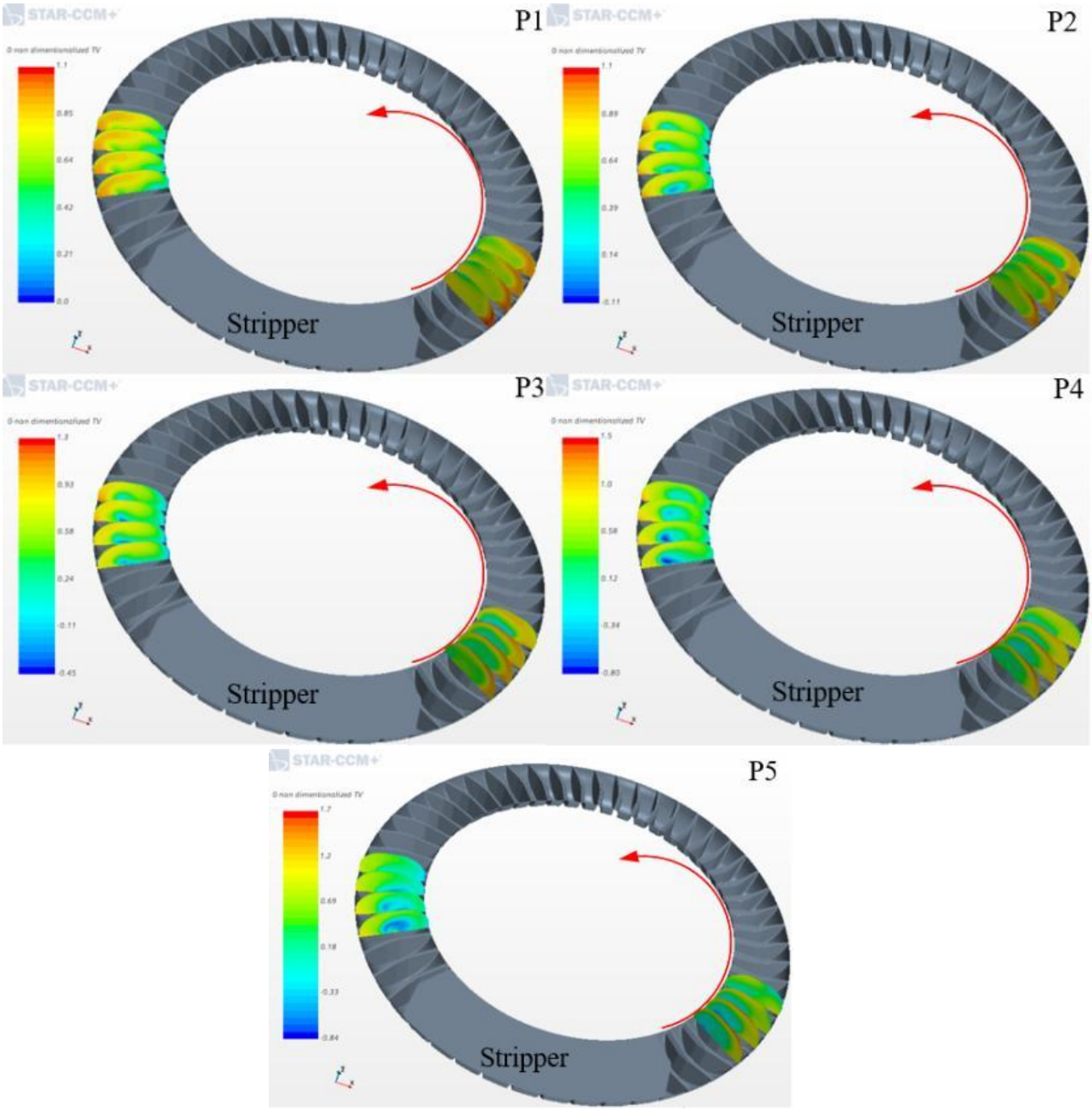

Fig. 45. Tangential velocity development from inlet to outlet at 1000 rpm for five working points.

Fig. 46. separation zone in five working points at 1000 rotational speed.

To have a better idea of separation and its effect on the efficiency the last three high-pressure working points of the 1000 rpm and last working point of the 3500 rpm, based on Ψ-Φ curves, compared. As it can

be seen from **Fig. *47*** the separation in 1000 rpm in all three Φ are bigger than the 3500 rpm study case at P5. The reason behind this difference is laid in the fact that the inlet mass flow in 1000 rpm working points is much higher than 3500 rpm working point (P5) combined with the lower rotational speed the flow starts to move backward and separates. This explains why the efficiency drops sharply at1000 rpm casing after its peak at P2.

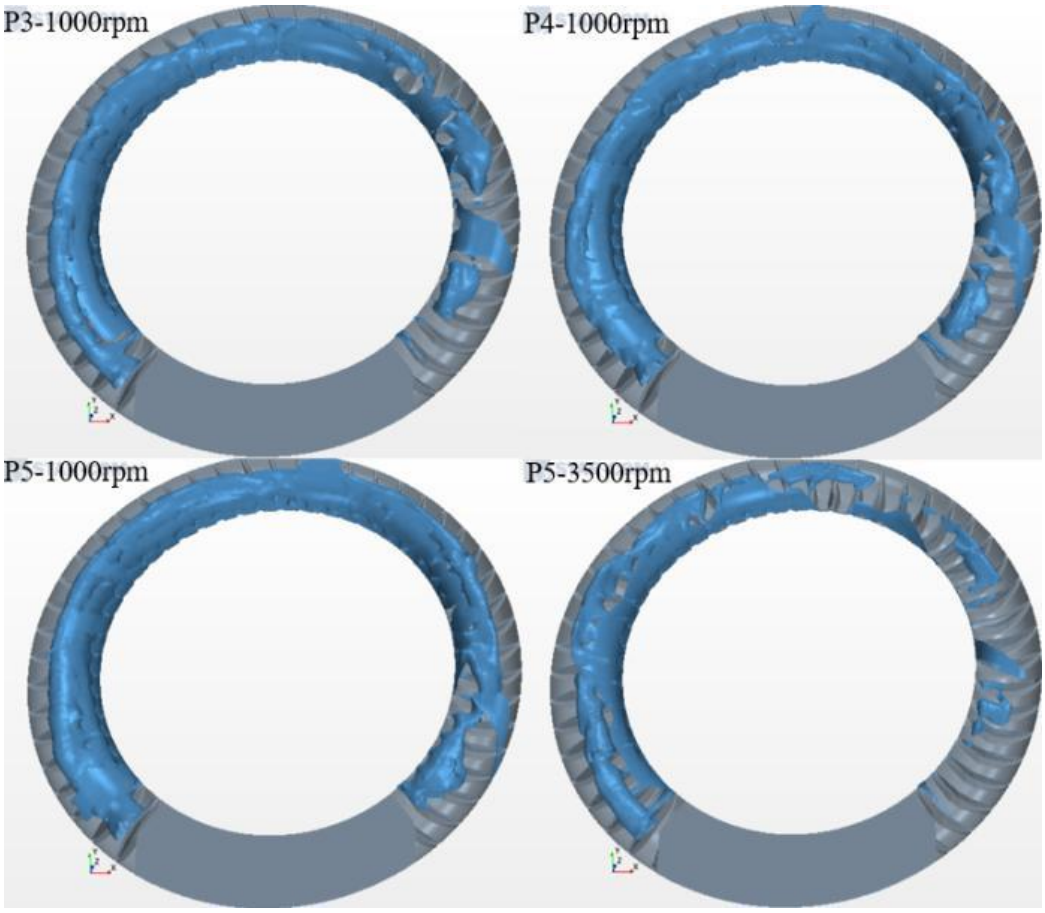

Fig. 47. comparing separation in three high-pressure working points with P5 at 3500 rpm.

As demonstrated before also for circulatory velocity it is possible to show the effect of similarity effect using tangential velocity at the same Φ for four rotational speeds. ***Fig. 48*** shows the similarity effect on tangential velocity in four rotational speeds with same range. Moreover, it shows how tangential velocity decreases moving from inlet to outlet in a coherent way in sense that in section close to outlet due to the presence of the pressure gradient, the flow starts to move backward, and negative tangential velocity developed in the center of the blades. These trend are identical for all four rotational speeds from inlet to outlet and small negligible differences in the figures have roots into the fact that they are representing instantaneous values.

Another important flow character which is needed to be addressed is development of the temperature, since in these machine pressure increases it is expected that the temperature increases accordingly but it is handy

to understand how circulatory velocity effects temperature changes and its rate. So, to better understanding of how temperature develops through these machines, a plain section perpendicular to the rotational axis considered to demonstrate the temperature distribution from inlet to outlet for all four rotational speed and five working points.

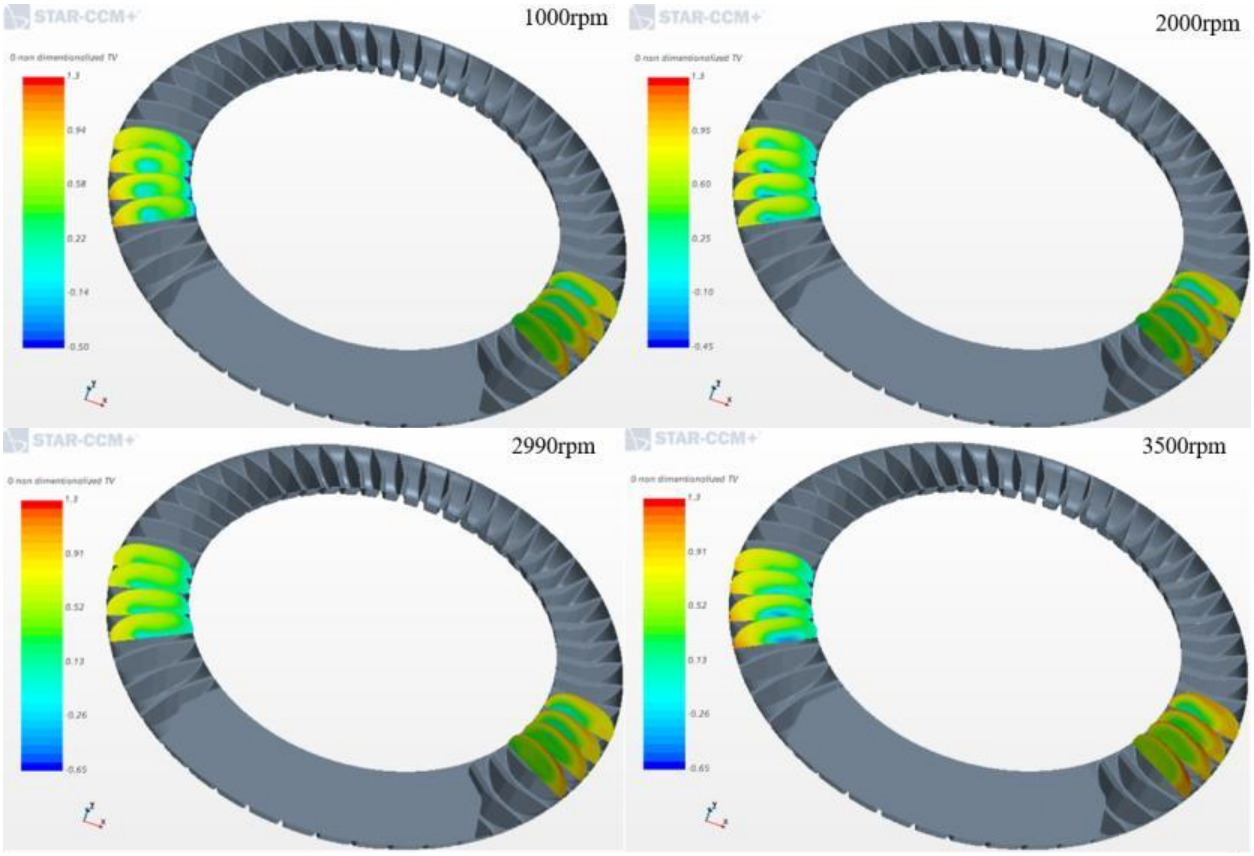

Fig. 48. Similarity effect for the tangential velocity at the same Φ=0.002 in all four rotational speed.

As the ***Fig. 49***suggests at 3500 rpm rotational speed it takes one third of the rotor, tangentially speaking, for P1 and P2 in which fresh inlet air temperature totally be affected and increase to 306 and 307 K respectively. While in P3 the fresh inlet air start to increase after one sixth of the rotor length and tops at 336 K also in P4 in needs shorter tangential length for inlet cold air to dissipate and near the outlet arrives at 348 K while at P5 in a much shorter length the temperature of cold inlet air increases and the blue region dissipates much faster compared to other working points and reaches to a maximum of 373 K in outlet. This results suggests that by increase of the pressure also the temperature rises as it was expected from ideal gas equation but here also temperature rises due to the losses in the process such as friction and turning flow and etc.

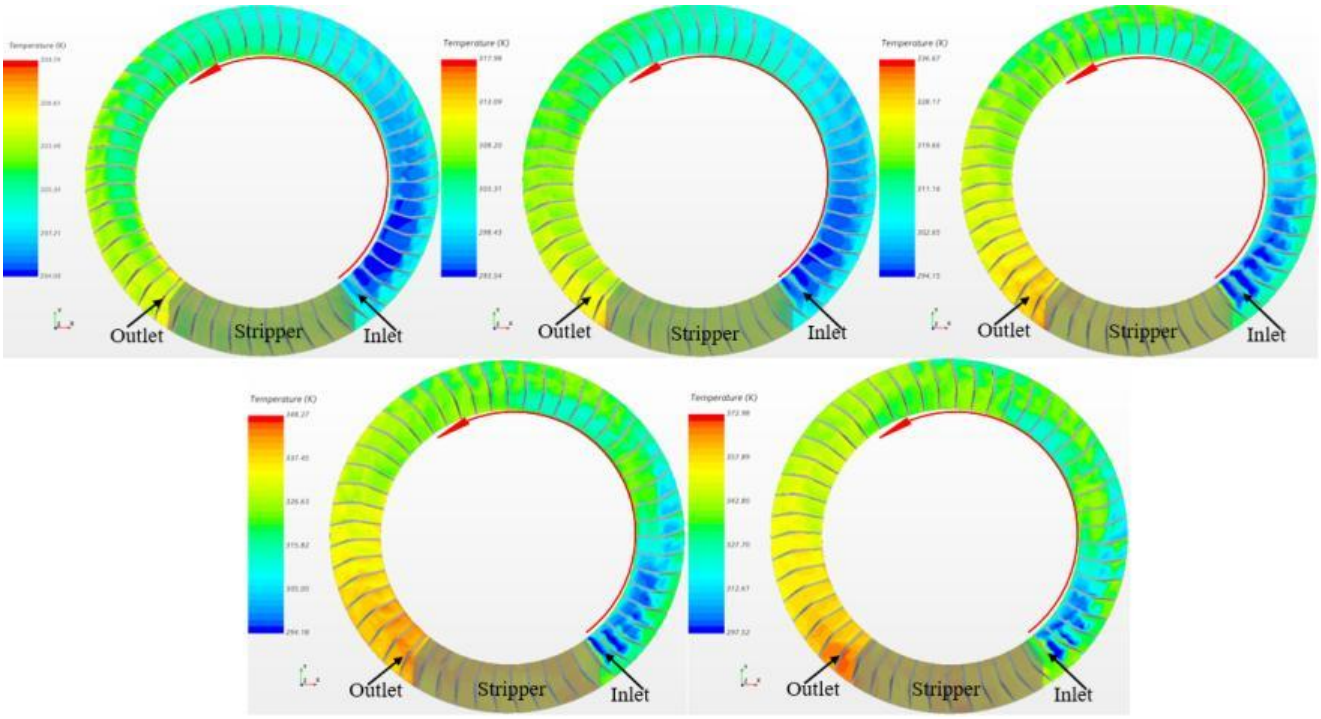

Fig. 49. Temperature distribution at 3500 rpm in all working points.

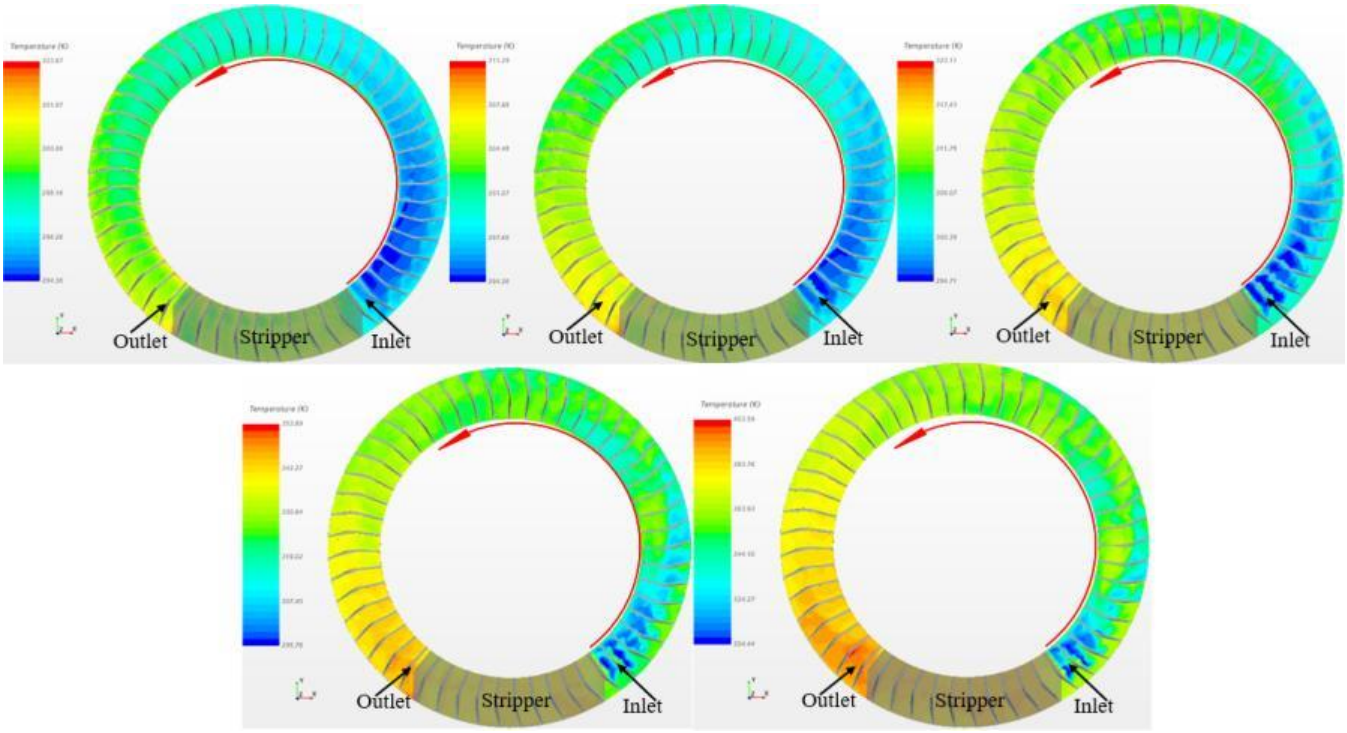

Fig. 50. Temperature distribution at 2990 rpm in all working points.

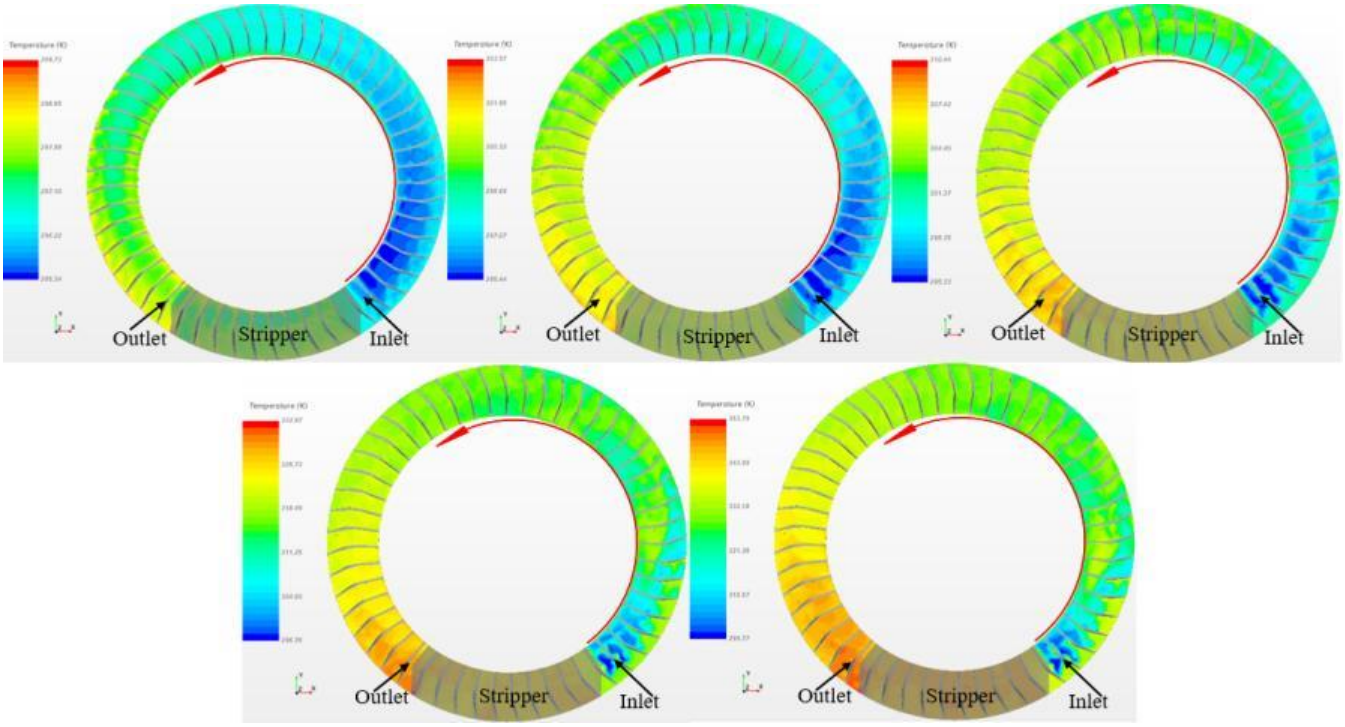

Fig. 51. Temperature distribution at 2000 rpm in all working points.

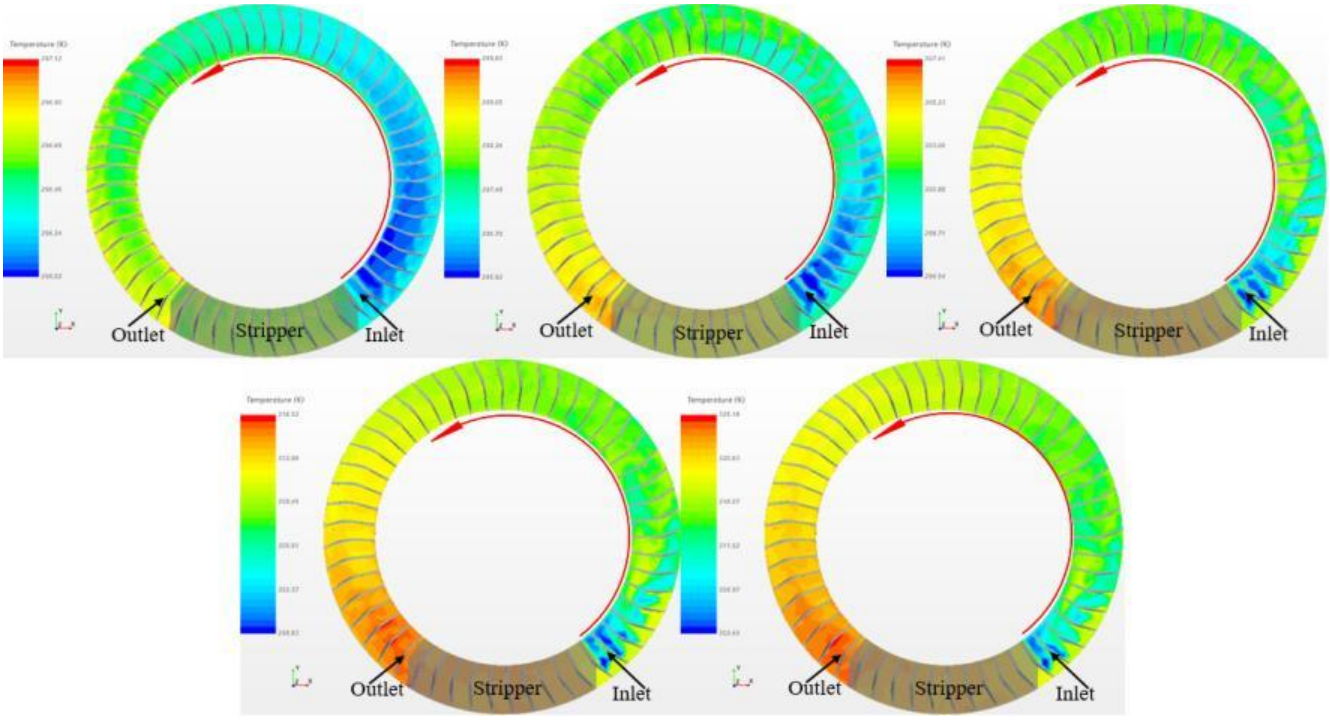

Fig. 52. Temperature distribution at 1000 rpm in all working points.

As demonstrated above, the flow field in this type of machine is very complicated and sensitive to small changes of mass flow. Hence to understand the flow development through the side channel a new method is proposed to show the results in a fully quantitative way which is not carried out by other scholars and literature, so the Idea is to follow the flow leaving one passage and entering another one by using a

streamlines to identify how a flow leaving one passage and re-entering the following passage. However, it must be noted that the streamline path considered is not a trajectory of a flow leaving a passage in time, it is a trace of the velocity in frozen instant of time. Moreover, the flow assumed to be permanent in casing and does not differ in time, which is not true, so to minimize the effect of these assumptions firstly for each passage more than one streamline were chosen to be more representative of the flow leaving the passage and then all the values for each passage along those streamlines have been measured averaged through one revolution of the machine. To that end it is crucial to locate exactly were in blade each streamline must be located and since it was known that the maximum axial velocity occurs at higher radius that region was considered for seeding point of streamlines. Since it was obvious that the flow close to the higher radius of the blade has the maximum axial speed where flow leaves the blade and enters the casing **Fig. *53***, In addition, it denotes the exchange of mass flow between the impeller and the side channel. Positive and negative axial velocity directions are distinguished by varying colors. The region shaded in red represents the outward mass flow from the impeller (+), while the green region signifies the inward mass flow entering the impeller (-). For this purpose, an average radius calculated where the axial velocity is positive through the whole rotor in all tangential locations ***Fig. 54***. Now that the location of positive axial velocity (average radius) is known, five sections, tangentially speaking, normal to the axial direction are created in the way that each section covers a blade surface. The first section starts from 50 degree, close to the inlet, with interwall of 50 degree between the sections, and the last one ends at 250 degree close to the outlet **Fig. *54***. each section was divided into equally spaced divisions in both theta and radial positions of 5 (Tangentially) and 20 (radially) segments, respectively using data post processing by MATLA **Fig. *55***. A large number of those divisions are selected in the way that the selected divisions all together cover at least 80 percent of the outgoing flow on each blade, then the number of tangential divisions for each section was calculated by MATLAB, then which resulted in 5 tangential divisions and 9 radial divisions and were used as seeding points of streamlines, which is 45 streamlines for each section **Fig. *56***. To have a well-developed flow inside the machine, one rotations of the rotor considered and then the flow features such as pressure, temperature, velocity, and density were calculated by making average values of those features on 45 streamlines for each section. The logic behind making average values of 45 streamlines for each section instead of using one streamline was to consider the flow leaving each blade as a column of flow so the results would be more representative and accurate which contains majority of the leaving flow at each blade.

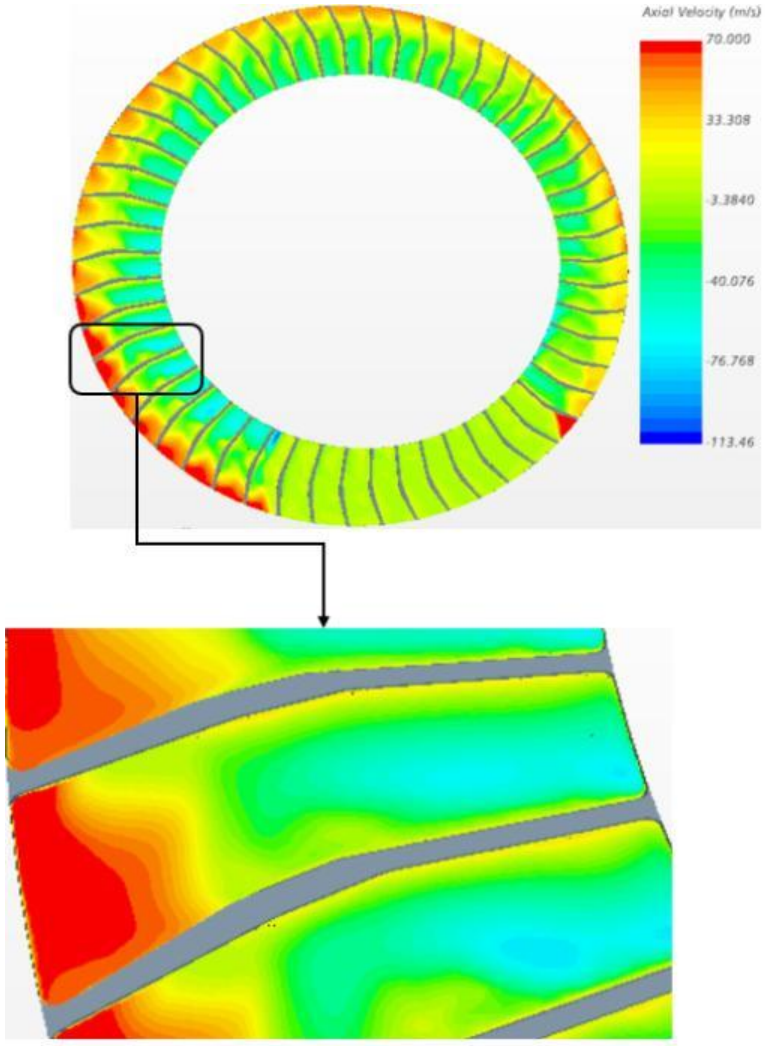

Fig. 53. Axial velocity distribution.

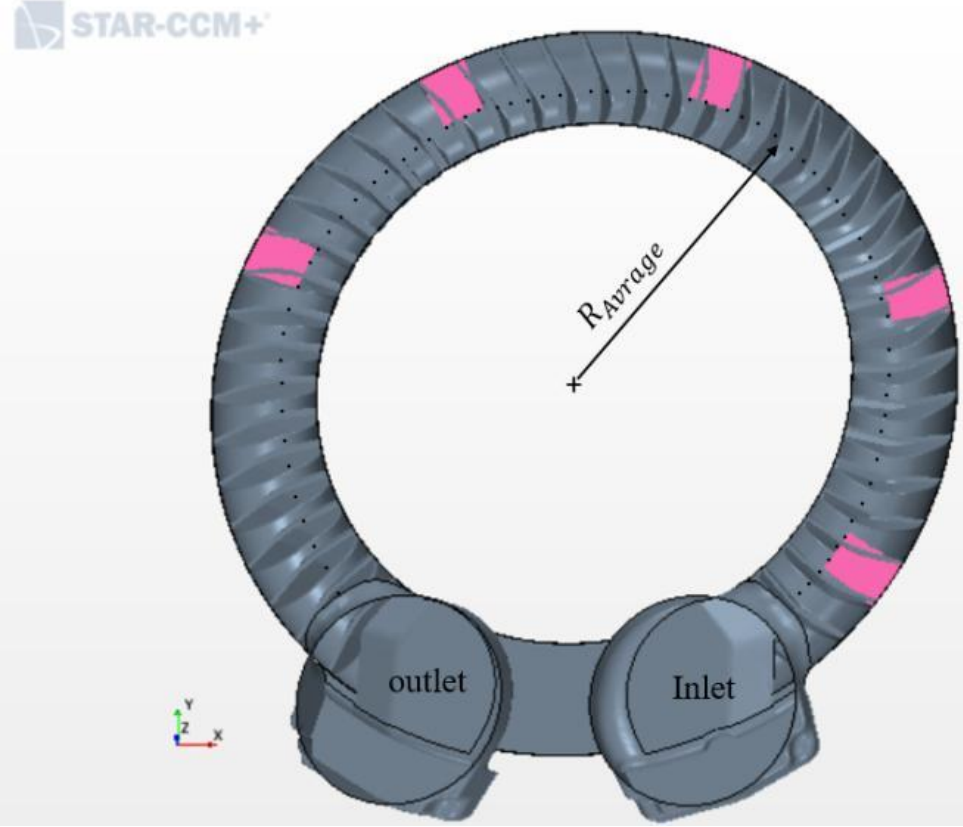

Fig. 54. Selected 5 sections and R average.

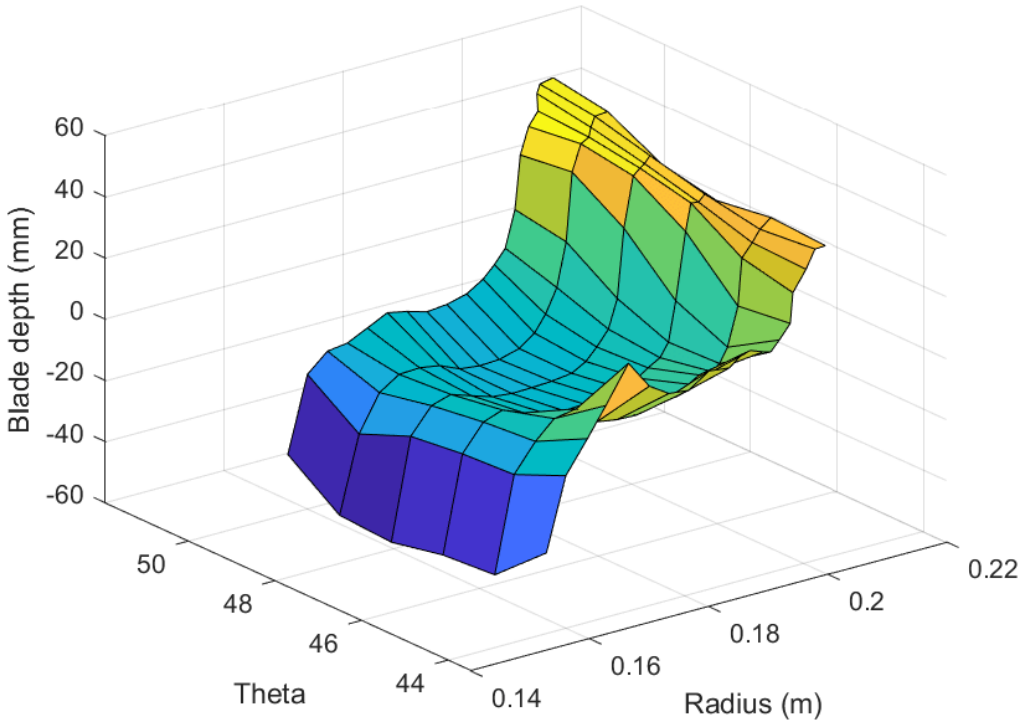

Fig. 55. The blade is divided equally in radial and theta direction.

Evaluated results showed that the streamline length getting shorter by moving from inlet to outlet and these changes were stronger in high pressure (low flow rate) working points compared to low pressure (high flow rate) working points, in the sense that the streamline length at section one in working point P1(low pressure) is three time longer that the streamline length at section one of P5 (high pressure). This pattern was common for all working points and the reason for that is an increase in circulatory velocity, which as a result increases the pressure and the flow particle passes shorter tangential distance between leaves a blade and entering the consecutive one. In **Fig. *57*** it is shown how much these lengths are changing; all the values have been averaged for each section and on all streamlines. It is clear from **Fig. *57*** that the streamline length shrinks moving in theta position toward outlet for all working points, for instance at P1 the streamline length reduces by 43 percent and at P5 reduces by 33 percent. Moreover, in **Fig. *58*** the number of blades each streamline passes between leaving the blade and entering another is depicted (left) alongside the visual graph of streamline length difference in P1 and P5.

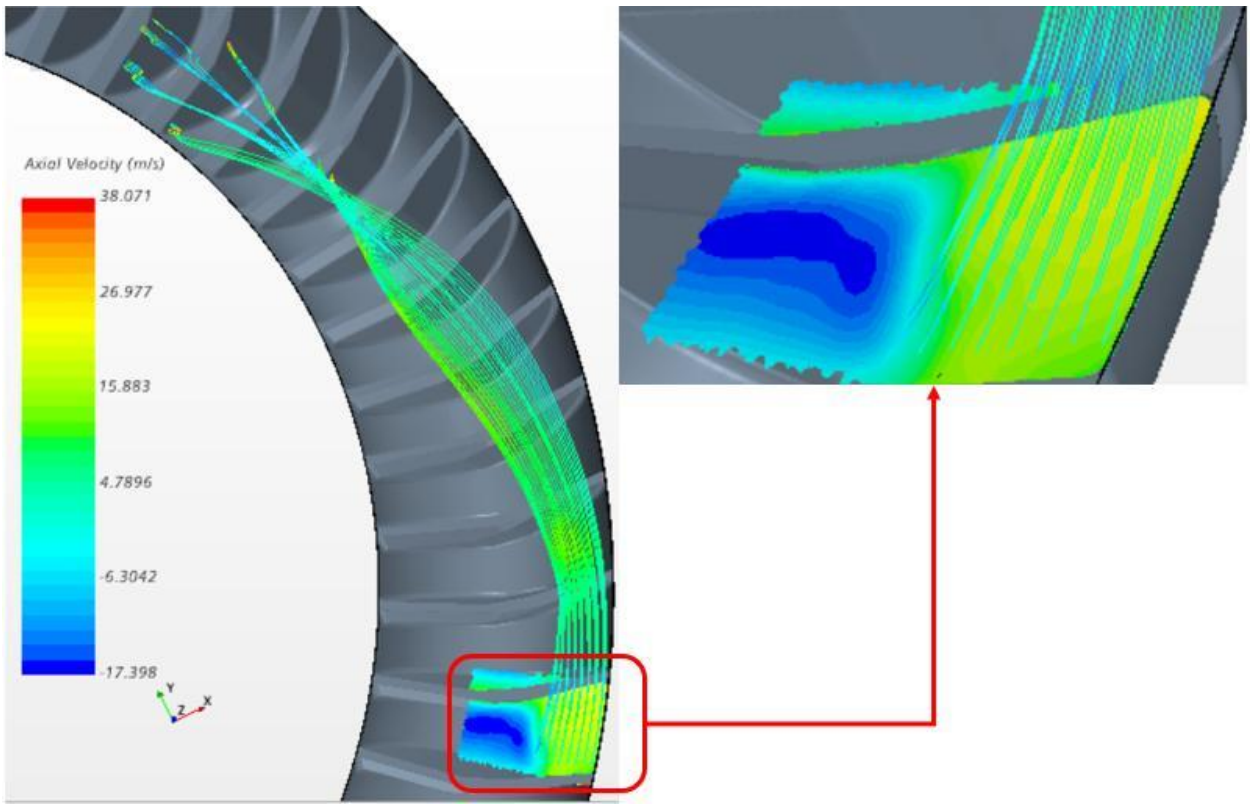

Fig. 56. 45 streamlines for the first section(left) and seeding points position of them at first section(right).

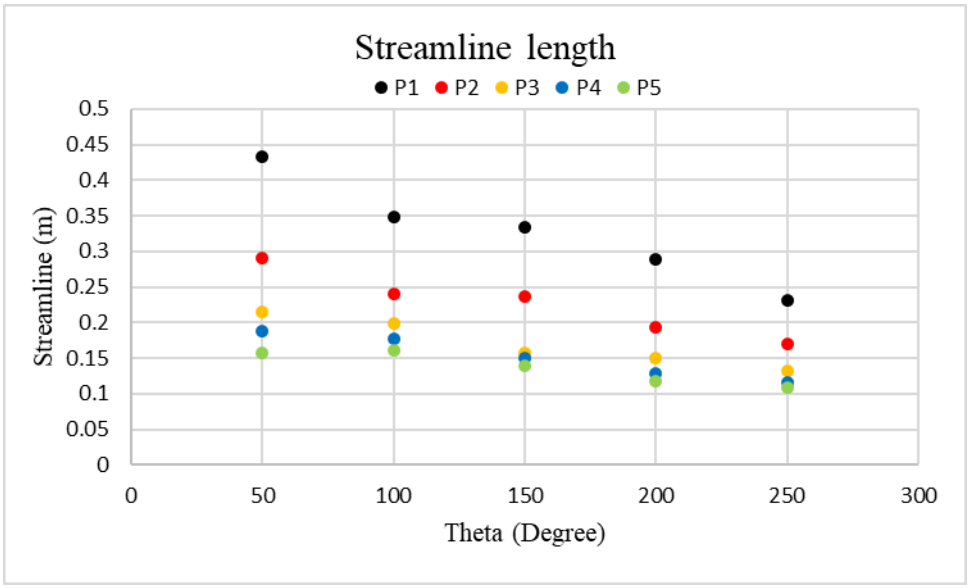

Fig. 57. Average length of streamlines at each section for five different working points.

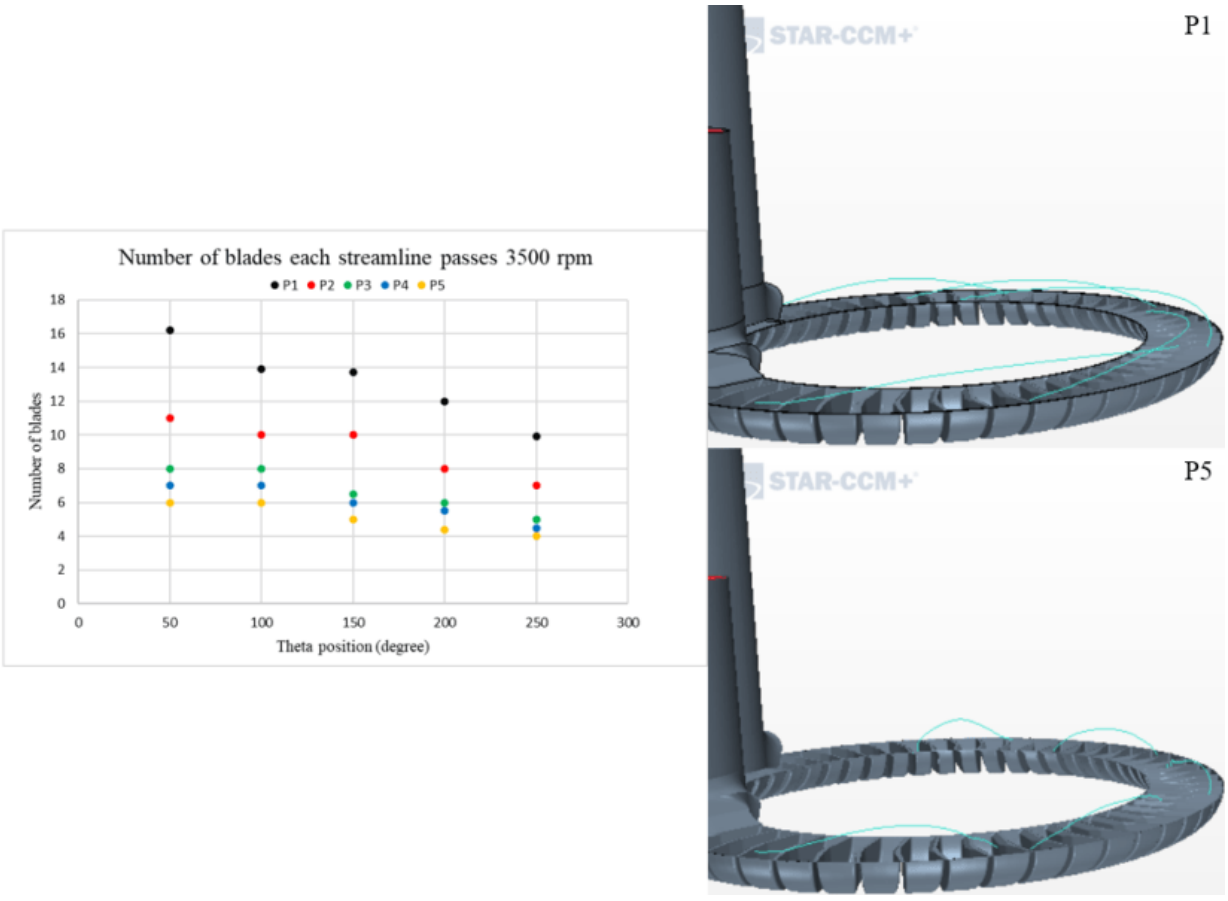

Fig. 58. Visually comparing streamline length in different working points at a fixed theta position(right) and showing the number of blades each streamline passes between leaving a blade and re-entering the following blade (left).

In the nutshell, as mentioned above, as the fluid receives energy (momentum) while it flows through the impeller and this energy is transferred to the slower fluid which is in casing (known as the annular channel) and thereby increasing its pressure hence the circulatory velocity is increased, moving from inlet to outlet

which causes much shorter streamlines and higher pressure. Hence, the higher the pressure is the shorter the streamline becomes which is due to a higher circulatory velocity, and lower tangential velocity. These latter mentioned velocities and their attribution in pressure generation will be discussed in following part:

To study how circulatory velocity is evolving from inlet to outlet, the circulatory velocity average on streamlines for all working points and the five sections depicted in **Fig. *59***. Data shows that the circulatory velocity's maximum constantly increasing going from working point P1 to P5, and also from section 1 to section 5 which are higher pressure working points and sections.

Every time the fluid passes through the rotor, receive the work from the rotor and energized goes to the next blade to repeat this cycle, this repetitive cycle with centrifugal for that rotation provides makes the circulatory velocity to increase.

On the other hand, Tangential velocity shows opposite trend in respect to the circulatory velocity in the sense that, with increase of pressure and moving from inlet to outlet the tangential velocity decreases the reason for that could be explained as follows **Fig. *61***. Instead of a row of stator blades as in a traditional turbomachine, the tangential velocity is reduced by the action of a tangential pressure gradient along the machine's perimeter between the exit conditions and the inlet circumstances. As a result, when the fluid enters the blade row again, its tangential velocity will have decreased, and its direction will have changed. As a result, during each loop of the spiral, the fluid is both decelerated by the tangential pressure gradient and propelled in the tangential direction as it passes through the blades in the channel's bladeless (casing) portion. Moreover, in **Fig. *62*** it is shown that the tangential velocity decreases for different working points and sections. The circulatory velocity in all working points starting from almost 80 m/s and but, the values continuously reduce in each section by moving up toward higher pressure (low flow rate) working points. However, at working points of P1 and P2 since the pressure raise in not high, the tangential velocity does not fluctuate that much and their maximum and minimum values almost stays in a constant range, but for higher pressure working points the minimum value at each sections gets lower and lower from P3 to P5 respectively.

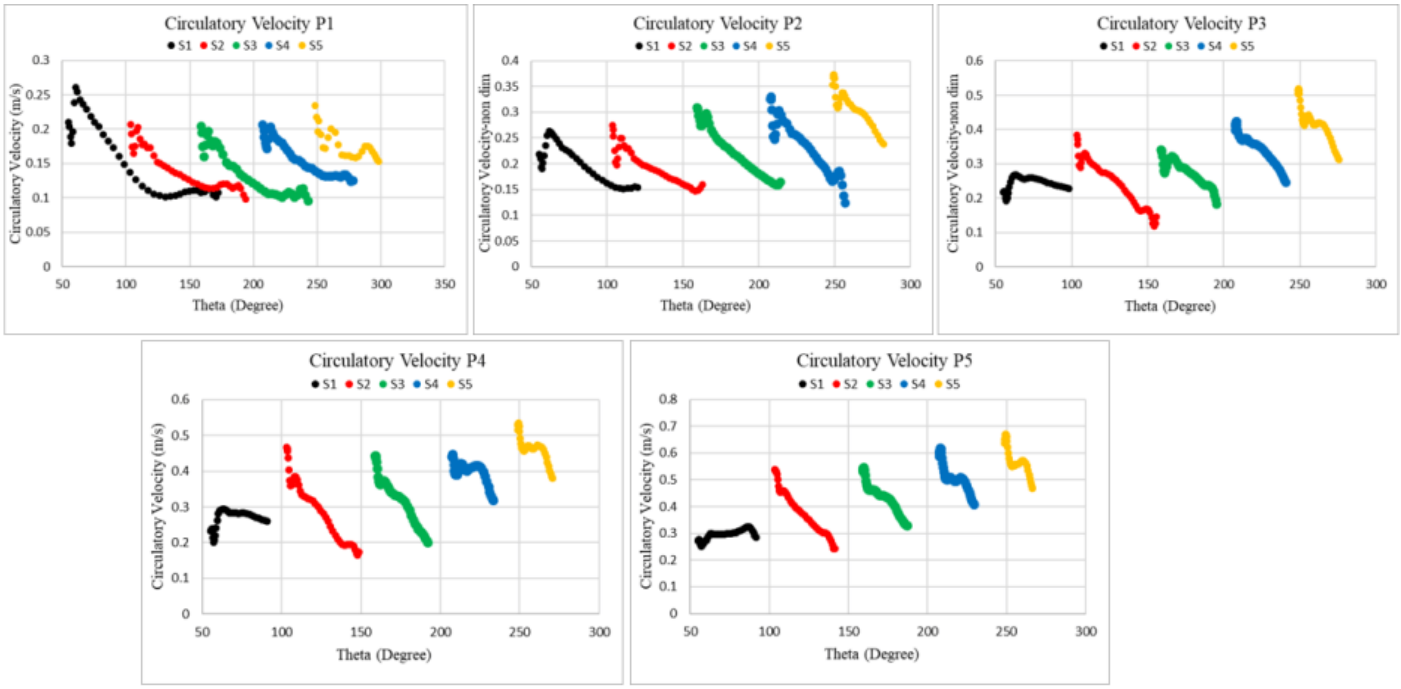

Fig. 59. Circulatory velocity for each working points and at five sections.

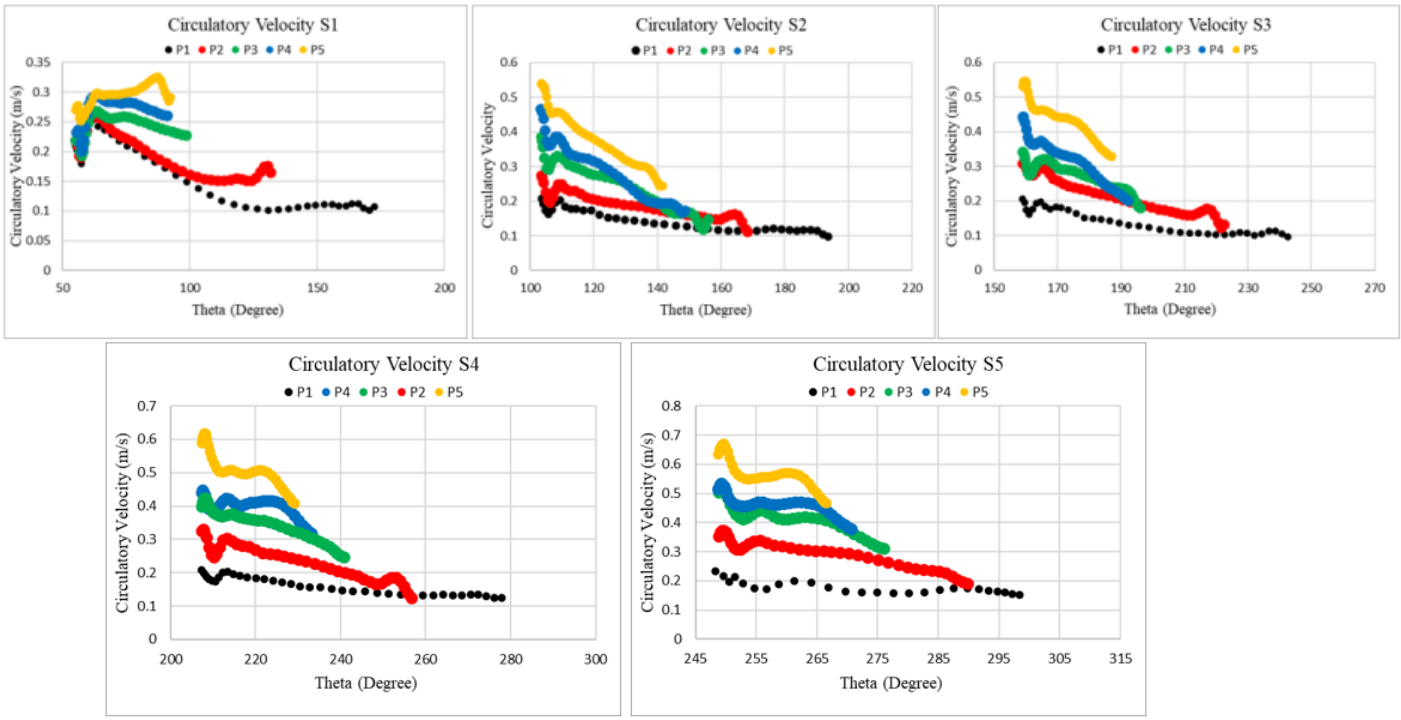

Fig. 60. Circulatory velocity for each section for all working points.

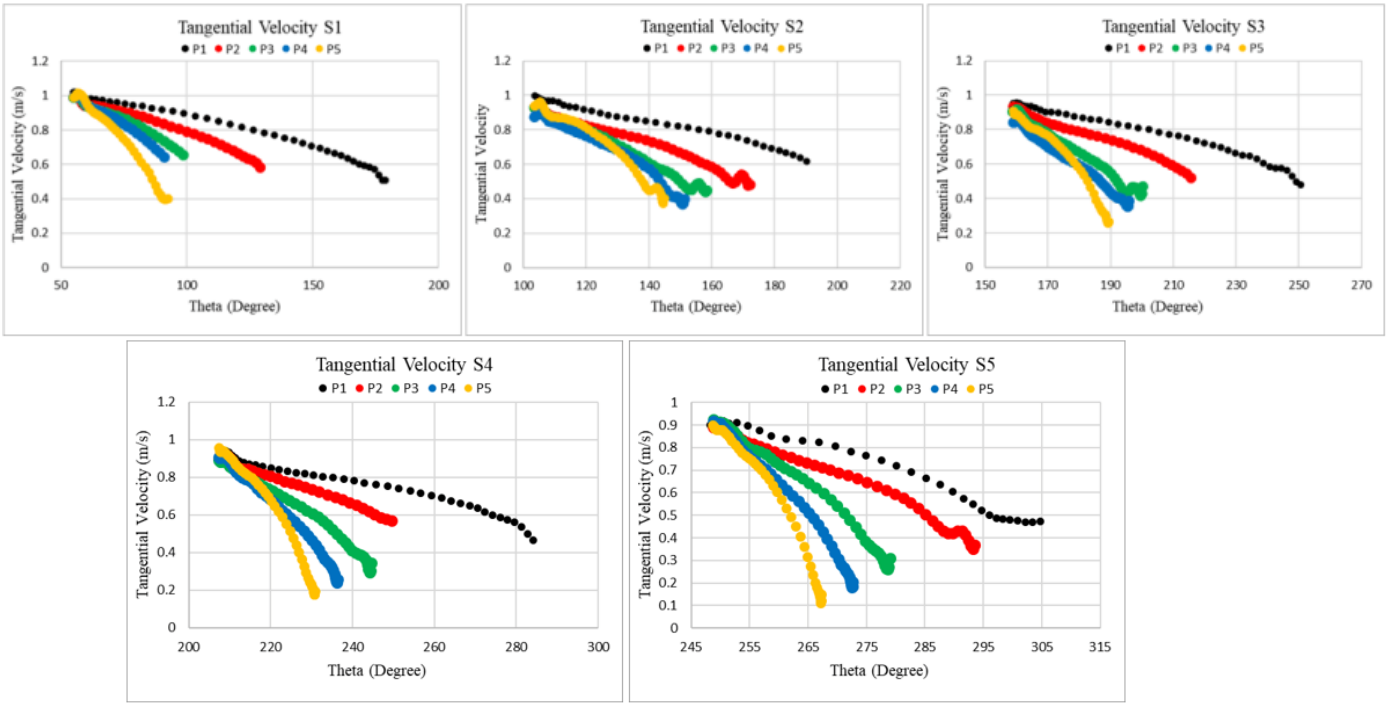

Fig. 61.Tangential velocity distribution against theta position at each section for five working points.

Moreover, joining the pressure graphs **Fig.** ***63*** for the same number of working points and sections shows the continuous trend of pressure raise in those sections and direct correlation between circular velocity and the pressure rise. Because the flow passes through the same blade row several times between the entry and the exit, the work done on it and hence the pressure increases and by each circulation of flow from next blade the circulatory velocity also increases. In these machines the pressure rise is considerably greater than that which can be obtained from a conventional turbomachine with the same tip speed. The specific speed is therefore low, and the machines operate in the usual range of positive displacement machines.

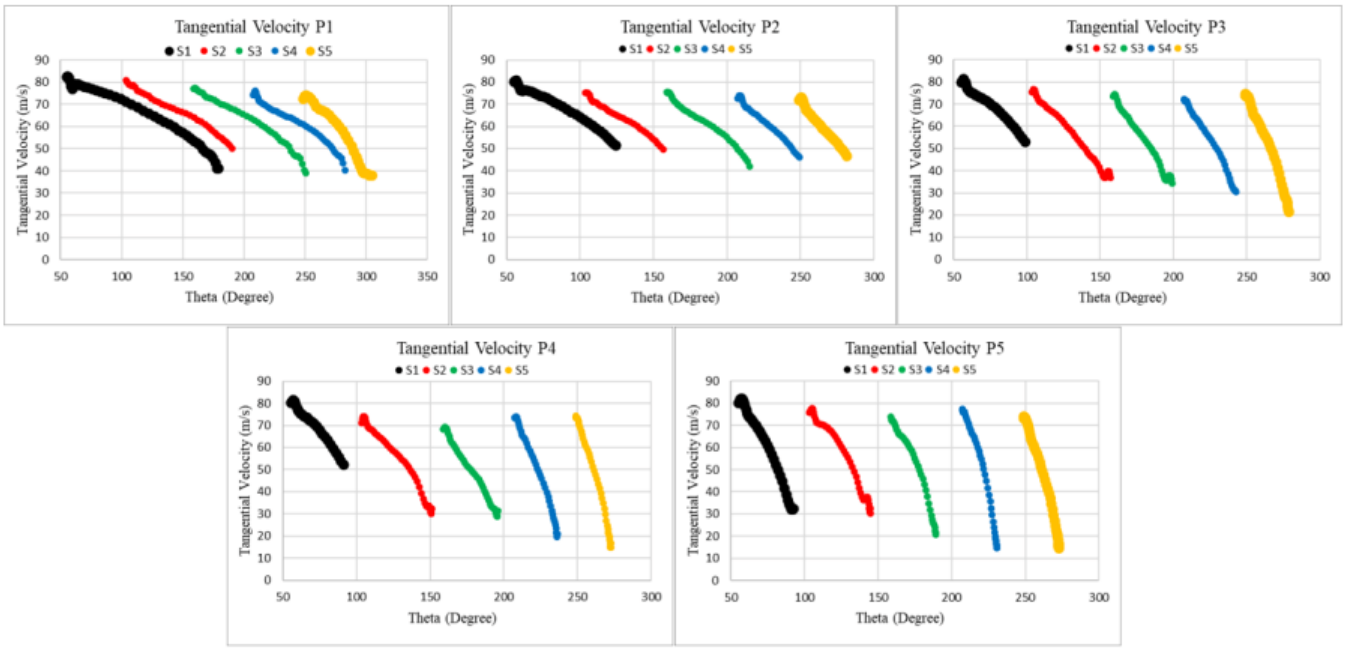

Fig. 62. Tangential velocity for all working points and at five sections.

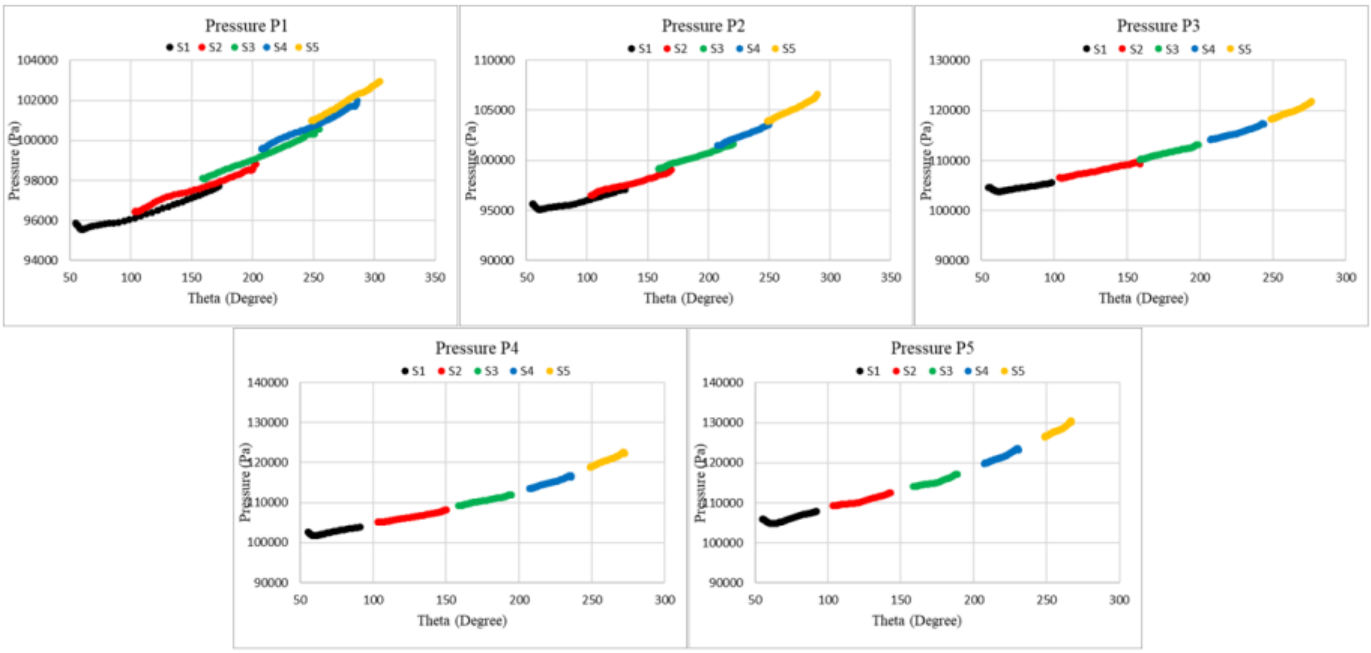

Fig. 63. Pressure rises in five forking points at five different sections.

4.2 E08 results with other rotational speed.

Since here the results of E08 with 3500 was reported, to see how and how much rotational speed will affect efficiency of a RFC when geometry is the same. Hence, the STD & UNSTD simulations for three rotational speeds (1000, 2000, and 2990 rpm) were done. As the results suggest the same trend as E08 3500 rpm is

repeated for the other rotational speeds in the sense that the efficiency is maximum at p2 which is low pressure point and by moving toward high-pressure working points efficiency drops **Fig. *64***. P1 in all of the rotational speeds has the lowest pressure and lowest efficiency because it is very close to the choking point of the machine. As illustrated earlier, in this type of machine the relation between pressure and efficiency is indirect. Moreover, it can be seen that the STD simulation at the design point (P4) and higher-pressure working points is slightly closer to experimental ones.

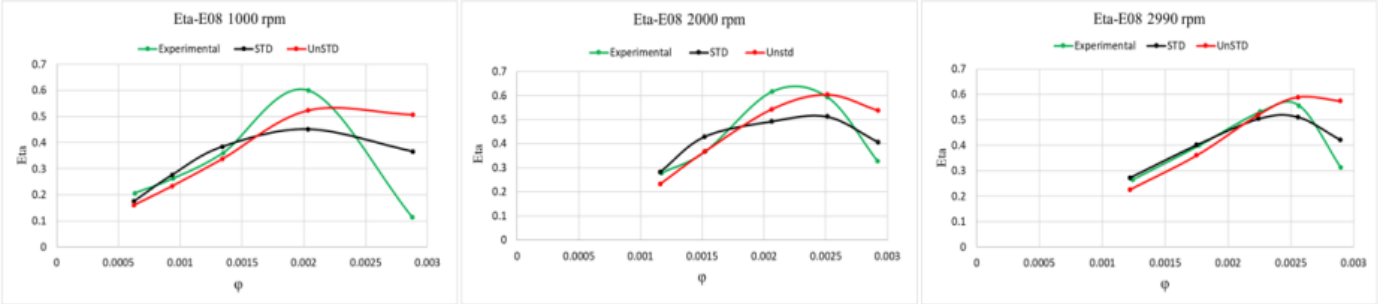

Fig. 64. efficiency of E08 geometry with rotational speed of 1000, 2000, and 2990 rpm

Considering **Fig. *64*** and **Fig. *30*** (efficiency of E08 at 3500 rpm) based on experimental results that peak efficiency at 1000 and 2000 rpm, is 60 percent and in 2990 rpm is 57 percent while at 3500 rpm is 50 percent. Which means efficiency drops by 10 percent by moving from 2000 to 2990 rpm and further drops at 16.7 percent for 3500 rpm in respect to the efficiency of 1000 rpm rotational speed. In **Fig. *65***, the pressure ratio that each machine produces at different rotational speed which indicates that by doubling the rotational speed from 1000 to 2000 rpm the pressure increased by 9.5 percent at design point and at the same point for 2990 and 3500 rpm the pressure increases by 20 and 24 percent respectively, while efficiency drop by 10 percent. This shows that even at modest flow rates, a somewhat substantial pressure rise can be achieved. This is as a result of a faster circulation velocity at a lower flow rate, which causes a bigger pressure rise. However, at low flow rates, more electricity is also needed. Regenerative turbomachines operate at their most efficient levels at comparatively high flow rates.

Moreover, it is clear from **Fig. 66** that in these machines with an increase in the rotational speed, and consequently pressure, the temperature also increases considerably. Below the non-dimensionalize temperature, divided by initial temperature, plotted against Φ, and shows by increase of the rotational speed of the machine from 1000 to 2000 rpm for low pressure working points the temperature is not changing much but in last two high pressure working points the temperature increases 4 and 7 percent in P4 and P5 respectively. Moreover, by increasing the rotational speed of the motor to 2990, the difference multiplies even more in the way that in the first two working points pressure is slightly higher in compare with first geometry (E08 1000 rpm) but at third working point the temperature is equal to temperature of fifth working point at first geometry. Also, the last two working points witnessing a 9.5 and 17 percent at P4 and P5 Respectively. And with increasing the rotational speed to 3500 the temperature increases 1, 8, 11, and 16 percent at P2, P3, P4, and P5 respectively. This increase of the temperature which accompanied by increase

of the pressure and rotational speed mostly is result of friction loss and circulatory losses in the machine [1].

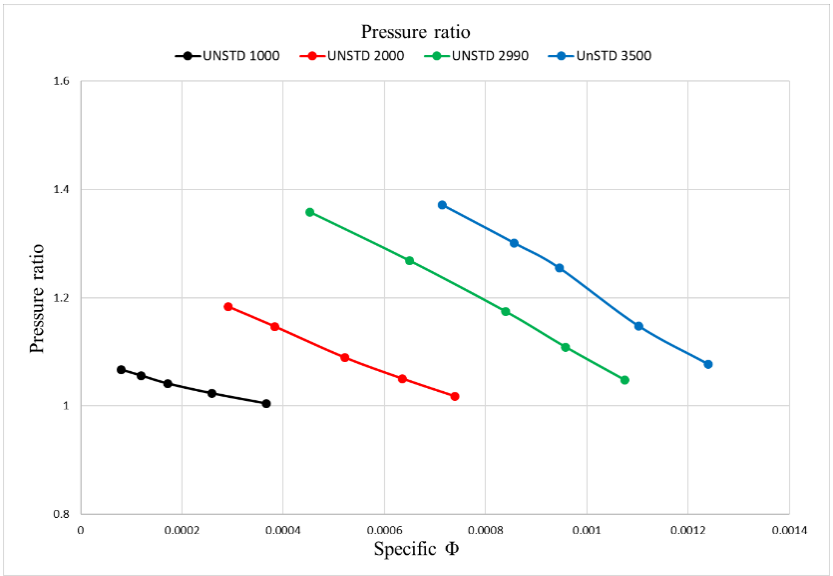

Fig. 65. Pressure ratio against the specific mass flow for all rotational speeds.

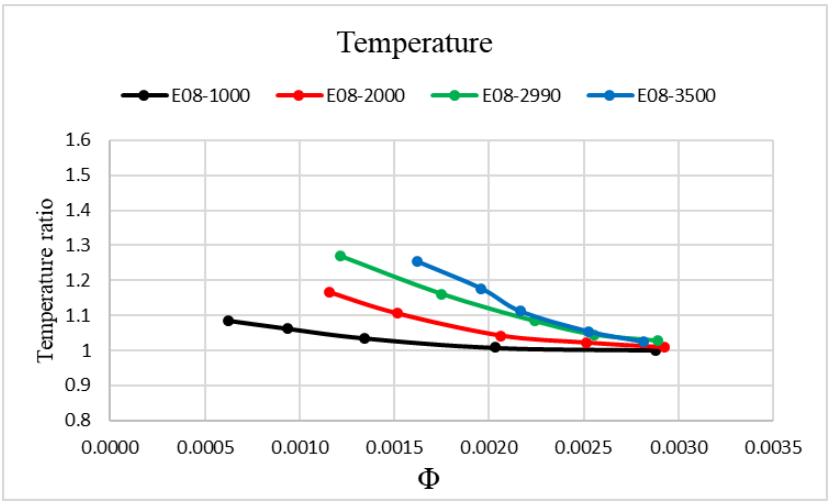

Fig. 66. Temperature ratio for different rotational speed of the E08 geometry.

4.3 STD & UNSTD difference

As shown above the steady simulation results were closer to the experimental data especially at high pressure working points (low flow coefficient) however the expectation at the beginning of this study was that the unsteady simulation results to be closer in experimental data since the unsteady simulation considers the circulatory effect of trapped flow. This phenomenon can be explained from different views and reasons which are brought as follows:

- Since the STD model is a frozen rotor state simulation, does not consider the effect of circulatory flows which trapped between blades and directly effects the incoming flow from inlet. At high flow

coefficients, the flow rate of the stripper leakage is low, and effects are relatively low. Vice versa, at low flow coefficients, a large fraction of the entire internal flow rate passes through the stripper leakage (100% at shut-off conditions) and large fluctuations of the entire flow rate are generated [64, 66, 67]. The way this works is that a small high pressure and temperature, compared to inlet flow, outlet flow ejects into the inlet through the existing gap between the impeller and the stripper and creates a blockage in machine which result in higher loss and has a detrimental effect on the performance of the machine, this kind of loss is called carryover loss or circulatory loss. However, in unsteady simulation the effect of this carry overflow considered but seems like it is overestimating it and make the pressure result at high pressure working points deviate a little more from experimental data in respect to steady simulation results.

- Another reason for such a difference is ascribable to the well-known limitation of the steady RANS approach in predicting the proper flow structures in the base region downstream of the blades. The blunt trailing edge generates large unsteady flow structures that affect the aerodynamics of the side channel and consequently of the impeller since the flow has a helical behavior. Such effects are not reproduced by steady RANS. Hence, the energization of the flow in the steady case is considerably higher thus resulting in a higher pressure rise of the machine [64], [67].
- To make this difference visually more clear **Fig. *67*** shows that how the hot carryover flow that comes from outlet section to inlet section through the stripper, and effects the cold and fresh incoming flow from the inlet and in result disturbs flow development in the unsteady simulation (left) while at steady simulation there is no incoming hot carryover flow to mix with the inlet flow and disturb the flow propagation in the machine (right). Hence, the steady simulation faces with less temperature changes and in result the flow gets more energized in respect to unsteady simulation and shows higher pressure.
- **Fig. *68*** Shows the temperature distribution on a plain section on the rotor to provide another view of how the carryover flow through the stripper affects the incoming cold flow from inlet and flow development across the machine. As can be seen in the steady simulation (left) the inlet flow does not affect by the hot flow under the stripper, so temperature of the flow gradually starts to increase as the flow moves through the machine and after almost passing through the one fourth of the rotor temperature sees a noticeable change in temperature. Meanwhile in unsteady simulation for the same geometry and same working points the incoming flow immediately affected with hot carryover flow from the stripper and the temperature increases much faster and in much shorter tangential length.
- In other hand, since the design point in the efficiency curve matches the experimental one, this small discrepancy could be attributed to certain weaknesses of the URANS model in predicting the real separation and vortices size and dissipation. Indeed, like many two-equation turbulence

models, the k-omega SST model assumes isotropy of turbulence, meaning it assumes that turbulence behaves the same in all directions. However, in cases where the turbulence is highly anisotropic (i.e., turbulent structures have different characteristics in different directions), the model may not provide accurate predictions of the dissipation of eddies. Furthermore, the k-omega SST model may not perform well for flows with tight curvature, such as flows around a sharp rotating ring with a highly curved surface. In such cases, the model's assumptions and transport equations might not fully capture the complex turbulent behavior. It can be concluded that for a such a 3D and unsteady flow in regenerative machines, the model overpredict the turbulent production, especially in adverse pressure gradient regions, leading to an overestimation of losses in the machine so it deviates from the experimental results more compared to steady simulations. It worth mentioning that if considered only the first three the results acquired from STD and Unstd are quiet close, however from 4th working point (design working point) the real deviation stars and in the 5th working point the difference maximizes.

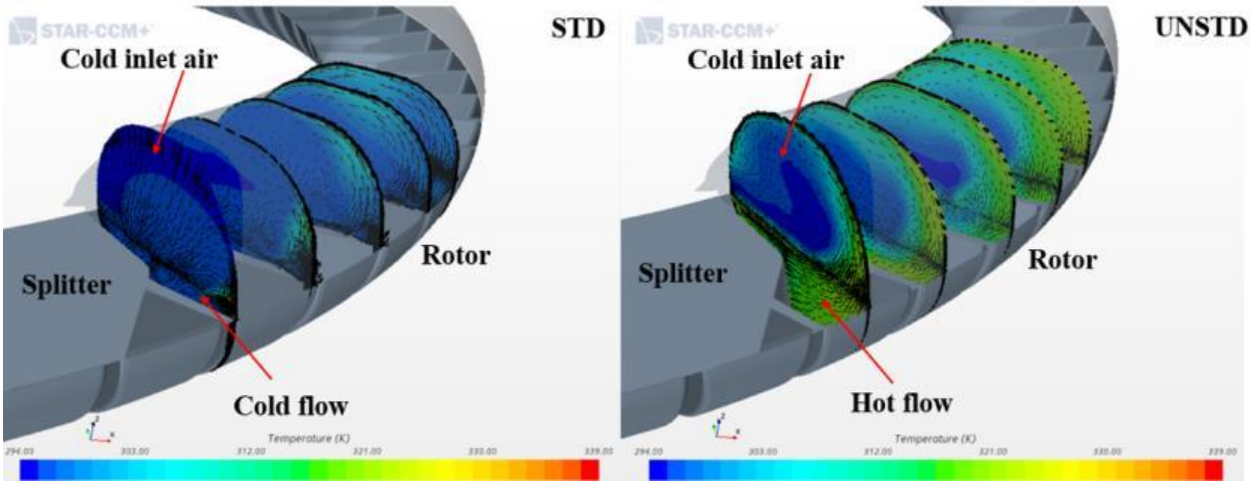

Fig. 67. effect of carryover flow on mixed temperature in steady (left) and unsteady (right) simulation.

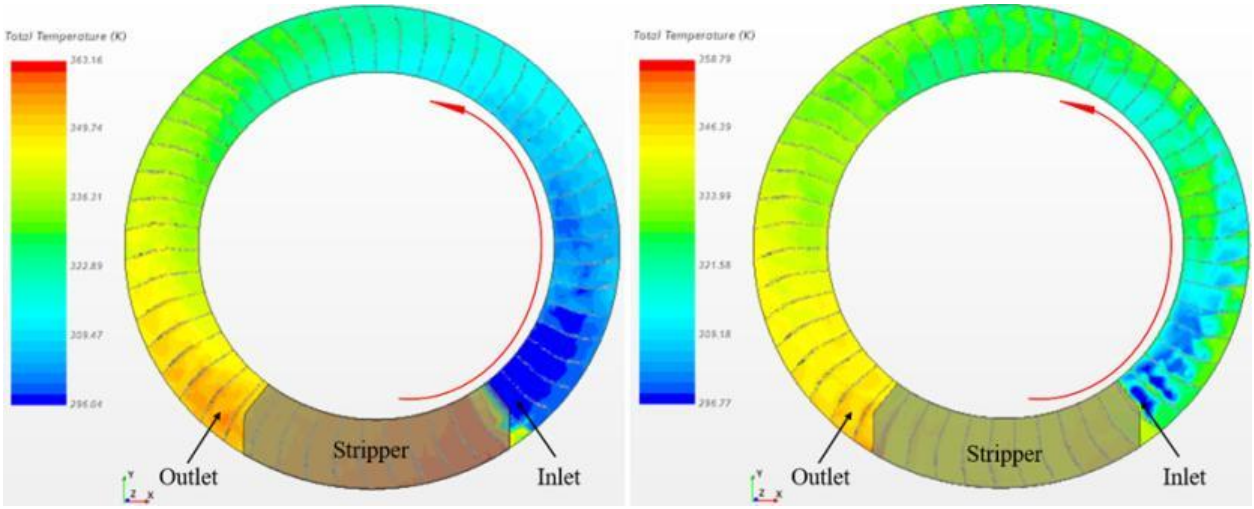

Fig. 68. Temperature distribution on axial plane in rotor STD (left) and Unstd (right).

5 Geometry

Geometry sensitivity analysis plays a pivotal role in the optimization and enhancement of regenerative fan compressors, particularly concerning the comprehension of the geometry's influence on efficiency. In the realm of regenerative fan compressors, where performance metrics such as efficiency are paramount, dissecting the impact of various geometric parameters becomes imperative. Through sensitivity analysis, researchers can discern which specific aspects of geometry wield the most substantial influence on efficiency. This elucidation not only facilitates a deeper understanding of the underlying mechanisms governing compressor performance but also guides targeted design modifications aimed at maximizing efficiency. By pinpointing critical geometric parameters, such as inner radius, depth of rotor, or stator configurations, sensitivity analysis empowers practitioners to iteratively refine compressor designs, thereby unlocking optimal performance levels. Ultimately, the integration of geometry sensitivity analysis into the design and optimization process of RFC's combining with flow characteristics in these machines, serves as a cornerstone for advancing efficiency, reliability, and overall performance in these crucial machines.

Hence, in this section the effect of geometry changes will be discussed for 12 geometries in which the rotational speed is constant at 2900 rpm. The characteristic curves, efficiency and of these machines will be compared and discussed as a sensitivity analysis to evaluate which geometrical parameter is affecting the performance of the machine. As mentioned in the previous chapter (4) due to the over prediction of losses in Unstd simulation and the fact that the STD simulation results are closer to the experimental measurements in this chapter in which the simulation goal is to highlight the effect of RFC geometric parameter effects on performance, it was decided to use the STD simulation results instead of Unstd results. In table 4 the specification of each geometry is introduced. The concept behind these changes is to keep the outer radius of the geometry constant and change the three parameters that includes:

- Inner diameter of the geometry, which affects the height of the rotor and stator,
- Depth of the Rotor (W_R)
- Depth of the Stator (W_S)

Fig. *69* shows the location of the constant and variable parameter of the geometry. Based on the changing parameters, these geometries were divided in four different groups of for geometry:

1. C01, C02, C03, C04
2. C03,C05, C06,C07
3. C01-C08-C09
4. C01-C110-C11-C12

As it can be seen some geometries belong to more than one family since each time only one parameter changes geometries can belong to more than one geometry.

The reason for such a selectin were in family group of one, all the parameter were constant only the inner radius was changing, for family group of 2, the only variable parameter was the depth of the stator while the inner radius was kept 288 mm, and for the third family group while the inner radius was kept constant at 300 mm the depth of the stator changed. However, for the last family group while the inner radius was kept constant at 300 mm the rotor depth changed.

Table 6. Geometries specifications.

Geometry	Depth of Stator W_S (mm)	Depth of Rotor W_R (mm)	Outer diameter of casing $2R_2$ (mm)	Inner diameter of rotor $(2R_1)$(mm)	Rotational speed rpm
C01	28	28	430.46	300	2900
C02	28	28	430.46	294	2900
C03	28	28	430.46	288	2900
CO4	28	28	430.46	276	2900
C05	30	28	430.46	288	2900
C06	32	28	430.46	288	2900
C07	34	28	430.46	288	2900
C08	30	28	430.46	300	2900
C09	34	28	430.46	300	2900
C10	28	30	430.46	300	2900
C11	28	32	430.46	300	2900
C12	28	34	430.46	300	2900

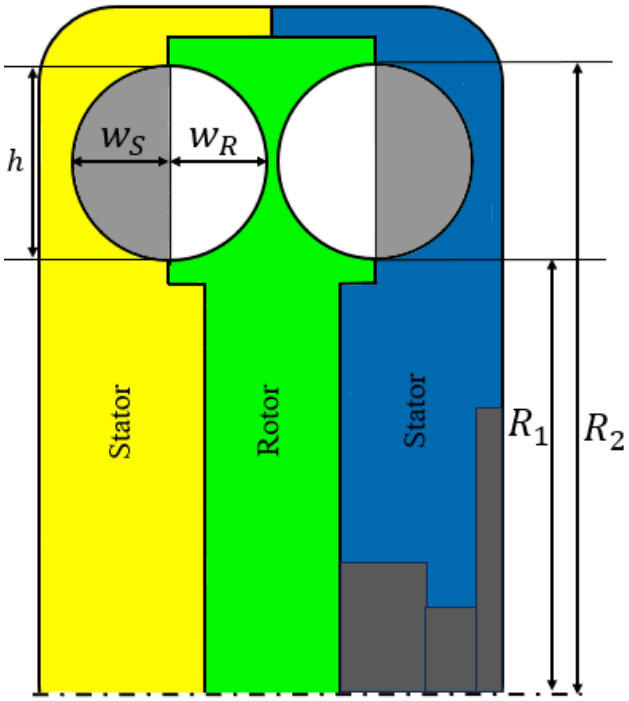

Fig. 69. the constant and variable parameters of the geometries.

5.1 Results and discussion

5.1.1 First family of geometries

The simulation results of the geometries are belonging to the first family are presented as follows. Configurations C01,C02,C03 and C04 have different inner diameter ranging from 300, 294, 288, and 276 mm respectively but the outer diameter for all of them kept constant at 430.46 mm.

Fig. 70 and **Fig. 71** show the effect of blade height (h) which here is controlled by variation of inner radius, on pressure and the efficiency of the machine, respectively. it can be seen from **Fig. 70** that the maximum pressure ratio is achieved with C04 where the inner diameter was smaller (largest h), and at low flow rate working point, also it shows that by increasing the inner diameter after a certain value the amount of the pressure ratio does not change that much. in another word with increasing the width of the blade (h) by 8.7 percent (difference between C01 and C04), the pressure ratio increases by 2 percent.

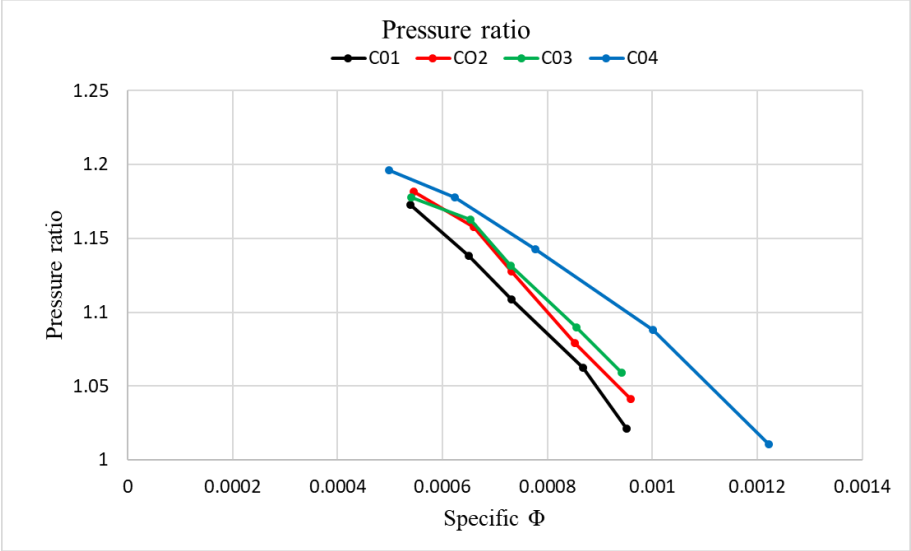

Fig. 70. Comparison between pressure ratio of geometries of family one.

Fig. 71 shows that, as it had been seen before in E08 geometries, where the pressure rise is maximum the efficiency is minimum. This trend can be seen in all working points of all four members of the first family. For instance, the C01 produced the lowest pressure ratio at all working points regarding the other three geometries, however it has higher efficiency at all working points in regard to the other three. The hierarchy in **Fig.** ***70***is reversed in **Fig.** ***71***for efficiency as it was expected from these machines. the efficiency of the C01 at the working point with the highest-pressure rise is 38 percent whereas the efficiency of the same working point at C04 (maximum pressure) is 30 percent which shows a 21 percent decrease in efficiency.

The reason for that lies in the fact that regenerative compressors draw more power at low flow rates since, increased number of circulations through the impeller blades at low flow rate producing very high pressure rise at low flow rates for RFC. However, these large number of circulations through the blades require a high amount of power draw. This is the reason why in RFCs we see a high-pressure ratio at low flow rates, but very low efficiency.

It must be mentioned that since the pressures rise at the first working points are very close to the chock point of the machine, the data is not coherent in those points as it shows in efficiency plot. In a nutshell the geometry with a bigger blade, while other parameter of the machine is kept constant, gives a higher efficiency.

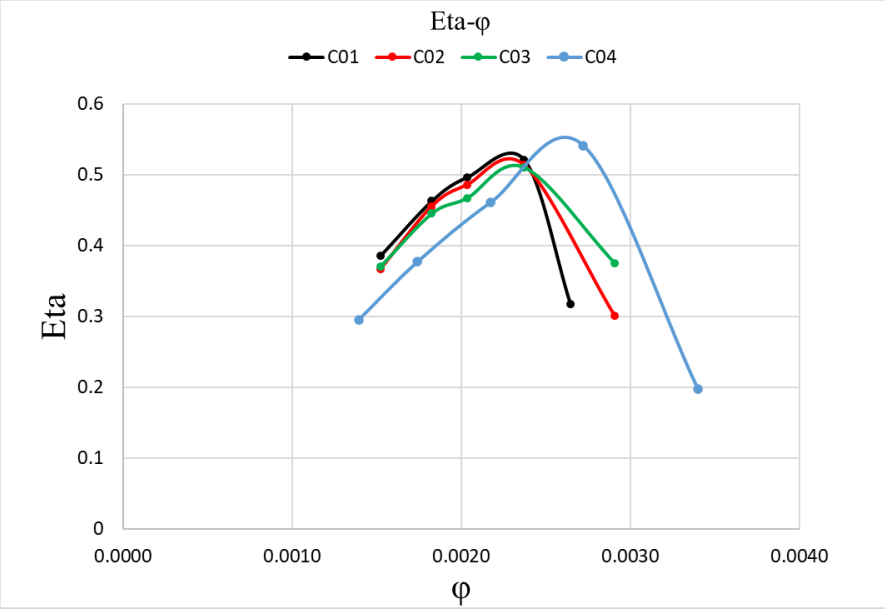

Fig. 71. Comparison between efficiency of geometries of family one.

Moreover, it was found that the geometries which produce higher pressure also produce high outlet temperature **Fig. 72**. It is obvious form **Fig. 72** that the C04 has by far higher temperature in all working points in regard to other three geometries whereas the maximum temperature at C01 is 317 kelvin where the maximum temperature at C04 is 330 kelvin which is 4 percent increase while for the minimum temperature, points are equal at 302 kelvin.

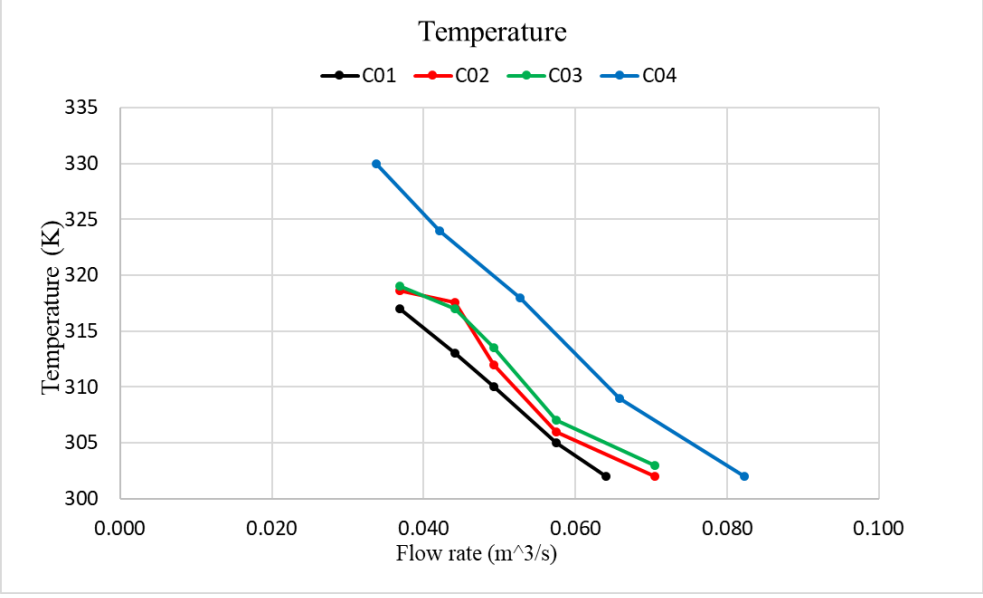

Fig. 72. Comparison between temperature rise of geometries of family one.

5.1.2 Second family of geometries

In the second family of geometries the outer diameter and inner diameter are fixed at 430.46 mm and 288 mm respectively hence configurations C03, C05, C06, and C07 have different casing depth $\boldsymbol{W_S}$ ranging from 28, 30, 32, and 34 mm respectively.

From plotted pressure ratio **Fig. 73**, it can be seen that when the inner and outer diameter of the machine is kept constant by increase of the casing depth $\boldsymbol{W_S}$ the pressure ratio increases at C05 with30 mm casing depth in compared to C03 with 28 mm casing depth in high-pressure working points while for the two low-pressure working points the pressure drops, however when the casing depth increases to 32 mm at C06 the pressure ratio drops somewhere between C03 and C05 at first two low pressure working points while at last three high-pressure working points the pressure ratio surpasses the C03 and C05. Moreover, increasing the casing depth further to 34 mm at C07 the pressure ratio sees another drop in pressure ratio for all working points in regard to C06. It can be concluded that there is a limitation on increasing the casing depth $\boldsymbol{W_S}$ which results in pressure rise and after that the further increase of the casing depth results in decrease in pressure ratio. In nutshell at low pressure working point the smallest casing depth C03 is superior to the higher depth geometries while in high-pressure working points the optimal casing depth is C06 geometry with casing depth of 32 mm.

This effect also was reported by Cates [46] but he did not provide any explanation regarding his observation. The flow separation at the channel walls is what is causing this trend. The fluid cannot adhere to the channel walls if the channel area is too large, which prevents normal fluid circulation. Extreme turbulence is caused by this flow separation at the channel walls. A smaller channel area, on the other hand, allows the fluid to adhere to the walls and receive optimal direction and circulation. The amount of energy delivered to the fluid and the pressure ratio increase when the impeller is rotated more frequently. Therefore, a reduced channel area also contributes to a better pressure ratio.

The efficiency plot **Fig. 74** shows that the maximum efficiency happens at second working point of C05 with 53 percent while the maximum efficiency at C03, C06, and C07 is 51, 47, and 50 percent respectively at their second working point. As was expected the minimum efficiency happened at C06 by 25 percent for the last working point where the pressure is maximum. In the next runner-up's are C07, C05, and C03. It must be mentioned that the C07 here does not follow the expectation since it has a lower pressure ratio, so it was expected to have the highest efficiency since it produced lowest pressure. This could be because of the fact that since the casing passed the optimal depth, the flow separation in the casing creates strong turbulence and the fluid which fails to circulate mixes with incoming stream of fluid coming from compressor inlet and creates a blockage effect, resulting in huge loss of efficiency.

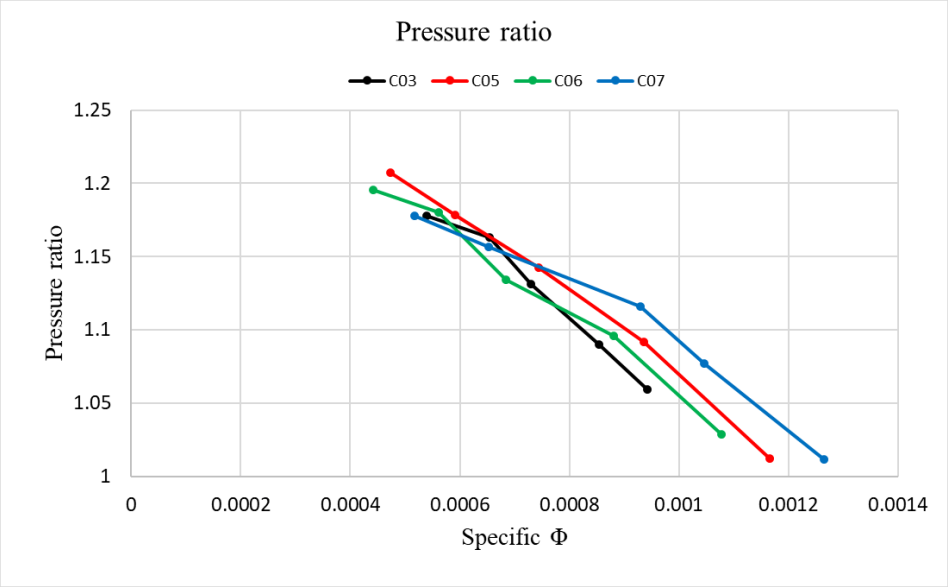

Fig. 73. Comparison between pressure ratio of the second family of geometries.

Moreover, the temperature plot **Fig. 75** in the second family of geometries demonstrates that the higher the pressure is the higher the temperature. The same effect was reported for the first family of geometries either. It is obvious form **Fig. 75** that the C06 has the higher temperature in all working points in regard to C03, C05 and C07 whereas the maximum temperature at C06 is 337 kelvin where the maximum temperature at C03 is 319 kelvin which is 5 percent increase while in regard to C05 and C07 is 1 and 0.2 percent increase. It can be seen that the C07 temperature is higher at high pressure working points compared to C03 and C05 which could be explained by the fact that due to the bigger casing depth the losses in those points are higher so producing higher temperatures despite the fact that aforementioned working points at C07 have lower pressure regarding C03 and C05.

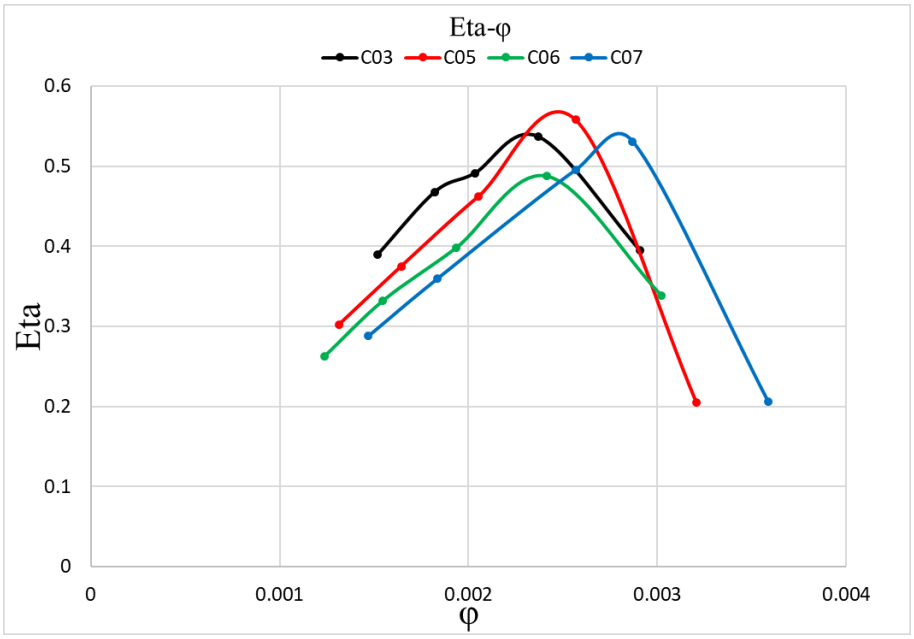

Fig. 74. Comparison between efficiency of the second family of geometries.

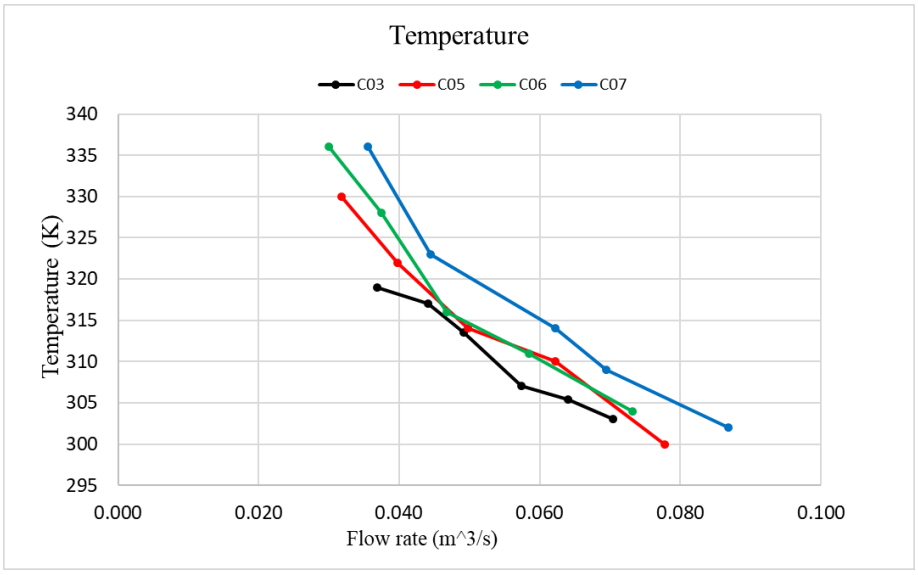

Fig. 75. Comparison between temperature rise of the second family of geometries .

5.1.3 Third family of geometries

In the Third family of geometries the outer diameter and inner diameter are fixed at 430.46 mm and 300 mm respectively hence configurations C01, C08, and C09 have different casing depth w_s ranging from 28, 30, and 34 mm respectively. It worth mentioning that the difference between the second family of geometries and the third geometries are in the inner diameter, in the sense that the third family has a bigger inner diameter (12 mm longer) hence it has a shorter blade radially speaking.

Fig. 76 and ***Fig. 77*** show again the effect of casing depth W_S, on pressure and the efficiency of the machine, respectively. it can be seen from ***Fig. 76*** that the maximum pressure ratio is achieved with C08 where the casing depth W_S was second smallest of the group (30 mm), also C08 geometry showed higher pressure ration in all working points in regard to the other two geometries. In next runner up in terms of maximum pressure ratio is C09 with casing depth W_S 34 mm, but it could be mentioned that in the first three working points (higher flow rate) the difference of the pressure ratio with C01 with casing depth W_S of 28 mm are very small, and in the last two high-pressure (low flow rate) working points the difference in noticeable.

These results suggesting that by increasing the casing depth W_S, the pressure ratio also increases but to a limit and further increase of the casing depth W_S will decrease the pressure rise. Moreover, this further increase of the casing depth W_S effects the pressure ratio especially at low-pressure (high flow rate) working points. Moreover, ***Fig. 77*** shows that the efficiency of the C01 geometry is highest (54%) among all other members of the third family, and in all working points. This partly due to the fact that in the smaller casing size the separation zone is not big enough to create tangible losses and in result effect the efficiency, while as it mentioned above when all parameters of machine are kept constant, in the machine with a bigger casing area, big separation happens and creates considerable losses which reducing the efficiency of the machine. this trend followed up by C08 (W_S 30 mm) and C09 (W_S 34 mm) having the second and third runner up position in efficiency graph with the values of 50% and 48% respectively.

In compared to the second family, the same trend happened for geometries with casing depth W_S 30 mm and produced the maximum pressure ratio with the fact that in second family the pressure ratio for first two low pressure (high flow rate) working points were lower than the smallest casing depth W_S (28 mm) while in third family were higher in all working points. Also, the geometry with casing depth W_S (34 mm) in the second family had lower pressure ratio in regard to the geometry with casing depth W_S (28 mm) C03 in the first 4 working points and for the fifth working points (highest pressure) was equal with the smallest casing depth. Whereas in third family geometry the geometry with the largest casing depth W_S had higher pressure ratio in all working points compared to the geometry with smallest casing depth W_S (28 mm) C01.

However, in regard to comparison of the efficiency graphs of these two families the maximum efficiency recorded by the C05 at 56% with bigger casing size (W_S 30 mm) in regard to the third family which the maximum efficiency happened at 52% in C01 which had the smallest casing depth (W_S 28 mm). in the second family, the second and the third runner up in efficiency were C03 (W_S 28 mm) and C07 (W_S 34 mm) with 54% and 53% which are both show higher value than their equivalent geometries in the third family of geometry C01, and C09 respectively. From these observation it can be concluded that the axial length of the blade has a superior effect on the efficiency compared to the casing depth W_S in the sense that the axially longer blades have better efficiency in these machines.

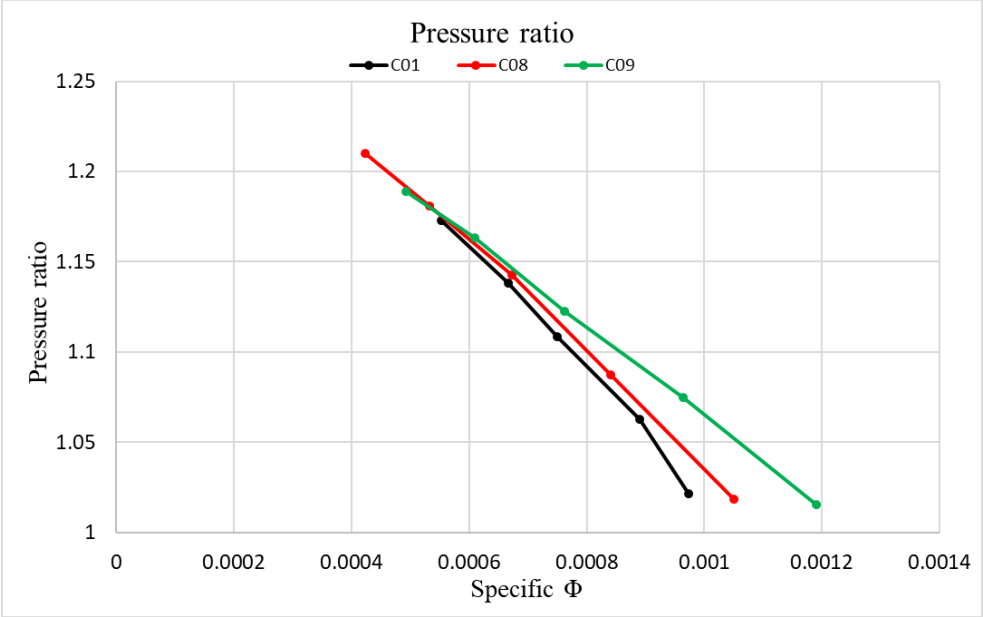

Fig. 76. Comparison between pressure ratio of the third family of geometries.

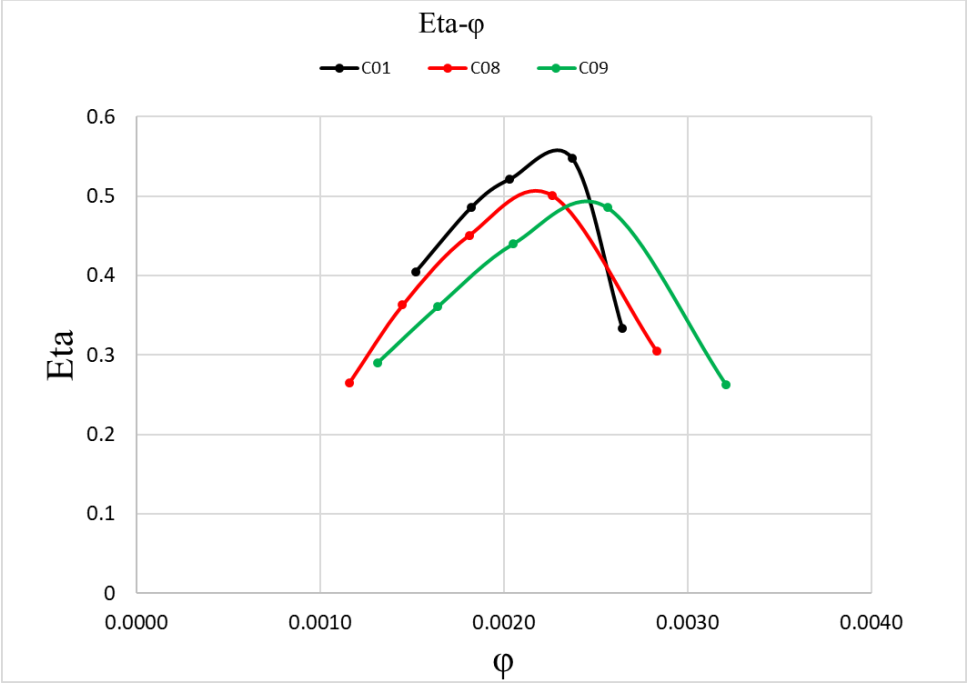

Fig. 77. Comparison between efficiency of the third family of geometries.

Moreover, the temperature plot **Fig. 78** in the third family of geometries demonstrates that the geometries with the higher pressure C08,C10, and C01 respectively, have the higher temperature. The same effect was reported for the first, and second family of geometries either. It is evident form **Fig. 78** that the C08 has the higher temperature in all working points in regard to C01, and C09 whereas the maximum temperature at

C08 is 329 kelvin where the maximum temperature at C10 is 328 kelvin which is 1 percent increase while in regard to C01 with 317 Kelvin has 3.7% percent increased.

In comparison between the temperature of the second and third family of geometries shows that the axially longer blades, second family of geometry's, produce more heat compared to the axially shorter blades machines.

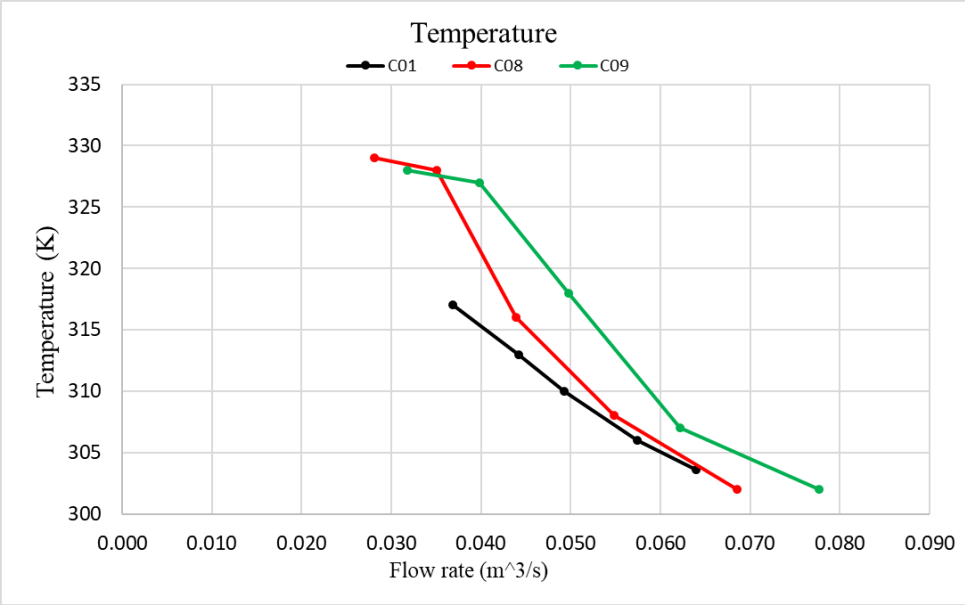

Fig. 78. Comparison between temperature rise of geometries of family three.

5.1.4 Fourth family of geometries

In the fourth family of geometries the outer diameter and inner diameter are fixed at 430.46 mm and 300 mm respectively hence configurations C01, C10, C11, and C12 have same casing depth $\boldsymbol{W_S}$ ranging however, the depth of the rotor $\boldsymbol{W_R}$ is changing from 28, 30, 32, and 34 mm respectively. In these set of geometries, the goal was to see the effect of blades depth on the pressure and the efficiency of the machine whereas in the previous groups the effect of the changes in the casing and axial length of the blade was considered.

As it shown in ***Fig. 79*** the larger the depth of the rotor $\boldsymbol{W_R}$ blades gets the higher the pressure becomes, which makes sense since the blades with higher depths $\boldsymbol{W_R}$ will carry more flow and subsequently resulting in more work exchange between the rotor and the air in the machine. by comparing the last two high pressure working points of C01 and C12, it can be seen that the pressure ratio increased from 1.14 in penultimate (P4) working point of C01 to 1.24 in equivalent working point at C12. Moreover, for the for the last working points the pressure ratio for C01 is 1.17 and for C12 is 1.27, all this difference in pressure ratio is result of changing rotor depth $\boldsymbol{W_R}$ from 28 mm in C01 to 34 mm in C12. Also, the **Fig. 79** suggests

that with increase of the blade's depth the slope of the pressure rise increases accordingly, whereas the C12 has the steepest slope followed by C11 and C10and then C01 at last.

Fig. 80 demonstrates the efficiency of fourth family of geometries in one graph. It is obvious that by moving from high flow rate (low-pressure) working points to low flow rates (high-pressure) working points the efficiency for all machines start at their lowest and reach at their peak in second working points and then start to drop down when pressure rises. The maximum efficiency value For C12 and C11 are 56%, and 53% respectively while the maximum efficiency at C10, and C01 are 51.5%, and 55% respectively. This results suggest that by decreasing the blades depth efficiency in high-pressure (low-flow rate) working points increases, while in low-pressure (high-flow rate) working points efficiency decreases not considering C01 first two working points.

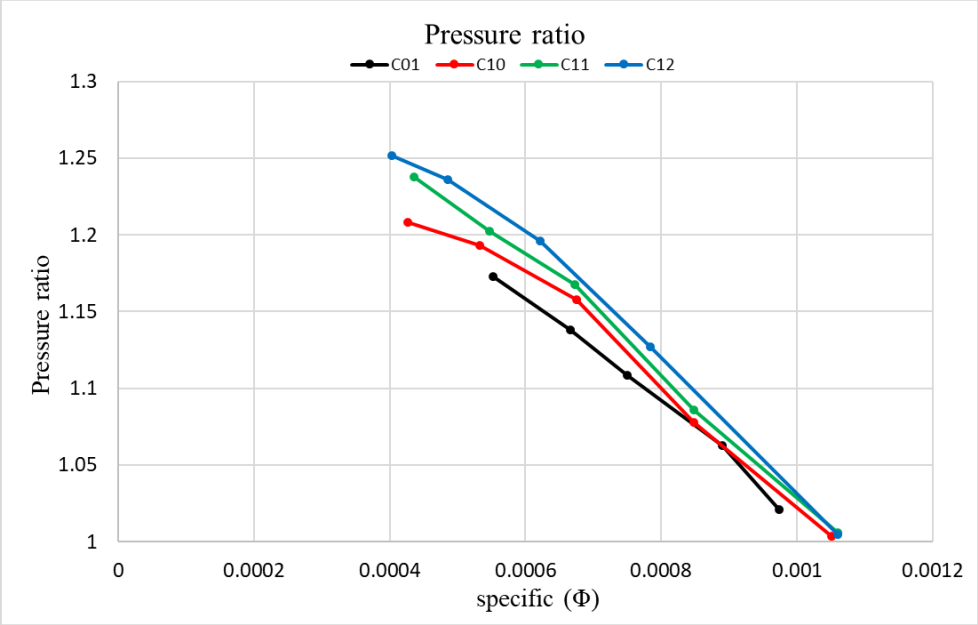

Fig. 79. Comparison between pressure ratio of the fourth family of geometries.

Fig. 81 shows the temperature variation between different working points for each geometry and also compares them with other family members of the fourth family. It suggests that by increasing the blade's depth from 28 mm to 30 mm the temperature rises almost in every working points, except for P1(highest flow rate) which drops by 4 kelvin to 302 kelvin. It is obvious that the higher pressure geometry (C12) has produced the highest temperature with the value of 331 Kelvin. And by further increasing the blades depth to 32 mm, in the first three working points the temperature despite the pressure rise doesn't change but in the last two high-pressure working points temperature drops by 2 Kelvin to 323, and 324 in C11. However, in C12 with 34 mm blade depth the temperature raises in all working points slightly above the C10 and reaches the maximum value of 327 Kelvin at highest pressure (low-flow rate) working point. This could be the effect of increase in the losses due to the high pressure produced.

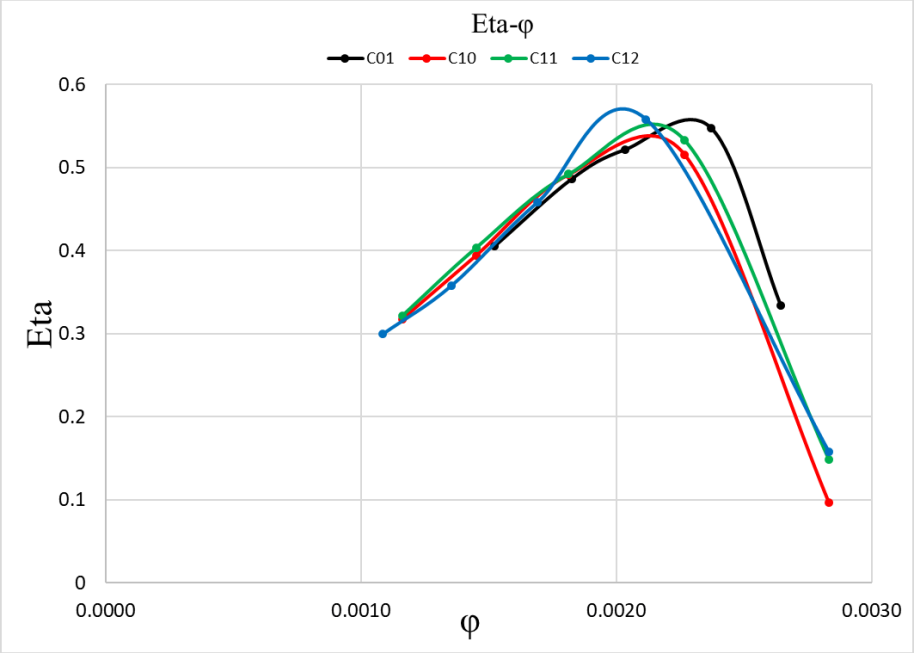

Fig. 80. Comparison between efficiency of the fourth family of geometries.

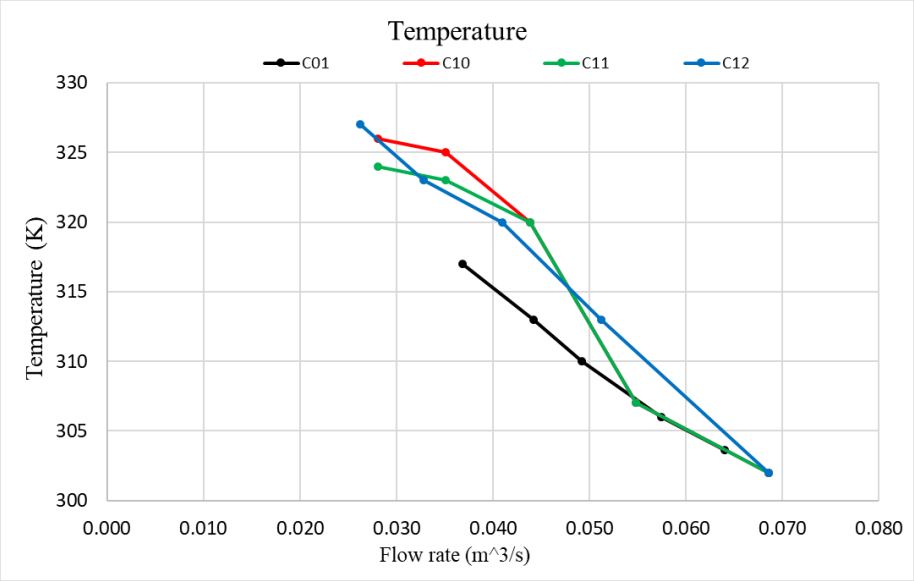

Fig. 81. Comparison between temperature rise of geometries of family three.

Table 7. effect of geometry changes on efficiency. (maximum changes are reported here).

Parameter (mm)	Variation range (mm)	Max. Efficiency (%)
Inner diameter	24	+3
Depth of Stator W_S (inner d 288)	2	+6
Depth of Stator W_S (inner d 300)	6	-12
Depth of Rotor W_R (inner d 300)	4	+4

- A small but significant fraction of the compressed gas was found to be carried through the stripper from the high-pressure region and expanded down to the inlet pressure as the blade pockets between the blades open into the annular channel at the inlet end. This is usually referred to as carry over loss and it represents a loss of efficiency.
- By reducing the mass flow rate, the effect of recirculating flow becomes more dominant due to its considerable higher temperature and volume regarding the inlet flow.
- The amount of the recirculating flow that passes through the stripper has indirect relation with the inlet flow rate, in the sense that at high inlet flow rate (low pressure working points) the amount of carryover flow through the stripper leakage is small but, at low inlet flow rate (high pressure working points) the amount of carryover flow through the stripper leakage is much higher and at shot off points almost 100 % of the flow passes through the stripper leakage.
- By moving toward outlet from inlet, tangentially speaking, the circulatory velocity increases due to the pressure rise and tangential velocity decreases due to adverse pressure gradient.
- The geometries with bigger rotor, radially speaking, produce higher efficiency compared to smaller rotor geometries, while the other variable is constant.
- By increasing the casing depth (casing size), the pressure increases up to a limit and after increasing further the casing size, the pressure drops, especially in low- flow rate working points.
- The effect of rotor length radially speaking has superior effect on efficiency of the machine compared to the depth of the casing, in way that in an equal situation for two RFC machine with a same casing depth, the machine with a longer blade size, axially speaking, has a higher efficiency.
- By increasing the rotor depth, the maximum efficiency of the RFC machine increases in general. However, this increase appears only on low- pressure (high flow rate) working points, and after maximum points they decrease with higher steep.

References:

[1] Sreekanth, M., Sivakumar, R., Sai Santosh Pavan Kumar, M., Karunamurthy, K., Shyam Kumar, M. and Harish, R. (2021). Regenerative flow pumps, blowers, and compressors – A review. Proceedings of the Institution of Mechanical Engineers, Part A: Journal of Power and Energy, 235(8), pp.1992–2013. doi: https://doi.org/10.1177/09576509211018118.

[2] Song. J. W.. Engeda. A., and Chung, M. K., 2003, "A Modified Theory for the Flow Mechanism in a Regenerative Flow Pump," Proc. Inst. Mech. Eng Part A, 217. pp. .111-.121.

[3] Yoo, I. S.. Park. M. R.. and Chung. M. K., 2OO.'i. "Improved Momentum Exchange Theory for Incompressible Regenerative Turbomachines." Proc. In.st. Mech. Eng. Part A. 219. pp. 67-81.

[4] Raheel. M. and Engeda. A. "A Systematic Design Approach for Radial Blade Regenerative Turbomachines." J. Propul. Power. 21(5). pp. 884-892.

[5] Meakhaii. T. and Park. S. O. "An Improved Theory for Regenerative Pump Performance," Proc. Insl. Mech. Eng. Part A. 219. pp. 213-222.

[6] Raheel, M., A Theoretical, Experimental and CFD Analysis of Regenerative Flow Compressors and Regenerative Flow Pumps for Microturbine and Automotive Fuel Applications Automotive Fuel Applications, Ph.D. thesis, Michigan State University, East Lansing, MI.

[7] Wilson, W. A., Santalo, M. A., Oelrich, J. A. A theory of the fluid-dynamic mechanism of regenerative pumps. Trans. ASME, 1955, 77, 1303–1316.

[8] El Hag, A. I. A theoretical analysis of the flow in regenerative pumps. PhD Thesis, University of Bath, England, 1979.

[9] Senoo Y., “Theoretical Research on Friction Pump”, Reports of Research Institute for Fluid Engineering, Kyusku University, Vol.5, No.1, 1948, pp 23-28.

[10] [14] Senoo, Y. (1956). A Comparison of Regenerative-Pump Theories Supported by New Performance Data. Journal of Fluids Engineering, 78(5), pp.1091–1095. Doi: https://doi.org/10.1115/1.4013932.

[11] [6] Senoo Y. (1954), “Researches on the Peripheral Pump”, Reports of Research Institute for Applied Mechanics, Kyusku University, Vol.3, No.10, pp 53-113.

[12] [15] Senoo Y. (1954), “Influences of the Suction Nozzle on the Characteristic of a Peripheral Pump and an Effective Method of their Removal”, Reports of Research Institute for Applied Mechanics, Kyusku University, Vol.3, No.11, August, pp 129-142.

[13] [19] Iversen, H. W., 1955,” Performance of the Periphery Pumps,” Trans. ASME, Vol. 77, No. 1.

[14] [8] [4] Wilson, W. A., Santalo, M. A. and Oelrich, J. A. A theory of the fluid-dynamic mechanism of regenerative pumps. Trans. ASME, 1955, 77, 1303–1316.

[15] Minoru Shimosaka and Yamazaki, S. (1960). Research on the Characteristics of Regenerative Pump: 1st Report, Influences of Flow Channel and Impeller. doi: https://doi.org/10.1299/jsme1958.3.185.

[16] Burton J. D., “The prediction and improvement of regenerative turbomachine performance”, The British hydromechanics research association, 9th member conference, Cranfield, September 1967.

[17] Gessner, R.L. (1967). Multistage, Gas-Bearing, Helium Compressor Development. pp.631–639. doi: https://doi.org/10.1007/978-1-4757-0489-1_65.

[18] Grabow G., “Influence of the Number of Vanes and Vane Angle on the Suction Behavior of Regenerative Pumps”, Proceedings Conference on Fluid Machinery (5th) Budapest. Hungry, September 15-20, 1975, Vol. 1, pp 351-364.

[19] Hollenberg J. W., “An investigation of the efficiency of regenerative blowers and pumps”, PhD thesis, Stevens institute of technology, 1978.

[20] Yamazaki S., Tomita Y., “Researches on the Performance of the Regenerative Pump with Non-radial Vanes”, Bulletin of JSME, Vol. 14, No. 77, 1971, pp. 1178-1186.

[21] Yamazaki S., Tomita Y., “Researches on the Performance of the Regenerative Pump with Non-radial Vanes”, Bulletin of JSME, Vol. 15, No. 81, 1972, pp. 337-343.

[22] Yamazaki S., Tomita Y., “Researches on the Performance of the Regenerative Pump with Non-radial Vanes”, Bulletin of JSME, Vol. 17, No. 106, 1974, pp. 459-466.

[23] [33] Sixsmith, H. and Altmann, H. (1977). A Regenerative Compressor. Journal of Engineering for Industry, 99(3), pp.637–647. doi: https://doi.org/10.1115/1.3439291.

[24] Sixsmith H., “The Theory and Design of a Regenerative Compressor, Presented at the Institute of Marine Engineers, London, May 7, 1981.

[25] Abdalla H.M.M., “A Theoretical and Experimental Investigation of the Regenerative Pump with Airfoil Blades, PhD thesis, September 1981, Applied Mechanics Branch, Royal Military College of Science.

[26] Grabow, G. Influence of the number of vanes and vane angle on the suction behavior of regenerative pumps. Second Conference on Flow Machines, Budapest, October 1966, pp.147–166.

[27] Dewitt, D. P. Rational design, and development of the regenerative pump. MS thesis, MIT, January 1957.

[28] Mason, S. C. Influence of internal geometry upon regenerative pump performance. BS thesis, MIT, May 1957.

[29] Whitehead, D. S., Harrison, S. and Rose, M. G. A Regenerative Compressor, 1982 (Cambridge University Engineering Department Technical Report, Cued/A-Turbo/Tr 114).

[30] Badami, M. and Mura, M. (2012). Comparison between 3D and 1D simulations of a regenerative blower for fuel cell applications. Energy Conversion and Management, 55, pp.93–100. doi:https://doi.org/10.1016/j.enconman.2011.10.003.

[31] Ritter, C., 1930,” Uber selbstansaugende Kreiselpumpen und Versuche an einer neuen Pumpe dieser Art,” PhD TU Dresden, Germany.

[32] Schmiedchen, W., 1932,” Untersuchungen ¨uber Kreiselpumpen mit seitlichem Ringkanal,” PhD TU Dresden, Germany.

[33] Pfleiderer, C., 1949,” Die Kreiselpumpen f¨ur Fl¨ussigkeiten und Gase,” Springer Verlag, dritte Auflage, Berlin.

[34] Weinig, F. S., 1955,” Analysis of Traction Pumps. Hydraulic Division of ASME,” No. 55 - Sa -35.

[35] Senoo, Y., 1958,” Comparison of Regenerative-Pump Theories Supported by New Performance Data,” Trans. ASME, July 1958.

[36] Grabow, G., 1992,” ¨Ubersicht ¨uber die Theorien zur Kl¨arung der Str¨omung in Seitenkanalmaschinen,” Verlag und Bildarchiev, W.H. Faragallah (Hrsgb.).

[37] Surek, D., 1992,” Anwendung theoretischer Grundlagen und ¨Ahnlichkeitszahlen zur Auslegung von Seitenkanalstr omungsmaschinen,” Verlag und Bildarchiv, W.H. Faragallah (Hrsgb.).

[38] Surek, 2000,” Druckschwingungsverteilung im Seitenkanal von Verdichtern,” Vakuum in Forschung und Praxis, Nr. 5, 326-332.

[39] Trautmann, C., Hellmann, D.-H., 1998,” F¨orderverhalten von Seitenkanalpumpen bei 3000 1/min,” Verlag und Bildarchiv, W.H. Faragallah (Hrsgb.).

[40] Beilke, J., 2005,” Numerische Untersuchungen zur instation ¨aren Str¨omung in Seitenkanalverdichtern,” Dissertation of Technical University of Freiberg, Germany.

[41] Fleder A., Böhle M. A systematical study of the influence of blade length, blade width, and side channel height on the performance of a side channel pump. ASME J. Fluids Eng., 2015, 137(12), pp. 121102-121102-10, doi: 10.1115/1.4030897.

[42] Quail F., Scanlon T., and Stickland M.. Design optimization of a regenerative pump using numerical and experimental techniques. International Journal of Numerical Methods for Heat & Fluid Flow, 2011, 21(1), pp: 95-111, doi: 10.1108/09615531111095094.

[43] Nejadrajabali J., Riasi A., Nourbakhsh S.A. Flow pattern analysis and performance improvement of regenerative flow pump using blade geometry modification. International Journal of Rotating Machinery, vol. 2016, Article ID 8628467, 16 pages, 2016. doi:10.1155/2016/8628467.

[44] Bicard R., "Investigation on the Inlet Design of the Regenerative Pump", M. I. T. B.S. Thesis, 1957.

[45] Shimosaka M., Yamazaki 8., "Research on the characteristics of Regenerative Pump", Bulletin of JSME, Vol. 3, No. 10, 1960, pp. 185-190.

[46] Cates P.S., "Peripheral-Compressor Performance on Gases with Molecular Weights of 4 to 400", A.S.M.E. Transactions 64-WA/FE-25, Meeting November 29- December 4, 1964.

[47] Cates P.S., "Performance Characteristics of a Peripheral Compressor", Technical Division, Oak Ridge Gaseous Diffusion Plant.

[48] Hollenberg J. W., "An investigation of the efficiency of regenerative blowers and pumps", PhD thesis, Stevens institute of technology, 1978.

[49] Hollenberg J. G., "Hydrogen Pipeline Transmission", Stevens Institute of Technology, Hoboken, New Jersey 07030.

[50] Sixsmith H., Watson M. J ., "A Helium Regenerative Compressor", Proceedings of the International Cryogenic Engineering Conference, 1980, pp155-164.

[51] Swift W- L" Nutt W. E-, Sixsmith H., "A helium regenerative compressor", Cryogenic Engineering Conference July 12-16, 1993, Albuquerque, NM.

[52] Crowe W. E., Schwarz H., "Development of UHTREX Gas-Bearing Compressors", Rotating Machinery for Gas- Cooled Reactor Application, TID-7690, November 4-6, 1963, pp 253-262.

[53] Crewdson E., "Water-Ring Self-Priming Pumps", Proceeding of the Inst. of Mech. Engr., Vol. 170, No.13, 1956, pp 407-417.

[54] Balje O. E., "Drag-Turbine Performance", Trans. of ASME, August. 1957, pp 1291-1304.

[55] Burton D. W., "Review of Regenerative Compressor Theory", Rotating Machinery for Gas-Cooled Reactor Application, TID-7631, April 2-4, 1962, pp 228-242.

[56] Whitehead D.S., Harrison 8., Rose M.G., "A Regenerative Compressor", Cambridge University Engineering Dept, (Technical Report) CUED/A-Turbo, 1982

[57] Kupryashin N.N., and Ryazanov S.D., "Analysis of the Operation of Radial- Vortex Type Centrifugal Pumps", Translated from Khimicheskoe i Neftyanoe, No. 4, pp 11-12, April, 1983.

[58] Jakubowski M., Kovitz AA, and Raynor 8., "Ideal Fluid Flow in an Enclosure of Toroidal Geometry, Int. J. Non Linear Mechanics, Vol. 6 (1971) pp 101-115 Pergamon press.

[59] Schivley G.P., Dussourd J .L., "An Analytical and Experimental Study of a Vortex Pump", Journal of Basic Engineering, December 1970, pp 889-900.

[60] Bullough W.A., "A Simple Drag Pump", "Proceedings of the 4th Conference on Fluid Machinery, Akademiai Kiado, Budapest, 1972, p. 211.

[61] Burton J. D., "The "Straight Through" Labyrinth Seal as Applied to the Regenerative Turbomachine", 5th International Conference on Fluid Sealing, Paper E1, Warwick England, 30th March-2nd , April, 1971.

[62] Andrew D.N., "The Calculation of Flow in Regenerative Turbomachines by a Streamline Curvature Method", Proc. Instn. Mech. Engrs., Part A: J. of Power and Energy, Vol. 204, 1990. pp 121-129.

[63] Bo¨hle, M. and Mu¨ller, T. (2009) ‘Evaluation of the flow inside a side channel pump by the application of an analytical model and CFD’, Volume 1: Symposia, Parts A, B and C [Preprint]. doi:10.1115/fedsm2009-78023.

[64] Wang, Y., Zhang, F., Yuan, S., Chen, K. and Wei, X. (2020). Effect of URANS and Hybrid RANS-Large Eddy Simulation Turbulence Models on Unsteady Turbulent Flows Inside a Side Channel Pump. Journal of Fluids Engineering-transactions of The Asme, 142(6). doi:https://doi.org/10.1115/1.4045995.

[65] Wilcox, D.C. 2008. “Formulation of the k- turbulence model revisited”, AIAA Journal, 46(11), pp. 2823-2838.

[66] Insinna, M., Salvadori, S., Martelli, F., Peroni, G., Simon, G., Dipace, A. and Raffaele Squarcini (2018). One-Dimensional Prediction and Three-Dimensional CFD Simulation of the Fluid Dynamics of Regenerative Pumps. doi: https://doi.org/10.1115/gt2018-76416.

[67] Badami M., “Theoretical and Experimental Analysis of Traditional and New Periphery Pumps”, Proceedings of the 1997 International Congress and Exposition, Feb 24-27 1997, Detroit, MI USA, pp 45-55.

[68] Engeda, A. 2003, "Flow Analysis and Design Suggestions (or Regenerative Flow Pumps." ASME Paper No. FEDSM2(K)3-45681.